KU LEUVEN

FACULTY OF BIOSCIENCE ENGINEERING

Looking through the clouds or fly below?

A multispectral biodiversity analysis with drones

Promoters:

Prof. Koenraad Van Meerbeek

Dr. Sam Ottoy

Department of Earth and Environmental Sciences

Division Forest, Nature and Landscape

Dissertation presented

in fulfillment of the requirements for the degree of

Master of Bioscience Engineering:

Agro- and Ecosystems Engineering

Esther TUBBAX

August 2022

This dissertation is part of the examination and has not been corrected after defense for eventual errors. Use as a reference is permitted subject to written approval of the promotor stated on the front page.

Acknowledgment

First of all, I would like to deeply thank my supervisors Koenraad and Sam. Koenraad, I am very grateful for your endless availability and always being ready to listen, give advice and guide me through the whole research process and yet let it be my own work entirely. Sam, thank you for sharing your passionate drone knowledge and pilot experience with me. Flying with such expensive equipment with no prior experience was scary at first but with your guidance it became a wonderful experience.

I would also like to thank Marjel Van den Boer for the high-quality photo reportage during our flight mission in Hechtel-Eksel. Your photos make my thesis and presentation much more illustrative. Additionally, thank you Stephanie Delalieux for your guidance using the MAPEO Field Software to pre-process our data.

Last but not least, I would like to express my sincere gratitude to my boyfriend, family and friends for always supporting and encouraging me during this master thesis as well as during my entire study. A special thanks to my dad for investing a lot of time in reading and giving suggestions during the writing process.

Thank you all for helping to turn this thesis into something I can be proud of!

Scientific Summary

Today, biodiversity is declining faster than ever known in human history. This huge loss of species causes a decrease in ecosystem functioning which is a direct threat to human existence. To be able to take conservation and restoration actions, inventory and monitoring biodiversity and the associated ecosystem functioning is crucial. Unmanned aircraft systems (UAS) are in this regard a cost-efficient method to collect high spatial resolution data compared to for example field surveys. However, the relation between UAS-based data and biodiversity is still underexamined.

In this master thesis, we tried to predict species diversity and productivity at the FORBIO tree experiment sites in Belgium, by collecting and linking multispectral drone imagery with ground truth data on species richness and composition. The mean, standard deviation and correlation of variance of the six different reflectance bands (red, green, blue, red edge, near-infrared and thermal), the normalised difference vegetation index and the subtracted plant height were used for modelling. The model coefficient of determination (R^2) values to predict species richness with spectral data, spectral heterogeneity data, plant height data and all data combined were respectively 0.16, 0.13, 0.26 and 0.33. These results showed that UAS-based tree height data are a better predictor of species richness compared to spectral data.

The models to predict plant height, used as a proxy for tree productivity, had R^2-values of 0.72 and 0.69 based on spectral data and species richness data, respectively. In 80% of the mixed plots, a positive net diversity effect was observed. The latter in combination with the model results confirms the biodiversity-productivity hypothesis. These thesis results indicate that UAS-based data can indeed be used in tree biodiversity and productivity studies in addition to field surveys.

List of Abbreviations and Symbols Used

a.s.l.	Above sea level
BVLOS	Beyond Visible Line of Sight
CRP	Calibrated Reflectance Panel
CRS	Coordinate Reference System
cv	Correlation of Variation
DLS 2	Downwelling Light Sensor 2
DSA	Drone Service Application
DSM	Digital Surface Model
DTM	Digital Terrain Model
E/MSY	Extinctions per million species-year
EASA	European Union Aviation Safety Agency
EF	Ecosystem Functions
EMR	Electromagnetic Radiation
ENS	Effective Number of Species
ES	Ecosystem Services
FAO	Food and Agriculture Organisation
FORBIO	FORest BIOdiversity and Ecosystem Functioning
GCP	Ground Control Point
GSD	Ground Sampling Distance
HTA	Helicopter Training Area
IPBES	Intergovernmental science-policy Platform on Biodiversity and Ecosystem Services
IUCN	International Union for Conservation of Nature and Natural Resources
LAI	Leaf Area Index
LiDAR	Light Detection and Ranging
LWIR	Longwave Infrared
MAP	Mean Annual Precipitation
MAT	Mean Annual Temperature
NDE	Net Diversity Effect
NDVI	Normalized Difference Vegetation Index
NIR	Near-infrared
PH	Plant Height

ROI	Region of Interest
RS	Remote sensing
sd	Standard Deviation
SR	Species Richness
SVH	Spectral Variance Hypothesis
SWIR	Shortwave infrared
TIR	Thermal infrared
UAS	Unmanned Aircraft System
VLOS	Visible Line of Sight

List of Tables

Table 2-1 Active geozones at the day of the flight missions 24

Table 2-2 Data and time of the flight missions 25

Table 3-1 Ground truth data per plot for one show case flight mission 44

Table 3-2 Extracted mean and standard deviation band values per plot for one show case flight mission 44

Table 3-3 Extracted correlation of variance band values, NDVI and plant height per plot for one show case flight mission 44

Table 3-4 Results of Bayesian generalised linear models with negative binomial distribution to predict the species richness. 45

Table 3-5 Results of Bayesian linear models with Gaussian distribution to predict the plant height 46

List of Figures

Figure 1-1 Relationship cosystem functioning and biodiversity 2
Figure 1-2 Cumulative extinction rate of vertebrates 4
Figure 1-3 Magnitudes of extinct and threatened species 4
Figure 1-4 Temporal plant biodiversity at different spatial scales 6
Figure 1-5 Electromagnetic spectrum 8
Figure 1-6 Spectral reflectance signatures of different land cover types 11
Figure 1-7 Spectral reflectance signature of healthy green vegetation 13
Figure 2-1 Situation three FORBIO sites 18
Figure 2-2 Experimental planting design FORBIO 19
Figure 2-3 DJI Matrice 210 RTK V2 drone with the Micasense Altum sensor 22
Figure 2-4 Bands captured by a Micasense Altum sensor 22
Figure 2-5 Pilot certificate of subcategories OPEN A1 and A3. 23
Figure 2-6 Kleine-Brogel controlled airspace area 24
Figure 2-7 Start screen of DJI Pilot App 26
Figure 2-8 Deliniation flight missions on FORBIO map 26
Figure 2-9 Visualisation of front and side overlap. 27
Figure 2-10 Take-off/landing point at the Hechtel-Eksel FORBIO site 27
Figure 2-11 Calibrated Reflectance Panel 28
Figure 2-12 Drone pilot with fluorescent vest 29
Figure 2-13 Mission profile selection MAPEO Field Software 30
Figure 2-14 Drone image upload MAPEO Field Software 31
Figure 2-15 Selection flight lines and validation MAPEO Field Software 31
Figure 2-16 Flight description MAPEO Field Software 32
Figure 2-17 Quality check MAPEO Field Software 33
Figure 2-18 Schematic overview steps to extract mean, standard deviation and correlation of variation of the raster layers. 34
Figure 3-1 Deliniation of show case flight mission on FORBIO map 39
Figure 3-2 DTM and DSM of show case flight mission 39
Figure 3-3 Unprocessed reflectance data of show case flight mission 40
Figure 3-4 NDVI of show case flight mission 40

Figure 3-5 Plot size reduction FORBIO experiment Zedelgem 41
Figure 3-6 DTM FORBIO site Zedelgem. 41
Figure 3-7 NDVI and mask layer of show case flight mission. 42
Figure 3-8 Plant height of show case flight mission. 42
Figure 3-9 Processed reflectance data of show case flight mission 43
Figure 3-10 Net diversity effect of FORBIO experiment Hechtel-Eksel and Gedinne 47
Figure 3-11 Net diversity effect of FORBIO experiment Zedelgem 47

Table of Contents

1 Literature Study 1
1.1 Biodiversity in Natural Ecosystems 1
1.1.1 Importance 1
1.1.2 Biodiversity Crisis 3
1.1.3 Ecosystem Monitoring 6
1.2 Remote Sensing with Drones 8
1.2.1 General Sensor and Platform Characteristics 8
1.2.2 Drones: The Way to Go? 9
1.2.3 Biodiversity Assessment with Drones 11
1.3 Research Goals 17
2 Materials and Methods 18
2.1 Study Sites 18
2.1.1 Hechtel-Eksel 19
2.1.2 Zedelgem 20
2.1.3 Gedinne 20
2.2 Field Data 21
2.3 Multispectral Data 21
2.3.1 Drone and Camera Characteristics 21
2.3.2 Data Collection 22
2.4 Preprocessing 29
2.4.1 Preprocessing using MAPEO 29
2.4.2 Preprocessing Raster Data per Plot 33
2.5 Species Richness and Productivity Calculation 35
2.6 Data Analysis 36
3 Results 39
3.1 MAPEO-preprocessed Data 39

3.2 Extracted Raster Data per Plot 41
3.3 Species Richness and Productivity Models 45
4 Discussion 48
4.1 Spectral Diversity is a Weak Predictor of Tree Species Diversity 48
4.2 Tree Productivity can be Predicted by Spectral Data 49
4.3 UAS-based Plant Height Data Confirms the Biodiversity-Productivity Hypothesis 49
4.4 Further Improving Drone Data Collection 51
5 Conclusion 54
6 References 55
7 Appendices 64
8 Popularised Summary 103

1 Literature Study

1.1 Biodiversity in Natural Ecosystems

1.1.1 Importance

Biodiversity, including all biotic variation at gene, species, and ecosystem level, is essential, not only for human existence but for all life on Earth (Cardinale et al., 2012). Its importance as being part of the biophysical ecosystem structure has gotten more recognition during the past decades (Haines-Young & Potschin, 2010). Ecosystems provide all kinds of socio-economic and ecological benefits to humans, called ecosystem services (ES). There are four categories distinguished by the Millennium Ecosystem Assessment: provisioning, regulating, cultural, and supporting ecosystem services, with the first three directly affecting human well-being and the latter maintaining the other three (Millennium Ecosystem Assessment, 2005). The biological underpinning that determines the supply of these ES are ecosystem functions (EF) (Oliver et al., 2015).

Understanding how biodiversity affects ecosystem functioning, and therefore human well-being, has grown significantly over the past decades (Cardinale et al., 2012). In many studies, biodiversity is considered to be a positive determinant of ecosystem functions and dynamics (Schwartz et al., 2000; Tilman et al., 2014). Increased species richness can result for example in higher productivity, better nutrient dynamics, or increased ecosystem stability (Singh, 2002; Tilman, 2001).

The term ‘overyielding’ is often used to refer to the higher productivity in a species-rich ecosystem. There are two main mechanisms that can explain this biodiversity-productivity hypothesis relation. On the one hand, there is the selection effect. In a polyculture, the chance of well-performing species being present is higher as well as the chance that they will become dominant and thus increase productivity (Jing et al., 2021). On the other hand, productivity can increase in polycultures due to complementarity between different species. This can have different causes. For example, resources can be used more efficiently when species differentiate from one another in niche e.g. differentiation in rooting depth and/or architecture (Van de Peer et al., 2018). Facilitation and mutualism between different species is another example that positively influences the species productivity (Jing et al., 2021). Contrary to

selection, complementarity can also explain cases of transgressive overyielding, i.e. mixtures that have a higher productivity than the most productive monoculture (Tilman et al., 2014). When considering wood production in forest systems, complementarity is a more important mechanism than selection (Jing et al., 2021).

An important part of biodiversity is functional diversity. It is the variety of functional traits (e.g. rooting depth, leaf phenology, flowering time) that influence aspects of ecosystem functioning like ecosystem dynamics, stability and productivity (Tilman, 2001). High functional diversity in a species pool can have an even higher importance for ecosystem functioning, due to complementarity between different species, mainly when considering multiple EF (Haines-Young & Potschin, 2010).

The impact of biodiversity on EF is nonlinear and saturates at high diversity (Figure 1-1). This means that, in general, loss of biodiversity in a species-rich ecosystem will not have the same impact as in a species-poor ecosystem. The lower the biodiversity already is, the higher the decrease in EF and ES delivery when losing extra species (Cardinale et al., 2012). Also, the capacity of an ecosystem to buffer environmental perturbations will decrease rapidly. The so-called 'insurance effect' of biodiversity will no longer ensure the stability of ecosystem functioning at a low number of species (Oliver et al., 2015).

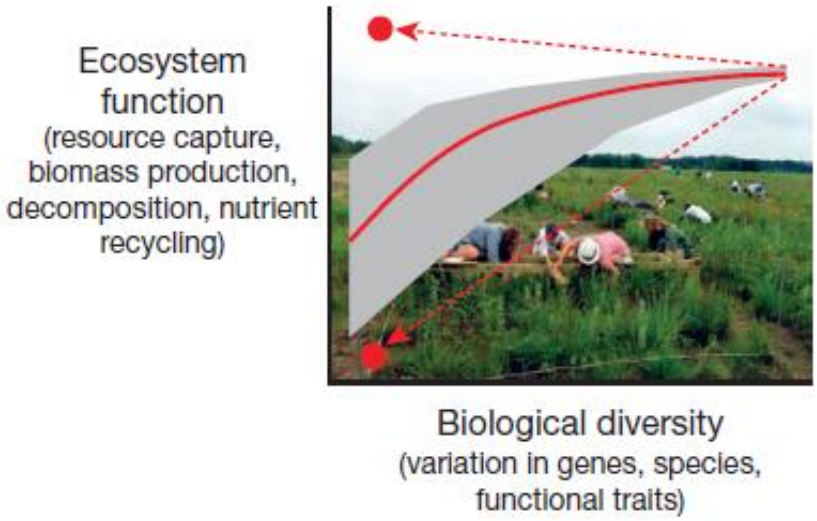

Figure 1-1 The nonlinear relationship between ecosystem functioning and biological biodiversity, based on several hundred experiments. The red line indicates the average change and the grey polygon the 95% confidence interval. The upper and bottom red dots show respectively the maximum and minimum value of the most and the least productive species grown in a monoculture (copied from Cardinale et al., 2012).

1.1.2 Biodiversity Crisis

In the past, in total five major mass extinctions have occurred and scientists suggest that today we are living in an ongoing sixth mass extinction with human activity as its main driver (Ceballos et al., 2010; Rampino & Shen, 2021; Roberts et al., 2021). Contrary to what many people think, extinction is an essential phenomenon for evolution since the balance between speciation and extinction determines diversification (Rull, 2022). The natural background extinction rate depends on natural selection processes such as competition, climatic changes and predation. When the extinction rate exceeds this background rate in orders of magnitude, one speaks of an episodic extinction (Rull, 2022). However, an episodic extinction burst is only considered as a mass extinction when also more than 75% of the living species are lost in a geologically short period of time (Barnosky et al., 2011).

Based on fossil records, the mean natural background extinction rate for all taxa is estimated at 0.1 extinctions per million species-year (E/MSY). In other words, globally one extinction per 100,000 species occurs on average every 100 years. Today, this rate is between 1,000 and 10,000 times higher (Ceballos et al., 2010; Singh, 2002; Figure 1-2). Unlike the rate, the magnitude of extinction has not yet reached the 75% boundary to speak of mass extinction. According to the Red List of Threatened Species drawn up by the International Union for Conservation of Nature and Natural Resources (IUCN), around 900 of the evaluated species went extinct in the past 500 years. This is only 0.04% of the 2.0 million known species and 0.01% of the 8.7 million estimated species (Bánki et al., 2022; Mora et al., 2011). However, these percentages are underestimations since only 142,577 species have already been assessed by the IUCN. The evaluated species are unevenly divided across different species groups, which makes it impossible to draw conclusions or make extrapolations for the insufficiently covered groups (IUCN, 2022).

The IUCN divides the assessed species into nine different categories depending on their risk of global extinction. Compared to the number of extinct species, the number of threatened species, which include all vulnerable, endangered and critically endangered species, are already much higher and increasing faster than ever seen in human history (Figure 1-3). Twenty-eight percent of all evaluated species are threatened and according to the seventh global assessment report on biodiversity and

ecosystem services, around 1/9th of all plant and animal species on Earth are threatened (IPBES, 2019; IUCN, 2022).

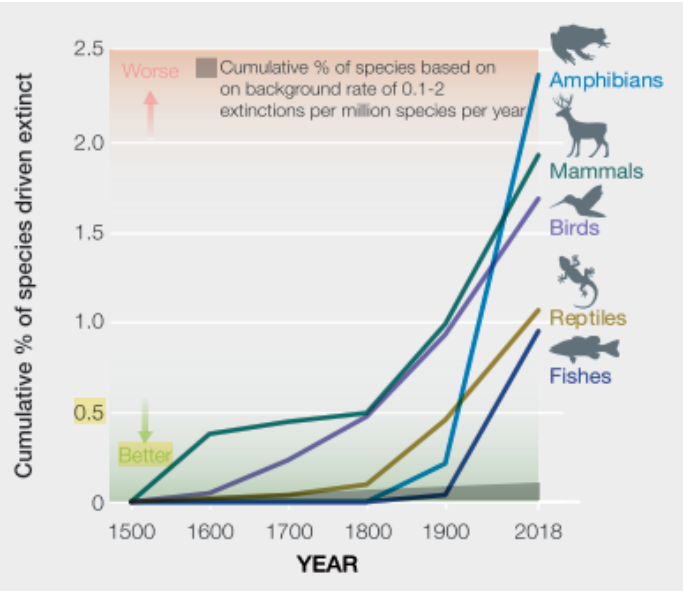

Figure 1-2 Cumulative extinction rate ('extinct' or 'extinct in the wild') of vertebrate species since 1500. The grey shape represents the extinction percentages expected with a background extinction rate of 0.1-2 E/MYS. In total 77% of described vertebrate species have been evaluated (copied from IPBES, 2019).

When extrapolating the current extinction rate and taking into account the large number of threatened species, the benchmark of 75% will be reached in a geologically short time interval of less than 1.8 million years (Rull, 2022). So, when no actions are undertaken to conserve biodiversity, we can state that today we are facing the start of a sixth mass extinction even though the extinction magnitude is not very large yet.

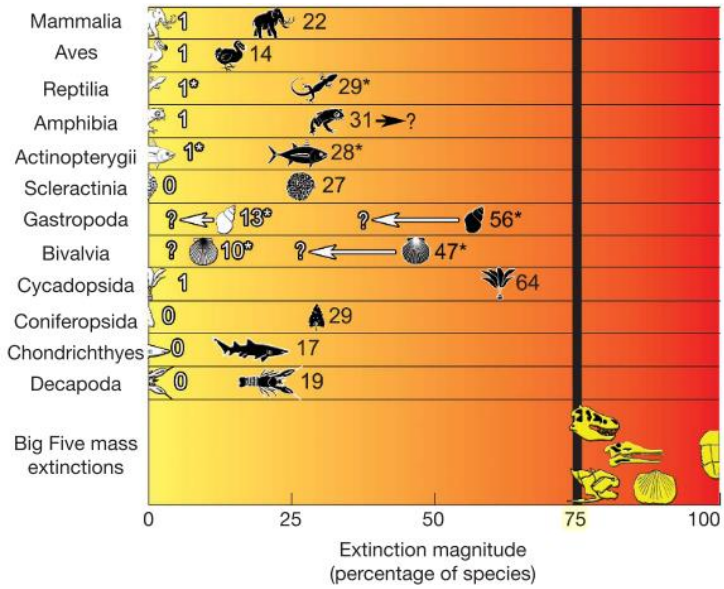

Figure 1-3 Magnitudes of IUCN-assessed extinct (white) and threatened species (black) for different taxa over the past 500 years (copied from Barnosky et al., 2011).

Both direct and indirect anthropogenic drivers are causing this huge global loss in biodiversity. Examples of direct drivers are changes in land and sea use, direct exploitation of organisms, climate change, pollution, and invasion of alien species. Indirect drivers are the underlying causes of these direct drivers, for example, human population dynamics, conflicts, epidemics, trade, etc. Without taking action to reduce the impact of these direct and indirect drivers, the global rate of species extinction will accelerate even more (IPBES, 2019).

Although there is a clear global decreasing trend in biodiversity, different patterns are observed locally and regionally (Vellend et al., 2017; Figure 1-4). Immigration and invasion become important additional inputs next to speciation when evaluating regional or local species pools (Singh, 2002). At the regional scale, biodiversity has increased over time due to the higher levels of established introduced species compared to the number of regionally extinct species (Sax & Gaines, 2003). Most of the introductions of non-native species are human-mediated, either accidentally or intentionally (Vellend et al., 2017). The species composition becomes more similar in different regions because these non-native species spread around the world. Part of these introduced species are invasive, for example because their natural enemies are not present. Therefore, native specialist species experience higher extinction rates (Millennium Ecosystem Assessment, 2005). This global biotic homogenisation is the reason why the increased regional biodiversity does not induce global biodiversity gain (Cardinale et al., 2012).

Locally, the temporal biodiversity trends strongly differ depending on the context. For example, overexploitation in an intensive agricultural system or excessive nitrogen deposition generally cause a local loss of biodiversity. Other drivers such as climate change, habitat fragmentation, and pollution can decrease, increase or have no effect on the number, composition, and distribution of species (Vellend et al., 2017). Local extinctions are also dependent on the coextinction of different species (Koh et al., 2004). When a certain species disappears, it can influence other species that locally depend on each other. Local biodiversity loss can have a direct impact on the local provision of certain ES, like flood and drought control, pollination, pest control etc. and therefore on the well-being of local communities (Díaz-Delgado et al., 2019; Haines-Young & Potschin, 2010).

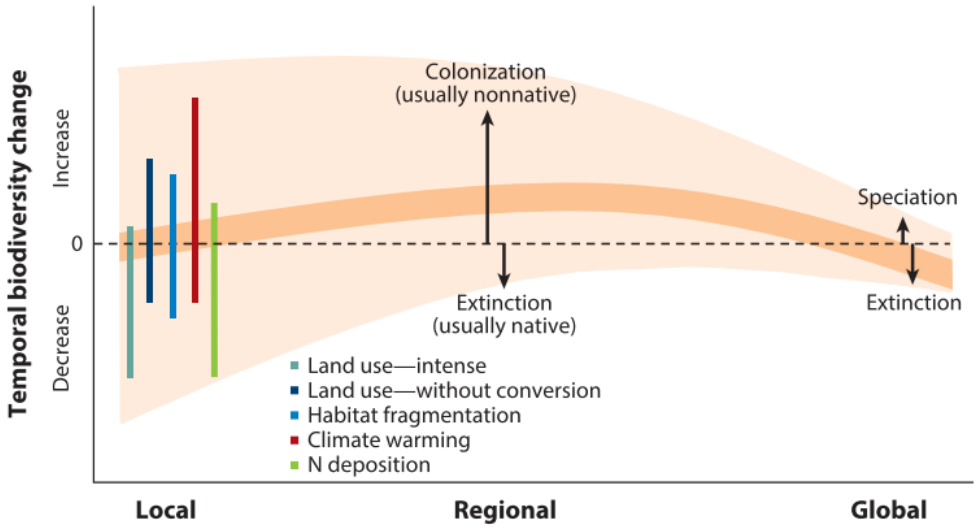

Figure 1-4 Temporal plant biodiversity change at different spatial scales. The large, shaded polygon represents the range of possible outcomes, with the central tendency indicated by the thick, darker curve. The coloured bars represent the range of local-scale outcomes of different drivers of change (copied from Vellend et al., 2017).

Not only species but also genetic diversity is declining due to human activity. According to the Food and Agriculture Organisation (FAO), already 75% of all genetic crop diversity is lost during the past century (FAO, 1999). Local varieties are lost because of the global use of genetically adapted and uniform, high-yielding crops. This loss poses a serious threat to global food security since the resilience against pests, diseases and climate change declines drastically (IPBES, 2019). The ability to breed crops in the future with desired traits such as drought tolerance decreases as well since the gene pool becomes smaller when numerous crop varieties disappear. The loss of genetic diversity today, which reduces the potential for subsequent evolutionary change, is even more alarming than the loss of species diversity (Singh, 2002).

1.1.3 Ecosystem Monitoring

Because of this ongoing loss of global biodiversity, the functioning and thereby the services delivered by natural ecosystems are highly threatened (Oliver et al., 2015). Therefore, conservation and restoration of biodiversity should be one of the major global priorities (Tilman et al., 2014). To do so, quick, efficient, and accurate inventory and monitoring of biodiversity and the associated ecosystem functioning in natural ecosystems is crucial.

First, it is important to point out that different measures can be used to evaluate and monitor biodiversity. Species diversity, being the most used measure of biodiversity, is often used as a synonym for species richness (Cardinale et al., 2012). However, it

actually should refer to both the number of species and the equitability between them (Whittaker et al., 2001). In other words, species diversity covers species richness on the one hand and species evenness on the other hand.

Functional diversity is an interesting facet of biodiversity to measure as well because of its strong relation with ecosystem functioning as discussed in section 1.1.1. Different measuring tools are used depending on the functional traits of interest, which as mentioned before influence the species' performance. Often knowing which species are present in a species pool is enough to evaluate the functional diversity because when species are described, most of their functional traits are listed as well. Lastly, genetic diversity is also often used as a measure of biodiversity because of its importance to maintain the stability of ecosystems. Molecular techniques are needed to sample the genetic variation among individuals of the same species (Singh, 2002).

To monitor species productivity, the above- and belowground biomass should be measured. This can be done directly by taking field samples and analyse the biomass in a laboratory. However, often less destructive methods are applied, mainly in forest systems, to measure the productivity. Diameter growth and tree height measures are used to monitor the standing biomass. Since the leaf area index (LAI)[1] is positively related to tree productivity, it is also often used as a measure (Arias et al., 2007).

To conduct a biodiversity assessment and inventory at a local or regional scale, often point sampling methods based on field visits are used (Singh, 2002). For productivity inventory, biomass estimates are often made in the field as well. Albeit being very accurate, field sampling has multiple limitations in this regard because these measurements are very costly and time-consuming. It is also not always easy to extrapolate these point measurements to a larger scale. Therefore, remote sensing can be an important alternative. Although it is often less accurate because it does not directly measure the variables of interest (see further), it is faster, non-destructive, relatively cheap and often easier to repeat and extrapolate (Jones & Vaughan, 2010).

[1] Leaf Area Index (LAI) is a unitless index defined as the one-side projected leaf area per unit ground surface (Arias et al., 2007).

1.2 Remote Sensing with Drones

1.2.1 General Sensor and Platform Characteristics

Remote sensing (RS) is defined as collecting information about a target from a distance without touching it (Khorram et al., 2012). More specifically, when talking about RS for earth observation, one often refers to the detection of electromagnetic radiation (EMR) by artificial detectors to study natural and non-natural ecosystems and their functioning (Jones & Vaughan, 2010). A wide variety of imaging sensors with different characteristics and applications is available. Each sensor has a specific spectral, spatial and temporal resolution and is active or passive sensing (Toth & Jóźków, 2016).

The spectral region of a sensor is determining for which applications the collected data can be used. The electromagnetic spectrum can be divided into three major groups that are used for RS: the optical part of the spectrum, which consists of visible and near-infrared radiation (NIR), the infrared part, and the microwave part of the spectrum (Figure 1-5). The infrared region is further subdivided in two subregions: the shortwave infrared (SWIR) and the longwave infrared (LWIR), also referred to as the thermal infrared (TIR). The longer the wavelength, the less energy the wave contains and thus the harder it becomes to get information about radiation further in the spectrum (Khorram et al., 2012).

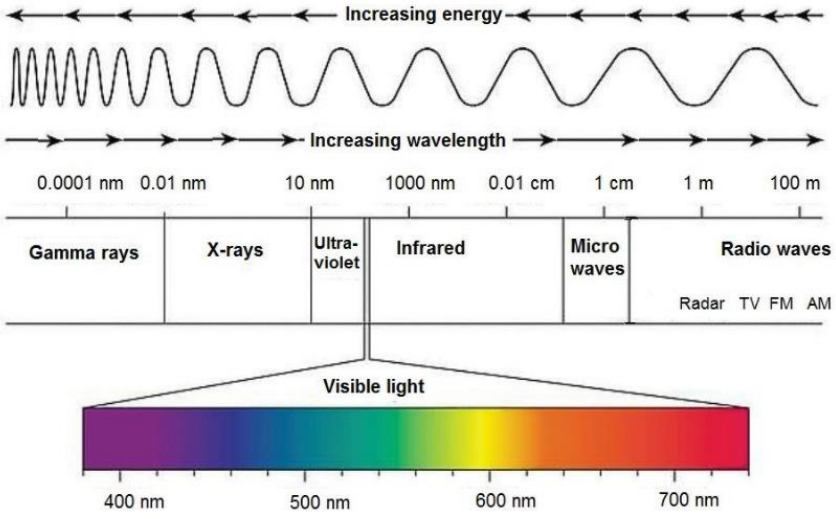

Figure 1-5 Electromagnetic spectrum with the optical (visible: 400-700 nm & near infrared part: 700-1000 nm), the infrared (shortwave infrared: 1-4 µm & thermal infrared: 4-6 µm & 8-14 µm) and the microwave (0.01-1 m) part of the spectrum often used for remote sensing applications (copied from Zhu et al., 2018).

The number and width of the measured electromagnetic bands determine the *spectral resolution* of a sensor. When hundreds of often single-nm spectral bands are measured, one speaks about hyperspectral imagery (Govender et al., 2007).

Multispectral imagery has a lower spectral resolution and thus fewer but wider bands are captured by the sensor (Toth & Jóźków, 2016). More information is averaged together and therefore less detailed information can be obtained per pixel with a multispectral sensor. However, for a lot of applications multispectral imagery is already detailed enough, definitely when the data can be collected at a high spatial resolution such as with UAVs (Dash et al., 2018).

The *spatial resolution* is often expressed in ground sampling distance (GSD) and can vary between a kilometre and centimetre resolution depending on the sensor, the platform and its intended flight altitude (Toth & Jóźków, 2016). The *temporal resolution* or repeat time is defined as how fast the same area can be revisited and resampled by the sensor. Lastly, the difference between *active and passive sensors* depends on the type of energy source used (Shaw & Burke, 2003). A passive sensor uses solar radiation as light source and captures the reflectance or emittance of objects, vegetation, or the atmosphere. Active sensors make use of their own energy source: the sensor sends out a signal and measures the difference in time, polarization and/or intensity of the returned signal (Zhu et al., 2018). Therefore, active sensors may be less dependent on environmental circumstances such as illumination conditions (Toth & Jóźków, 2016). An example of an active sensor is a light detection and ranging (LiDAR) sensor, where a laser pulse is used to measure the distance to the surface, from which a digital elevation model can be constructed.

This wide variety of sensors can be attached to different types of platforms: spaceborne platforms (satellites) or airborne platforms (e.g. aircraft, drones, hot air balloons). Satellites often have a high temporal resolution, but a relatively low spatial resolution. Aircraft, on the contrary, have a high spatial resolution but the flights are very costly and therefore difficult to repeat. Unmanned aircraft systems (UAS) – also called drones, unmanned aerial vehicles or remotely piloted aircraft systems – can collect spatially very detailed data and these flights are easy and relatively cheap to repeat. Therefore, UAS, such as drones, are very useful for numerous applications, for example, to assess the biodiversity of ecosystems.

1.2.2 Drones: The Way to Go?

UAS technology has developed rapidly over the last decade with new imaging sensors and better data processing methods (Toth & Jóźków, 2016). This increasing interest in

drone applications is reflected by the increasing trend of drone-related research (Chabot, 2018; Tsiamis et al., 2019). The use of drones shows some clear advantages compared to other RS techniques and field surveys. First of all, the use of UAS is highly flexible and easy to repeat, because the flying path is not fixed as with satellites and UAS are easy to transport (Dash et al., 2018; Pajares, 2015). UAS can operate both rapidly and at a relatively low cost (Candiago et al., 2015). In contrast, aircraft operations are in a lot of cases expensive because an entire flying crew needs to be stand-by, often for several days, to be able to take off when the weather conditions are favourable (Jones & Vaughan, 2010). A European license to fly with a UAS in open class A1 and A3 – as specified by the European Union Aviation Safety Agency (EASA) – can be obtained by everyone after taking a free online theoretical exam and is valid in all countries in Europe. A licence in these subclasses of the open category is in most cases sufficient to conduct biodiversity assessment flights since you generally do not need to fly over or near uninvolved people (EASA, 2021). The data captured by UAS generally has an extremely high spatial (centimetres) resolution because of their low overflight height (Pajares, 2015). Furthermore, drones can give access to inhospitable places where field operations would be too dangerous or destructive, e.g. mountainous areas, large wildfires, flooded areas etc. (Jones & Vaughan, 2010). Satellites can also measure such data, but the overpass time of satellites is fixed, and natural disasters are not, neither in place nor in time.

However, like every technique, UAS also has some disadvantages. Compared to satellites and aircrafts the spatial coverage of a drone flight is small due to the low flying altitude and the limited battery power. Because of that spatially specific context, it will not always be possible to extrapolate developed analysing techniques or conclusions to other areas of interest. UAS are, like aircraft, less stable platforms than satellites. They are more sensitive to wind and other disturbances, which can result in a less accurate positioning (Jones & Vaughan, 2010). UAS do not have a fixed overpass time like satellites, which could be a drawback for long-term monitoring applications. However, some studies show that combining spatially-detailed UAS data with satellite imagery can deliver results with higher utility than both separate datasets (Dash et al., 2018). Depending on the type of sensor attached to the UAS, the flight possibilities will be limited to certain weather conditions. A drone flies below the clouds, but a passive sensor onboard still uses the sun as an energy source and therefore it is

better to execute a flight during constant light intensity to have a representative reflectance for the whole research area. Nevertheless, depending on the intended application useful imagery can be captured even in presence of full cloud cover (Dash et al., 2018). Drones can have an extra sensor on top to capture the incoming solar radiation so that the reflected radiation can be corrected for it. Another limiting factor in the use of UAS is the different flight area restrictions present in almost every country. Although the UAS open class A1 and A3 licence allows pilots to fly in all European countries, they still need to follow the specific flight area restrictions in their region of interest. In certain areas, interference with other aerial vehicles and both security and privacy issues make that strict rules need to be followed when using UAS.

1.2.3 Biodiversity Assessment with Drones

Spectral Signature of Vegetation

When sensors measure radiation in multiple bands over a sufficiently wide range of the electromagnetic spectrum, the result, a spectral signature, can be used to identify materials and/or characteristics of the measured object or surface (Shaw & Burke, 2003). Vegetation can be distinguished from water, soil, or man-made materials through its specific spectral signature, but also different vegetation types or species can be differentiated (Figure 1-6). However, the latter can only be done with a high spatial and spectral resolution being available. In that case, different parts of the spectral signature of vegetation can even provide information about health, possible water stress, leaf maturity, etc. (Jones & Vaughan, 2010).

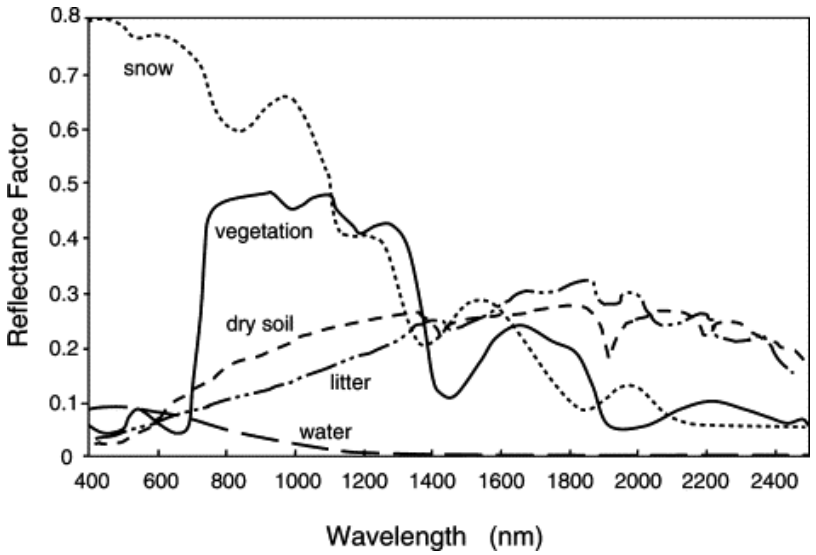

Figure 1-6 Spectral reflectance signatures of different land cover types: healthy vegetation, dry soil, grass litter, water, and snow (copied from Huete, 2004).

To be able to extract plant biophysical parameters and physiological characteristics of vegetation from reflectance data, the interaction between vegetation and incoming radiation needs to be well understood (Pajares, 2015). The typical spectral reflectance of a single healthy leaf is low in both the visible and SWIR part of the spectrum and high in the NIR part of the spectrum (Figure 1-7).

In the visible part of the spectrum, around 80 to 90% of the photosynthetic active radiation is absorbed by different leaf pigments (Jones & Vaughan, 2010). Chlorophyll is the dominant photosynthetic pigment in green plants and strongly absorbs red and blue wavelengths. Therefore, a small reflectance peak can be seen around the green waveband for healthy vegetation, which we perceive as green because of the same reason (Govender et al., 2007). The chlorophyll concentration decreases when leaves are exposed to environmental stress or are senescing during autumn. In that case, carotene and xanthophyll, absorbing blue wavelengths, and anthocyanin, absorbing blue and green wavelengths, become more dominant, hence the reflection in the red waveband increases (Jones & Vaughan, 2010). To conclude, reflectance data of the visible part of the spectrum allows to distinguish vegetation depending on their colour and maturity.

The dominant factor controlling the leaf reflectance in the NIR part of the spectrum is the cell structure. Typically, between 40 and 50% of the incoming radiation is reflected, but it can vary depending on the cellular arrangements within the leaf that determine internal scattering (Govender et al., 2007). Dicots generally have a dorsiventral leaf structure with a lot of air and asymmetric structures which causes scattering inside the leaf while monocots have a more compact leaf structure that allows less scattering and thus more absorption and less reflectance (Jones & Vaughan, 2010). Also, sun leaves and older leaves generally have a less compact structure and can therefore be distinguished from shadow leaves and younger leaves based on NIR reflectance data. The sharp increase between the red waveband and the NIR plateau is called the red edge and can be used as a proxy for plant stress (Huete, 2004).

Three water absorption bands can be found in the SWIR around 1450 nm, 1950 nm and 2500 nm (Jones & Vaughan, 2010). When a leaf is under water stress less radiation will be absorbed in these bands and thus more light is reflected. The lignin and cellulose content are two other main factors influencing the reflectance in the SWIR region. In the TIR part of the spectrum, vegetation reflectance is too low to

measure with remote sensing applications (Zhu et al., 2018). However, the emissivity in these wavelengths is high when vegetation wants to get rid of excess energy. It is related to the leaf temperature and transpiration and can therefore be linked to changes in plant metabolism (Jones & Vaughan, 2010).

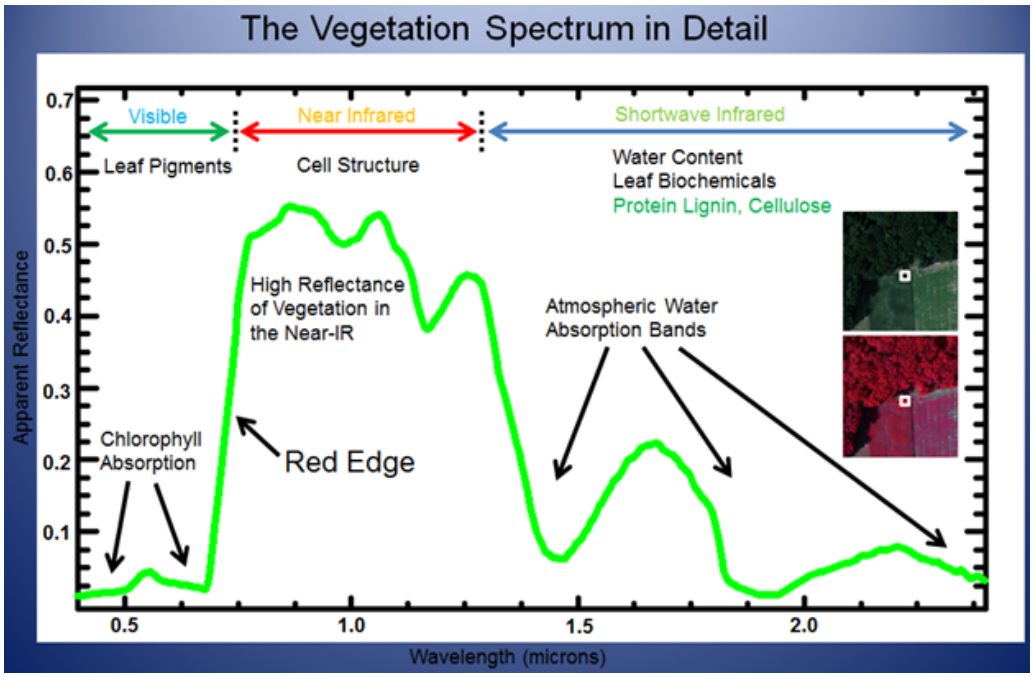

Figure 1-7 Typical spectral reflectance signature of healthy green vegetation (copied from Kirkaya, 2020).

This typical spectral reflectance signature is solely determined by the radiative characteristics of individual leaf components. It is the result of single-leaf measurements with a spectroradiometer that uses a perpendicular incoming light beam. However, the reflectance data collected with a UAS is the result of the interaction between incoming radiation and the entire vegetation canopy rather than single leaves (Pajares, 2015). Overall, the reflectance is lower than of a single leaf measurement because of variations in leaf orientation, illumination angle, and shadow. A part of the reflected signal is also attenuated due to interaction with the soil or other non-foliage background surfaces (Jones & Vaughan, 2010). The latter is less pronounced when using UAS compared to for example satellites because there are no mixed pixels in cm-resolution images. On the other hand, volume scattering, being the scattering caused by transmission and reflection across the multiple leaf layers in the canopy, can compensate for that reduction in reflectance. In canopies with a high LAI, more volume scattering will take place resulting in higher reflectance, mainly in NIR, compared to canopies with a low LAI.

Translation to Biodiversity Measures

With passive sensors on board a UAS, a stack of images is created for every pixel with every image representing another waveband (Shaw & Burke, 2003). That results in a 3D data cube, with two spatial dimensions (x and y) and one spectral dimension (z), which contains the different spectral channels. There are different approaches to translate this spectral data cube in information for assessing biodiversity.

A simple, widely-used method to distinguish vegetation is calculating spectral indices from certain bands of the spectral signature. One of the most known ratios is the normalized difference vegetation index (NDVI). A band in the near-infrared part of the spectrum is compared with a band in the red part of the spectrum by taking the normalized difference as the name suggests (Zhu et al., 2018):

$$NDVI = \frac{NIR-RED}{NIR+RED} \quad (1.1)$$

As discussed in the previous section, plants subjected to stress show a higher reflectance in the red waveband and a lower reflectance in the NIR part of the spectrum, resulting in a smaller normalised difference. Studies show that this ratio is indeed correlated with the amount of physiological stress, but also with the amount of vegetation cover, the plant condition, and the photosynthetic activity (Dash et al., 2018). Therefore, variation in NDVI can be used as a proxy for species richness (Peng et al., 2019). Other commonly-used indices to distinguish different vegetation types that simultaneously correct for soil background are the soil-adjusted vegetation index, and the modified soil-adjusted vegetation index (Govender et al., 2007).

The spectral variation hypothesis (SVH) suggests that high biodiversity may show high spectral heterogeneity and low biodiversity low spectral heterogeneity (Rocchini et al., 2007). Therefore, the calculation of spectral heterogeneity captured by UAS throughout a study area may be used as a proxy for the functional diversity or species diversity (Peng et al., 2019). The standard deviation (sd) or another measure to capture the variance can be calculated for single, multiple or combination of bands and then be linked with the species richness. The variance metrics show a positive correlation with the species diversity according to the SVH. However, an important condition is that the grain size of the studied ecosystem matches the spatial resolution of the RS-data. When collecting for example high spatial resolution data of plant individuals that

are larger than the pixel size, an object-based classification needs to be done before applying the SVH. Otherwise, the spectral variation inside one object will also be considered as species diversity. Furthermore, all the pixels that add additional unwanted variation, such as roads, need to be masked out. In some studies or study areas, no evidence is found confirming the SVH, often because of not applying one of these conditions (Gholizadeh et al., 2020; Möckel et al., 2016; Peng et al., 2019). Hyperspectral data seems to be better for linking spectral heterogeneity with species richness compared to multispectral data because the right selection of bands is very crucial (Rocchini et al., 2007).

Most forest biodiversity studies using UAS-collected multispectral data, indirectly estimate biodiversity through species classification rather than directly determining a measure of biodiversity (Franklin & Ahmed, 2018; Peng et al., 2021; Xu et al., 2020). This method requires knowledge about the spectral signature of the different species present in the study area but has an overall high accuracy. Segmentation of deciduous tree species is found more difficult than conifer tree species, generally resulting in a lower classification accuracy (Franklin & Ahmed, 2018). Several studies indicate that adding a structural component significantly improves the accuracy of classification (Gini et al., 2018; Peng et al., 2021). UAS-derived photogrammetric products can be used in that regard as alternative for expensive LiDAR surveys (González-Jaramillo et al., 2019).

The direct method of using spectral heterogeneity as proxy of species diversity, is mostly tested with satellite imagery for forest ecosystems (Gholizadeh et al., 2020). Generally, low but significant determination coefficients are found using simple univariate models to link spectral heterogeneity with local species richness (Peng et al., 2019; Rocchini et al., 2018). Some studies document that the success of the SVH might be season dependent and strongly is affected by the choice of spectral heterogeneity measures (Madonsela et al., 2021). Overall, no consistent success of using specific vegetation or spectral heterogeneity indices to predict species richness is achieved. Only a limited amount of studies have assessed the possibility of UAS, or remote sensing in general, to monitor forest biodiversity over time (Gholizadeh et al., 2020). Another bottleneck nowadays in forest remote sensing is model transferability. Most of the UAS-based models are region and vegetation specific whereby it is not yet

possible to apply them to other study areas or make useful comparisons (Peng et al., 2019; Toivonen et al., 2021).

To conclude, the development of methods for estimating functional and species diversity based on fine-scaled UAS data has still a big growth potential. A lot of different spectral indices have been developed and evaluated to predict plant alpha-diversity. However, because of the large variability in RS platforms, sensors and vegetation types, consensus about an optimal spectral index that directly relates species diversity with spectral data is yet to be found.

1.3 Research Goals

Biodiversity loss is one of the most pressing global problems nowadays. Hand in hand with species, a lot of ecosystem functions and services are diminishing. To be able to take conservation and restoration actions, capturing accurate data frequently throughout time is needed. UAS imagery with high spectral, spatial, and temporal resolution could be crucial means to do so.

Given the potential of using multispectral drone data, drone flight missions were conducted at the different sites of the FORBIO tree experiment to assess the effectiveness in predicting tree species diversity and productivity. We extracted both spectral and plant height data from the UAS imagery and used it to build models to predict tree species richness on the one hand and tree species productivity on the other hand by combining the multispectral data with ground truth data. We also documented a pipeline of the steps of collecting, processing and analysing drone data that can be used as manual for future research using drones. In this thesis, the following more specific research questions will be answered:

- Is it possible to predict species identity, composition and/or richness based on multispectral drone data?
- Which bands or band combinations are most suitable to do so?
- Will adding a structural vegetation component, i.e. plant height, increase the accuracy?
- Can the productivity be modelled based on multispectral drone data?
- Is the biodiversity-productivity hypothesis valid?
- How can the process of collecting drone data be optimized?

2 Materials and Methods

2.1 Study Sites

The study was performed in the three sites of the FORBIO (FORest BIOdiversity and Ecosystem Functioning) experiment distributed across Belgium: Hechtel-Eksel, Zedelgem and Gedinne (Figure 2-1). Between 2009 and 2012 the FORBIO experiment was established to assess the effect of tree species diversity on forest biodiversity and ecosystem functioning. This long-term tree experiment is part of the largest worldwide network of biodiversity experiments TreeDivNet (Verheyen et al., 2013). Each FORBIO site is subdivided into different plots where trees are planted in monocultures or mixtures with two to four species (Figure 2-1). Because the abiotic conditions are constant at a site while the species diversity differs between the plots, forest biodiversity dynamics can easily be evaluated. Although the experimental design is similar for each site, the soil and climatological characteristics differ.

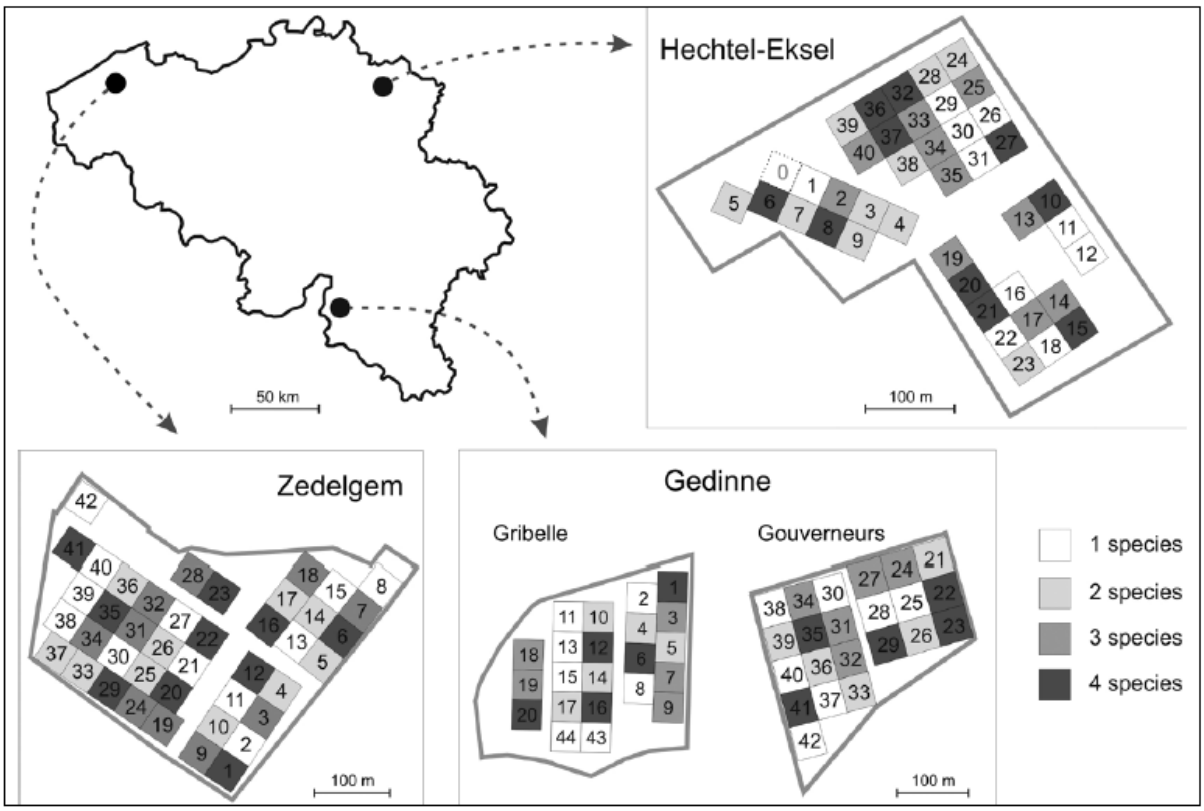

Figure 2-1 The three FORBIO sites situated on the map of Belgium together with their experimental designs. The colour of each plot indicates the number of species planted in mixture or monoculture (copied from Verheyen et al., 2013).

2.1.1 Hechtel-Eksel

The Hechtel-Eksel site is approximately 8 ha in size and located in the Campine ecoregion on a dry sandy soil (51°10'N 5°19'E, 55-56 m a.s.l.). The region has a mean annual temperature (MAT) of 9.0°C and a mean annual precipitation (MAP) of 799 mm. In late autumn of 2012, in total 23,040 trees were planted in 40 different plots, each with a plot size of 36 m x 36 m. As at each site, the trees were planted on a 1.5 m x 1.5 m grid, resulting here in a density of 576 trees per plot. Plot 0 was left unplanted for spontaneous succession. In the mixed plots, trees of the same species were planted in small patches of 3 x 3 trees, except sometimes at the edges where larger cells were used (Figure 2-2). In plots with three or four species, these 3 x 3 cells were randomly arranged and in plots with two species a checkerboard pattern was used (Verheyen et al., 2013). This design is found in all three sites. The following five different species were planted at the Hechtel-Eksel site: silver birch (*Betula pendula* Roth.), Japanese larch (*Larix kaempferi* Sarg.), Scots pine (*Pinus sylvestris* L.), Douglas fir (*Pseudotsuga menziesii* (Mirb.) Franco) and sessile oak (*Quercus petraea* (Mattuschka) Liebl.). The planted trees originate from the nursery Opdebeeck, located in Putte (Verheyen et al., 2013).

Distance (m)		0.75	2.25	3.75	5.25	6.75	8.25	9.75	11.3	12.8	14.3	15.8	17.3	18.8	20.3	21.8	23.3	24.8	26.3	27.8	29.3	30.8	32.3	33.8	35.3	36.8	38.3	39.8	41.3
	X/Y	1	2	3	4	5	6	7	8	9	10	11	12	13	14	15	16	17	18	19	20	21	22	23	24	25	26	27	28
0.75	1	2353	2381	2409	2437	2465	2493	2521	2549	2577	2605	2633	2661	2689	2717	2745	2773	2801	2829	2857	2885	2913	2941	2969	2997	3025	3053	3081	3109
2.25	2	2354	2382	2410	2438	2466	2494	2522	2550	2578	2606	2634	2662	2690	2718	2746	2774	2802	2830	2858	2886	2914	2942	2970	2998	3026	3054	3082	3110
3.75	3	2355	2383	2411	2439	2467	2495	2523	2551	2579	2607	2635	2663	2691	2719	2747	2775	2803	2831	2859	2887	2915	2943	2971	2999	3027	3055	3083	3111
5.25	4	2356	2384	2412	2440	2468	2496	2524	2552	2580	2608	2636	2664	2692	2720	2748	2776	2804	2832	2860	2888	2916	2944	2972	3000	3028	3056	3084	3112
6.75	5	2357	2385	2413	2441	2469	2497	2525	2553	2581	2609	2637	2665	2693	2721	2749	2777	2805	2833	2861	2889	2917	2945	2973	3001	3029	3057	3085	3113
8.25	6	2358	2386	2414	2442	2470	2498	2526	2554	2582	2610	2638	2666	2694	2722	2750	2778	2806	2834	2862	2890	2918	2946	2974	3002	3030	3058	3086	3114
9.75	7	2359	2387	2415	2443	2471	2499	2527	2555	2583	2611	2639	2667	2695	2723	2751	2779	2807	2835	2863	2891	2919	2947	2975	3003	3031	3059	3087	3115
11.25	8	2360	2388	2416	2444	2472	2500	2528	2556	2584	2612	2640	2668	2696	2724	2752	2780	2808	2836	2864	2892	2920	2948	2976	3004	3032	3060	3088	3116
12.75	9	2361	2389	2417	2445	2473	2501	2529	2557	2585	2613	2641	2669	2697	2725	2753	2781	2809	2837	2865	2893	2921	2949	2977	3005	3033	3061	3089	3117
14.25	10	2362	2390	2418	2446	2474	2502	2530	2558	2586	2614	2642	2670	2698	2726	2754	2782	2810	2838	2866	2894	2922	2950	2978	3006	3034	3062	3090	3118
15.75	11	2363	2391	2419	2447	2475	2503	2531	2559	2587	2615	2643	2671	2699	2727	2755	2783	2811	2839	2867	2895	2923	2951	2979	3007	3035	3063	3091	3119
17.25	12	2364	2392	2420	2448	2476	2504	2532	2560	2588	2616	2644	2672	2700	2728	2756	2784	2812	2840	2868	2896	2924	2952	2980	3008	3036	3064	3092	3120
18.75	13	2365	2393	2421	2449	2477	2505	2533	2561	2589	2617	2645	2673	2701	2729	2757	2785	2813	2841	2869	2897	2925	2953	2981	3009	3037	3065	3093	3121
20.25	14	2366	2394	2422	2450	2478	2506	2534	2562	2590	2618	2646	2674	2702	2730	2758	2786	2814	2842	2870	2898	2926	2954	2982	3010	3038	3066	3094	3122
21.75	15	2367	2395	2423	2451	2479	2507	2535	2563	2591	2619	2647	2675	2703	2731	2759	2787	2815	2843	2871	2899	2927	2955	2983	3011	3039	3067	3095	3123
23.25	16	2368	2396	2424	2452	2480	2508	2536	2564	2592	2620	2648	2676	2704	2732	2760	2788	2816	2844	2872	2900	2928	2956	2984	3012	3040	3068	3096	3124
24.75	17	2369	2397	2425	2453	2481	2509	2537	2565	2593	2621	2649	2677	2705	2733	2761	2789	2817	2845	2873	2901	2929	2957	2985	3013	3041	3069	3097	3125
26.25	18	2370	2398	2426	2454	2482	2510	2538	2566	2594	2622	2650	2678	2706	2734	2762	2790	2818	2846	2874	2902	2930	2958	2986	3014	3042	3070	3098	3126
27.75	19	2371	2399	2427	2455	2483	2511	2539	2567	2595	2623	2651	2679	2707	2735	2763	2791	2819	2847	2875	2903	2931	2959	2987	3015	3043	3071	3099	3127
29.25	20	2372	2400	2428	2456	2484	2512	2540	2568	2596	2624	2652	2680	2708	2736	2764	2792	2820	2848	2876	2904	2932	2960	2988	3016	3044	3072	3100	3128
30.75	21	2373	2401	2429	2457	2485	2513	2541	2569	2597	2625	2653	2681	2709	2737	2765	2793	2821	2849	2877	2905	2933	2961	2989	3017	3045	3073	3101	3129
32.25	22	2374	2402	2430	2458	2486	2514	2542	2570	2598	2626	2654	2682	2710	2738	2766	2794	2822	2850	2878	2906	2934	2962	2990	3018	3046	3074	3102	3130
33.75	23	2375	2403	2431	2459	2487	2515	2543	2571	2599	2627	2655	2683	2711	2739	2767	2795	2823	2851	2879	2907	2935	2963	2991	3019	3047	3075	3103	3131
35.25	24	2376	2404	2432	2460	2488	2516	2544	2572	2600	2628	2656	2684	2712	2740	2768	2796	2824	2852	2880	2908	2936	2964	2992	3020	3048	3076	3104	3132
36.75	25	2377	2405	2433	2461	2489	2517	2545	2573	2601	2629	2657	2685	2713	2741	2769	2797	2825	2853	2881	2909	2937	2965	2993	3021	3049	3077	3105	3133
38.25	26	2378	2406	2434	2462	2490	2518	2546	2574	2602	2630	2658	2686	2714	2742	2770	2798	2826	2854	2882	2910	2938	2966	2994	3022	3050	3078	3106	3134
39.75	27	2379	2407	2435	2463	2491	2519	2547	2575	2603	2631	2659	2687	2715	2743	2771	2799	2827	2855	2883	2911	2939	2967	2995	3023	3051	3079	3107	3135
41.25	28	2380	2408	2436	2464	2492	2520	2548	2576	2604	2632	2660	2688	2716	2744	2772	2800	2828	2856	2884	2912	2940	2968	2996	3024	3052	3080	3108	3136

Figure 2-2 Experimental planting design of a two-species mixture plot (no. 4 in Zedelgem). Each tree is represented by a number and the colours indicate the species: silver birch (yellow) and Scots pine (pink)

2.1.2 Zedelgem

The Zedelgem site is situated closer to the North Sea in the Cuesta ecoregion on a sandy to loamy sand soil (51°9'N 3°7'E, 11-16 m a.s.l.). The climate in Zedelgem is a bit milder with lower temperatures in the summer and higher temperatures in the winter (MAT = 9.5°C, MAP = 687 mm). This site, established on former agricultural land in the winter of 2009-2010, is approximately 9.5 ha large. At each of the 42 m × 42 m plots, 784 trees were planted, resulting in a total of 32,810 trees divided over the 42 plots. Again, five different species were used in mixture or monoculture: silver birch, common beech (*Fagus sylvatica* L.), Scots pine, pedunculate oak (*Quercus robur* L.) and small-leaved lime (*Tilia cordata* Mill.). In half of the plots the same provenance, i.e. Vekedelle West, of pedunculate oak was planted. In plots with numbers 21 to 42, a mixture of three different provenances was used. This was done to be able to evaluate the effect of genetic diversity on forest biodiversity and ecosystem functioning (Verheyen et al., 2013).

2.1.3 Gedinne

The Gedinne site is situated in the Ardennes ecoregion in the southern part of Belgium and divided into two subsites: Gribelle (49°60'N 4°59'E, 367-376 m a.s.l.) and Gouverneurs (49°59'N 4°59'E, 421-426 m a.s.l.). Both the subsites are about 4.5 ha in size and have a moderately dry loam soil. Compared to the other two sites, the climate is colder and wetter (MAT = 6.9°C, MAP = 1021 mm). In early spring of 2010, in total 44 plots were planted at the Gedinne site, 22 at each subsite. Most of the plots have a size of 42 m x 42 m, except for thirteen plots that measure 42 m x 37.5 m, with 700 trees per plot. Following tree species were planted, again in mixture or monoculture: sycamore maple (*Acer pseudoplatanus* L.), common beech, sessile oak, hybrid larch (*Larix x eurolepis* Henry), and Douglas fir. Similar to the Zedelgem site, at half of the plots, three different provenances of common beech were used to assess the genetic diversity (Verheyen et al., 2013).

2.2 Field Data

In this study, no field data was collected, because the planting data were considered as ground truth data and were readily available. For each site, the number of species, the number of trees per species and the total number of trees planted were available per plot. The delineation of the plots in the coordinate reference system (CRS) Belgian Lambert 72 (EPSG:31370) was also available for each site.

2.3 Multispectral Data

2.3.1 Drone and Camera Characteristics

The drone used to perform the flights is a DJI Matrice 210 RTK V2 (Figure 2-3). The drone weighs approximately 4.91 kg, batteries included, and has unfolded the following dimensions: 883 mm x 886 mm x 398 mm (DJI, 2019). It is a multi-rotor drone with four propellers attached to independently driven motors. By changing the speed of different propellers, it can easily turn around its roll, yaw and pitch axis. The two D-RTK antennas allow for more accurate positioning data and ensure a more stable flight because it interferes less with metal objects (DJI, 2019). Through this D-RTK module, a connection can be made with a ground station or an RTK network. The M210 RTK V2 has an advanced power management and is powered by two TB55 Intelligent Flight batteries with a voltage of 22.8 V and a capacity of 7,660 mAh each. With fully charged batteries and no payload, the drone has a maximum flight time of 33 minutes. To fly the drone, the remote controller with a CrystalSky Monitor attached was used (DJI, 2019).

To ensure safety, the M210 RTK V2 contains a built-in DJI AirSense that automatically gives an alert of aircraft nearby on the CrystalSky Monitor. Also, when the drone loses connection with the remote controller or the battery is low, it will automatically return to the last recorded Home Point and trigger the landing protection. The landing protection will check if the ground is suitable for landing and the pilot can still alter the orientation with the remote controller to ensure a perfect landing (DJI, 2019).

1. D-RTK antennas
2. Propellers
3. DLS 2
4. Batteries
5. MicaSense Altum sensor
6. Landing gears

Figure 2-3 Image of used DJI Matrice 210 RTK V2 drone equipped with the Micasense Altum sensor (Van den Boer, M., 2021).

A Micasense Altum sensor was attached to the M210 RTK V2 (Figure 2-3). This is a multispectral sensor that captures six different bands (red, green, blue, red edge, near-infrared and thermal) with a high spatial resolution (Figure 2-4). The sensor stores files for each band in a 16-bit TIFF with a resolution of 2064 x 1544 pixels except for the thermal band which has a lower resolution of 160 x 120 pixels (Micasense Inc., 2021). At a flying height of 120 m, the GSD of the thermal band and the five other bands are respectively 5.82 cm and 81 cm. The Micasense Altum sensor is also integrated with a Downwelling Light Sensor 2 (DLS 2) on top of the drone (Figure 2-3). This sensor stores information about the ambient light and sun angle during the flight in the metadata of the image files (Micasense Inc., 2020). That information can be used during processing to correct for changing light conditions as discussed in section 1.2.2.

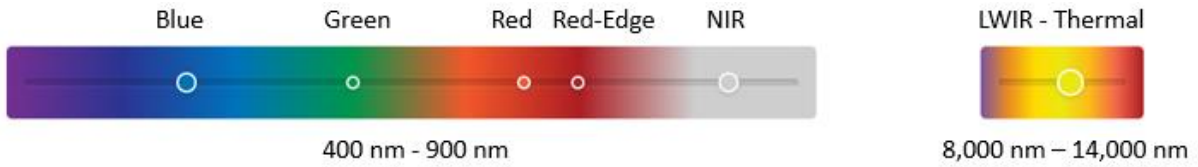

Figure 2-4 The six different bands captured by a Micasense Altum sensor: blue, green, red, red-edge, NIR and thermal (modified from AgEagle Sensor Systems Inc., 2021).

2.3.2 Data Collection

Following sections primarily describe the steps of collecting, processing and analysing drone data during this research. However, it is also intended as a manual that can be used for future research.

Pre-flight Activities

Flying a drone is subject to legal regulations. To be allowed to operate as a pilot in the subcategories OPEN A1 and A3, which cover the conditions of this study, I followed an online training continued by an exam provided by the Belgian Civil Aviation Authority in cooperation with EASA (Figure 2-5). To get the certificate, good knowledge about air traffic safety, restrictions and regulations, limitations to human performances, general knowledge of UAS, privacy, insurance and security is required.

Figure 2-5 Pilot certificate of subcategories OPEN A1 and A3.

Next to the regulations, various other restrictions can apply. The Skeyes drone guide (https://map.droneguide.be) was consulted to plan the flight mission dates and times for each site based on the UAS geographical zone statuses. When certain geo zones are active, it can impose a restriction on the flying height and/or time. For most geo zones this is announced well upfront, but for Helicopter Training Areas (HTA) the activation is only communicated one day in advance. The Hechtel-Eksel site is situated near the military basis of Kleine-Brogel, whereby during the day you cannot fly with a UAS because it is inside the controlled airspace area (Figure 2-6). For these flights (performed after the operational hours), the military basis was informed well in advance. In Zedelgem, an HTA was active on the day of the flight mission (Table 2-1).

Figure 2-6 Location of the Hechtel-Eksel FORBIO site inside the Kleine-Brogel controlled airspace area (blue contour). This is an active geozone (EBBL_Kleine-Brogel CTR) where no drone flights can be executed during the day (copied from Skeyes, 2021).

Table 2-1 Duration of the active geo zones at the day of the flight missions at each FORBIO site (only the ones applicable to drone flights, that have a relatively low flight height < 60 m).

Site	Date	Active geo zone	Duration
Hechtel-Eksel	20/07/2021	EBBL_Kleine-Brogel CTR	06:30 – 17:30
Zedelgem	25/08/2021	HTA10A	09:00 – 12:30
		HTA10A	13:30 – 16:00
Gedinne	26/08/2021	/	/

Besides checking the local flying restrictions, weather forecasts were also consulted to plan the flight missions. Rain and/or strong winds make missions dangerous because of unclear vision or abrupt changes in the flying path. Additionally, the drone and sensor equipment cannot withstand such harsh conditions. The UAV forecast app was used to check the weather conditions the day of the mission and again right before take-off.

Landowners of each site were asked for permission and they were informed at what exact time the drone flights would take place. Lastly, the details of the mission and the licenced pilots that would execute them were registered in the Drone Service

Application (DSA) Planner provided by Skeyes. Skeyes needs to approve the mission in advance. On the day of the flight, you need to inform them once more via DSA Fly when the drone is in the air, when it is landed and when the drone operation is finished. In that way, they can alert you by phone if you must land immediately due to certain unforeseen circumstances e.g. an aircraft in distress.

Flight planning and execution

The flights were executed on three different days in the summer of 2021 (Table 2-2).

Table 2-2 Data and time of each flight mission in the different FORBIO sites.

Site	Subsite	Date	Start time
Hechtel-Eksel		20/07/2021	17:30
Zedelgem		25/08/2021	12:30
Gedinne	Gribelle	26/08/2021	10:30
	Gouverneurs	26/08/2021	12:50

First, different flight missions were configured in the DJI Pilot app (Figure 2-7). This allows the drone to fly autonomously and you can apply the same settings (e.g. flight altitude, % overlap between the images…) for every flight, resulting in better and more consistent data. A polygon of the preferred flight area was drawn by visually marking the border points of the plots on a satellite base map. To limit the flying time and avoid crossing walking paths, the plots were subdivided into blocks for different flight missions (Figure 2-8). Respectively four, five, three and two flight missions were made for the sites in Hechtel-Eksel, Zedelgem, Gribelle and Gouverneurs. In Hechtel-Eksel, plots 24, 28, 32, 36 and 39 were not included in the flight mission plans because the flight would take too long. Plot 8 at the Zedelgem site was not included because of its proximity to a power line.

Figure 2-7 Start screen at DJI Pilot App with two different options: manual flight or mission flight (copied from DJI, 2019).

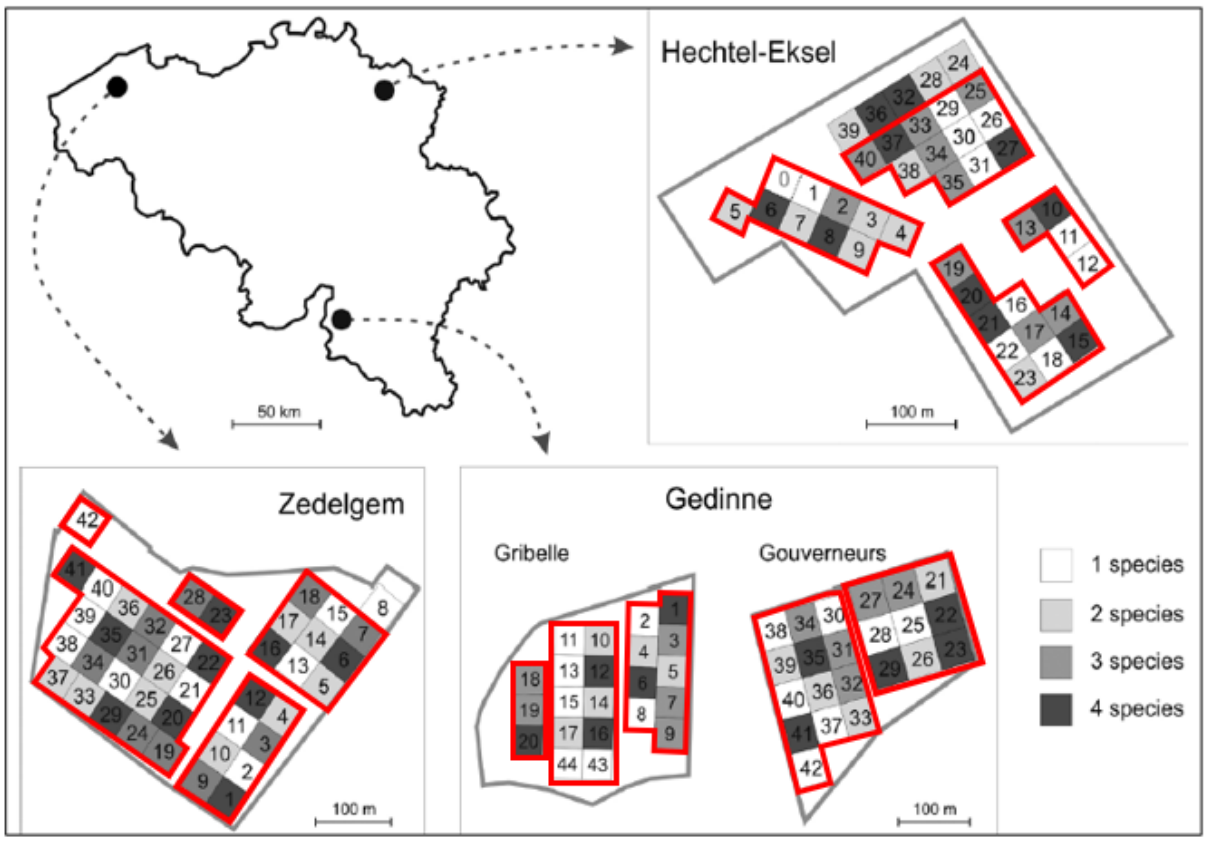

Figure 2-8 The three FORBIO sites situated on the map of Belgium together with their experimental designs. The colour of each plot indicates the number of species planted in mixture or monoculture. The red contours indicate the different flight missions (modified from Verheyen et al., 2013).

For every flight mission, the flight height was set at 40 m above ground level and the front and side overlap both at 75% (Figure 2-9). The MicaSense Altum camera was selected and the photo mode was set at ‘distance interval shot’ in order to have consistently a photo taken at the same distance.

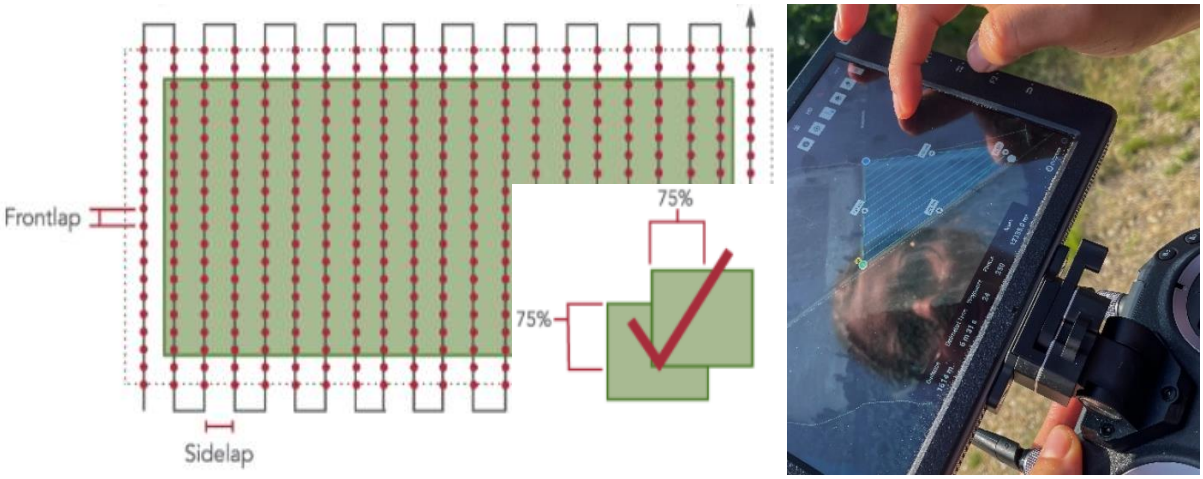

Figure 2-9 Visualisation of front and side overlap of 75% in a flight mission plan: left theoretical, right on the field (AgEagle Sensor Systems Inc., 2021; Van den Boer, M., 2021).

After the flight missions were made and saved, a proper take-off/landing point was chosen. It needs to be a flat surface, clear of objects where a good view over the flight path is ensured (Figure 2-10). Next, the drone compass was calibrated by turning the drone around all its six axes as indicated on the Aircraft Status Bar in the DJI Pilot app. At the sites in Flanders (Hechtel-Eksel and Zedelgem) connection was made with the mobile RTK-network FLEPOS and at the Gedinne site with the mobile RTK-network Walcors. By connecting via the DJI Pilot app to these networks, more accurate positioning is established, which will ensure a more stable flight.

Figure 2-10 Photo of the take-off/landing point at the Hechtel-Eksel FORBIO site (Van den Boer, M., 2021).

Then it was checked if the drone was fully equipped and ready to take off:

- Sufficient battery level of the remote controller, Intelligent Flight Batteries and display device depending on flight time
- D-RTK antennas locked properly
- Propellors having free rotation
- MicaSense Altum sensor
    - Protective cover removed
    - MicroSD card inserted
    - Connected with DLS 2
- DJI Pilot app having a connection with the drone

Lastly, right before and after every flight, a reflection calibration was executed. This was done by capturing an image of the Calibrated Reflectance Panel (CRP) by holding the drone about 1 m above it while making sure it is not covered by any shadow of a person or object nearby (Figure 2-11). In the case that no DLS 2 is connected to the drone's camera, these images can be used during processing to correct for the incident light conditions at the time of the flight. However, this radiometric correction assumes a rather constant reflectance during the flight because no real-time atmospheric conditions are measured. Therefore, it is less accurate than the DLS 2 where the images of the CRP are used to calibrate the DLS 2. Integrating CRP and DLS 2 significantly improves the radiometric correction for changing atmospheric conditions (C. Wang, 2021).

Figure 2-11 Calibrated Reflectance Panel to correct for incident light conditions at the time of the flight mission (copied from AgEagle Sensor Systems Inc., 2021)

During the flight, it was important to make sure the drone was always in the visible line of sight (VLOS) of the pilot. If not, when the drone was beyond the visible line of sight (BVLOS), the pilot was always in contact with someone that had the drone in VLOS.

This is needed to make sure the pilot can take over the drone at any time. Because of the same reason, the operating pilot could not be disturbed during the flight by passers-by. Therefore, a fluorescent vest with the inscription ‘Pilot DO NOT DISTURB’ was worn during the flights (Figure 2-12).

Figure 2-12 Photo of drone pilot with fluorescent vest with the inscription ‘Pilot DO NOT DISTURB’ (Van den Boer, M., 2021).

After the flight, the reflection calibration was executed again as explained before and - when necessary - Skeyes was informed via the DSA Fly that we landed again. After inspection, the drone was folded and stored. The data was uploaded immediately via the microSD card to an external disk. At home, all the batteries were recharged to be fully operational for the next flight.

2.4 Preprocessing

2.4.1 Preprocessing using MAPEO

First, multiple flights were pre-processed with PIX4Dmapper. However, this photogrammetry software had difficulties processing the large datasets on computers with limiting computing power, resulting in calibration problems and poor imaging. The key point image scale, the number of key points and the calibration method were adapted trying to improve the processing, but it did not result in the desired quality.

Therefore, the MAPEO services of VITO were used for the image pre-processing. Each flight mission is processed separately in MAPEO Field Software 1.0.5 using the following steps. To upload a new mission, first, the right mission profile ‘Micasense Altum’ was selected out of a list with different pre-programmed sensors (Figure 2-13). For the data quality check later, the default settings were used. If the used sensor is not present in the dropdown menu, the characteristics can be added manually.

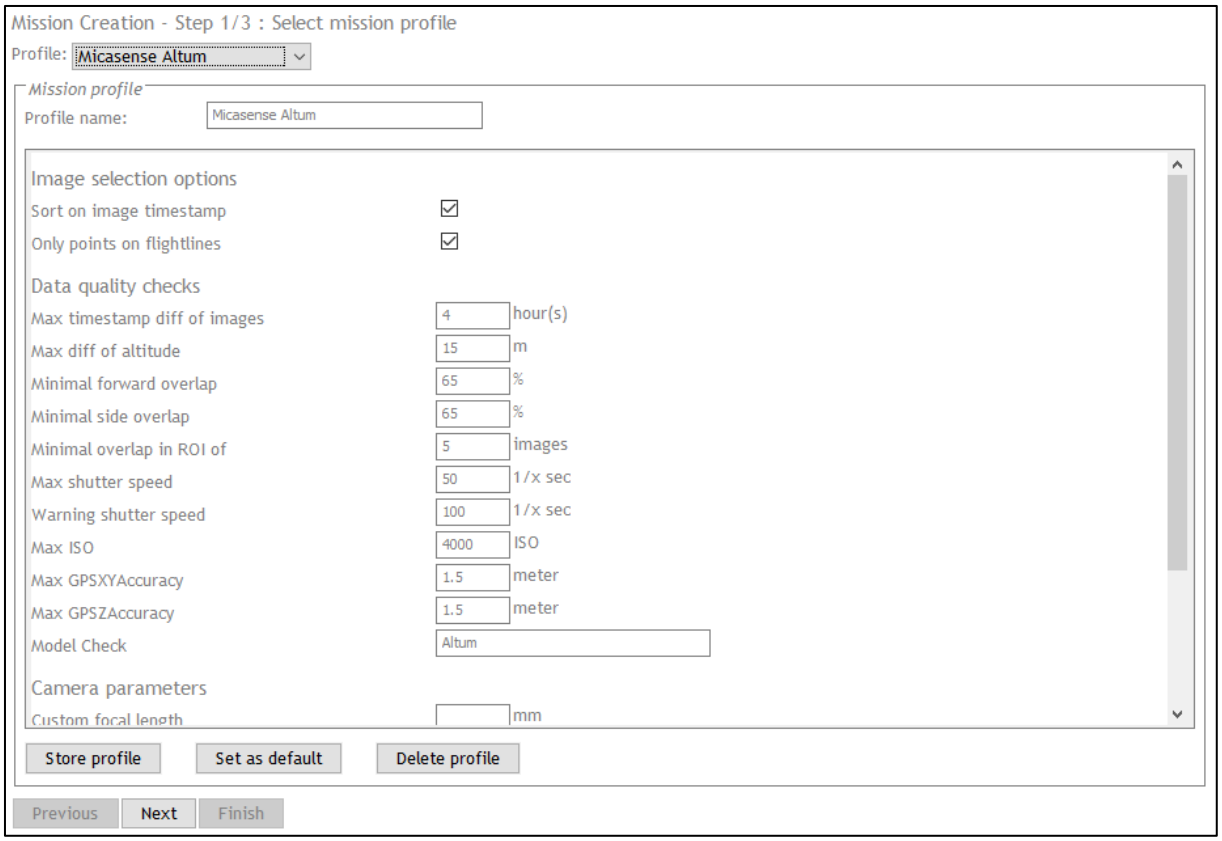

Figure 2-13 First step of mission creation to pre-process drone data with MAPEO Field Software. A mission profile can be selected out of a dropdown menu or can be manually added.

Next, the mission data was uploaded (Figure 2-14). This includes a folder with all the images of the mission, together with the before and after flight images of the Calibrated Reflectance Panel, and a kml-file of the region of interest (ROI). Then, the first and last images of the flight path were selected on the map and the flight height was set at 40 m. As result, the flight lines were drawn automatically (Figure 2-15). The next step was validating the overlap of the images inside the ROI: the bluer the colour, the better the result (Figure 2-15). In this step, ground control points (GCP) could be added if measured in the field, which was not the case in this research. As the last step of the mission creation, the flight description was added (Figure 2-16). Only the mission's name needed to be filled in because the other fields were pre-filled automatically since we used a pre-programmed sensor.

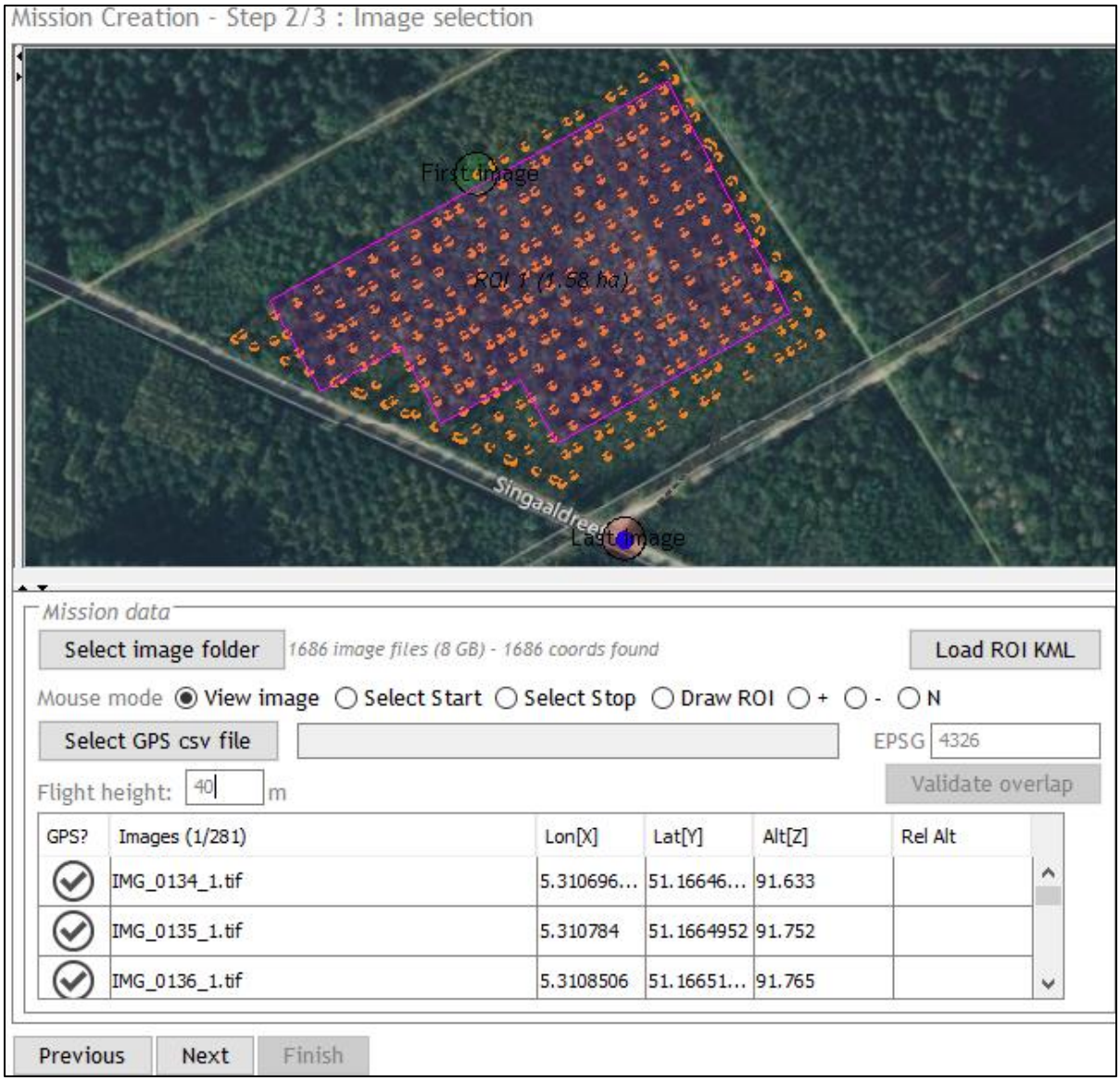

Figure 2-14 Second step of mission creation to pre-process drone data with MAPEO Field Software. Drone images can be uploaded by 'select image folder' and the right flight height needs to be given.

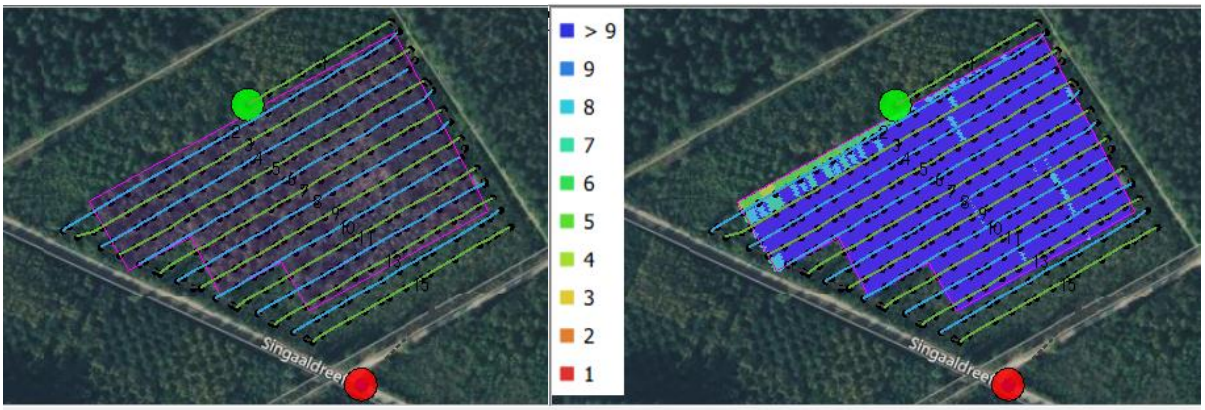

Figure 2-15 Second step of mission creation to pre-process drone data with MAPEO Field Software. The first and last images need to be selected whereby the flight lines are drawn automatically (left). By validating overlap inside the region of interest, an overview of the overlap quality is given in a colour scale (right): the bluer, the better.

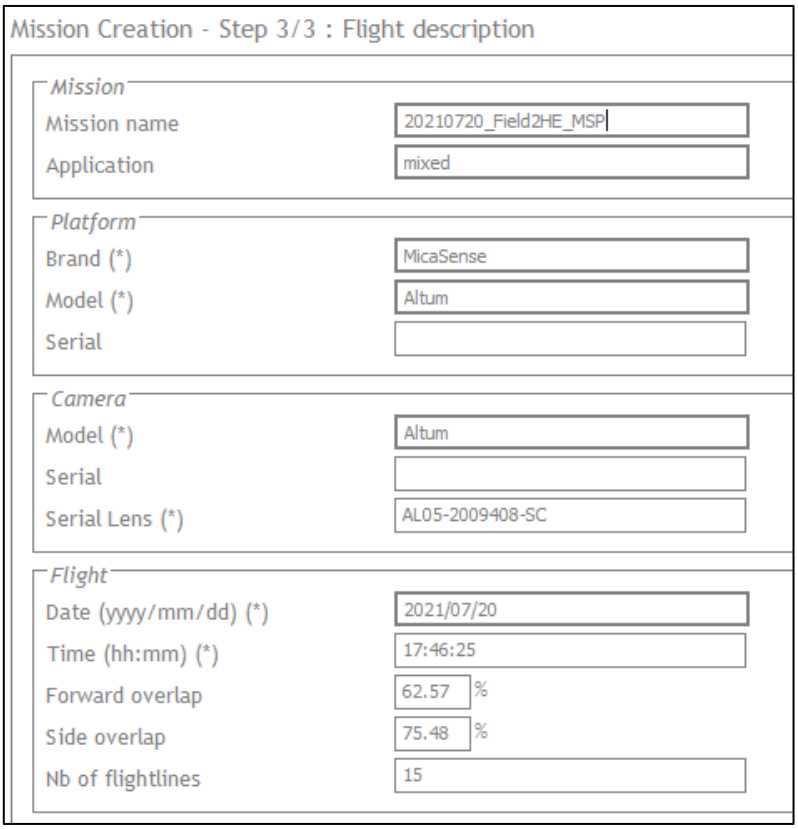

Figure 2-16 Third and last step of mission creation to pre-process drone data with MAPEO Field Software. In this step the flight description needs to be given. When a pre-programmed sensor is used only the mission name should be filled in.

Before uploading the mission for pre-processing, the quality checks were consulted (Figure 2-17). At this point, input data could be adapted to improve the quality depending on the type of error. In this research, no improvements were possible with the available data. However, if for example some images do not have valid coordinates, these images could be removed to improve the processing quality. Next, the data was uploaded for standardized photogrammetric and radiometric processing. As output, a multiband raster image, a digital terrain model (DTM), a digital surface model (DSM) and an NDVI raster image were created per flight mission.

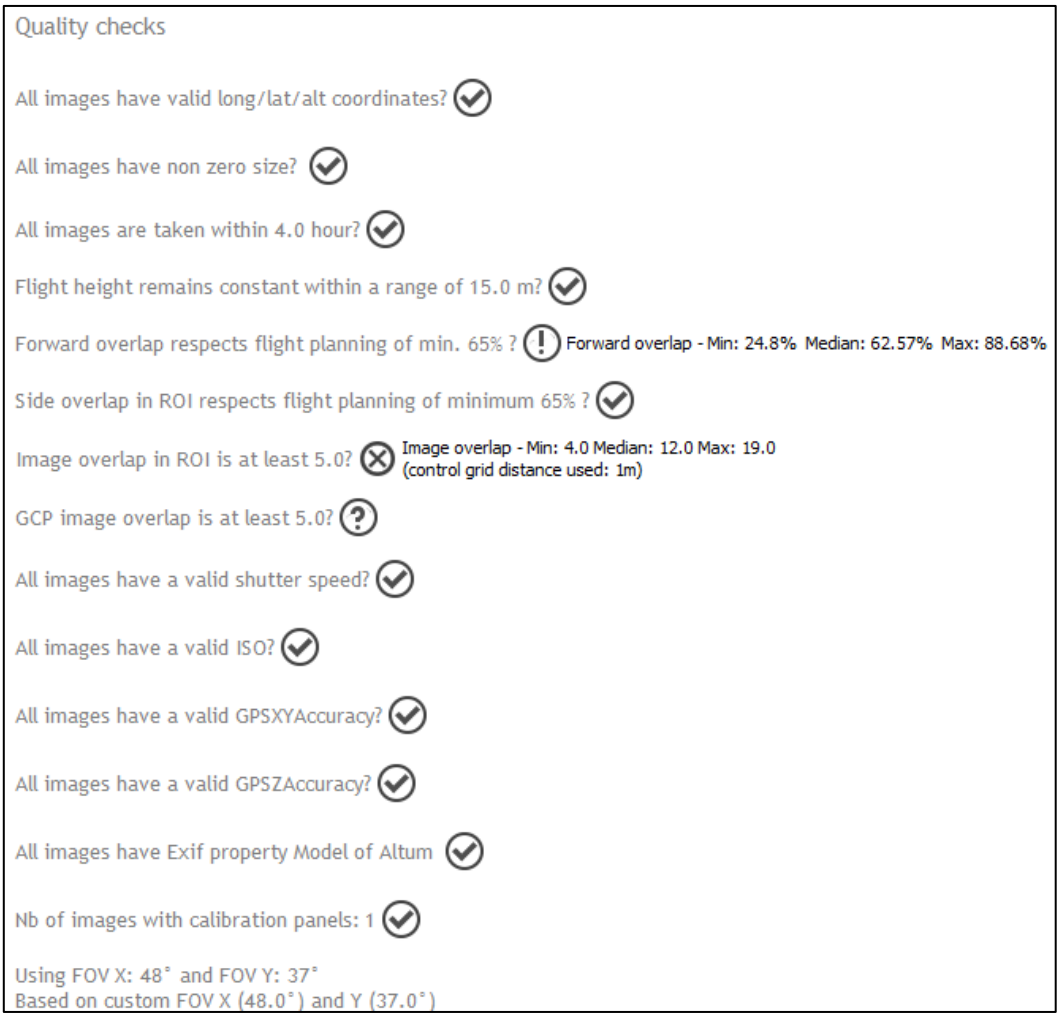

Figure 2-17 Quality check step to pre-process drone data with MAPEO Field Software. A check mark indicates that the quality is good, an exclamation marks points out there might be a problem and a cross mark shows that there is a problem.

2.4.2 Preprocessing Raster Data per Plot

All analyses were performed using R version 4.2.1 (R Core Team, 2022). A schematic overview of the steps to extract the raster data per plot is given in Figure 2-18 and explained here in more detail. First, the perimeter of each site (shapefile) was imported and transformed from Belgian Lambert 72 (EPSG:31370) to World Geodetic System 1984 (WGS 84) with the sf package (Pebesma, 2018). Using the same package, the plot sizes were reduced by 4 m at each side to minimize edge effects and correct slight positioning errors in the drone data. For example, a plot size of 42 m x 42 m was reduced to 34 m x 34 m. Before further processing, the data was reviewed by removing some plots. The data of plots 5 and 9 in Hechtel-Eksel and plot 21 in Gouverneurs were not used because after MAPEO pre-processing, in more than half of these plot sizes data was missing due to some malfunctioning during data capturing or processing.

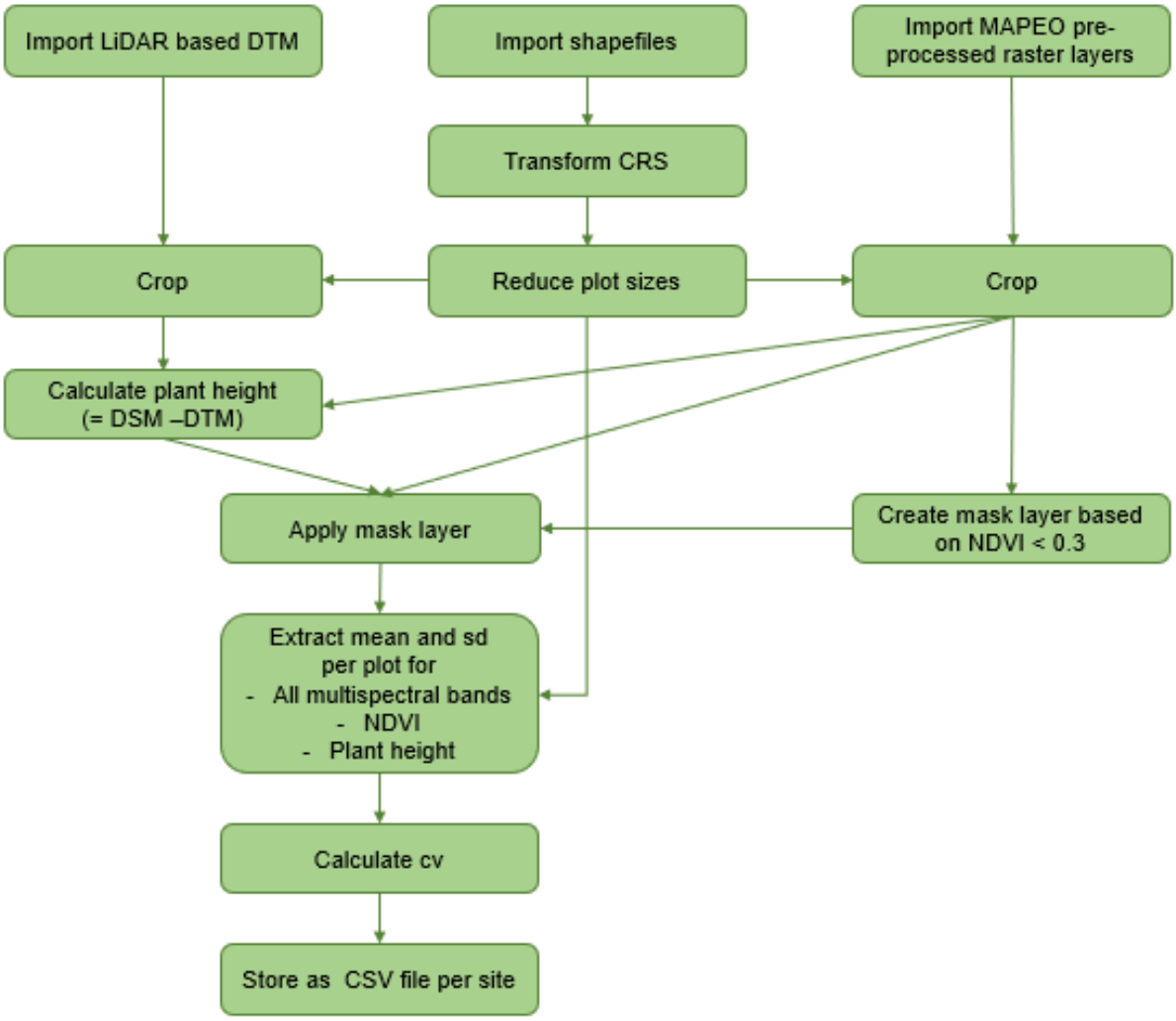

Figure 2-18 Schematic overview of the steps followed to extract the mean, standard deviation (SD) and correlation of variation (CV) of the different raster layers per plot in each FORBIO site.

Next, DTMs of Flanders and Wallonia were requested and downloaded (Agentschap Digitaal Vlaanderen, 2014; Service public de Wallonie, 2014). Both these DTMs are a result of LiDAR data acquisitions from a period between 2013 and 2014. The ground resolution of both datasets is 1 m and their CRS is Belgian Lambert 72 (EPSG:31370). These data were used instead of the DTM results from the MAPEO processing because they have higher accuracy.

All following steps were applied to the data of each flight mission separately. The MAPEO pre-processed raster layers (multiband rasters, NDVI rasters, DSM rasters) and the DTM rasters of Flanders and Wallonia were imported in R using the raster package (Hijmans, 2022a). Then they were cropped to the extent of the corresponding site. With the dplyr package, the plots reduced in size were masked out the resulting raster datasets to only keep information from inside the plots (Wickham et al., 2022).

Based on the NDVI, a mask layer was created to mask out pixels with no vegetation or dead vegetation inside the plots. All pixels with an NDVI value larger than 0.3 were given the value one and the other pixels a value of zero. This boundary was chosen because healthy vegetation generally has an NDVI larger than 0.3 (Jones & Vaughan, 2010). The created mask layers were multiplied with all the other raster layers and then the zero values were replaced by NA-values. All resulting raster datasets were exported to TIFF files.

The next step was to extract a mean value and the standard deviation (sd) for each of the variables per plot. This was done by first importing the masked layers using the terra package (Hijmans, 2022b). With the exactextractr package, the mean and sd were extracted per plot per flight mission (Daniel Baston, 2022). Next, the correlation of variance (cv) was calculated per plot for all the reflectance bands, the NDVI and the plant height by dividing the sd by the mean.

2.5 Species Richness and Productivity Calculation

The alpha diversity in each plot was calculated based on the number of trees per species present in each plot. Examples of some popular indices to calculate alpha diversity are the Shannon index, Simpson index, species richness, and Rao quadratic entropy index (Leinster & Cobbold, 2012). However, effective numbers of species (ENS) are recently more used as a measure because they make diversity comparisons and percentage changes meaningful (Leinster & Cobbold, 2012). Therefore, this last index was calculated as measure of alpha diversity. As the evenness for all plots equals one, both $ENS_{Simpson}$ and $ENS_{Shannon}$ are equal to the species richness (SR). Therefore, I only consider SR in what follows.

To calculate the plant height, the DTM raster layers were subtracted from the DSM raster layers to generate a canopy height model. The plant height was corrected by lowering it by 39 m for all plots and sites. An error in the MAPEO pre-processed DSM was observed, which resulted in a plant height much higher than observed during the flights. The average drone-based calculated plant height per plot in Hechtel-Eksel was compared with the average in situ height measurements per plot in Hechtel-Eksel from 2019. This difference was assumed to be an approximation of the error and therefore subtracted from the plant height in each plot at the different sites. The cv was recalculated as well with the new mean plant height.

The mean plant height per plot was considered as proxy for forest productivity. Plant height is generally a good indicator of tree productivity in the first years, mainly in dense plantations, because height growth is still more prominent than diameter growth. The net diversity effect (NDE) in each mixture plot per site was calculated as well (Loreau M. & Hector. A., 2001). For this analysis the sites were evaluated separately, because of the different soil and climatological conditions. The mean plant height of every species in monoculture (PH_i) was extracted from the data. Then, the expected plant height (PH_{exp}) in a mixture was calculated based on the proportion of the different species (p_i) present in the plot using equation 2.1. Finally, to evaluate the overyielding, the NDE was calculated by comparing the expected plant height with the observed plant height (PH_O; equation 2.2; Van de Peer et al., 2018). A positive NDE will be obtained when high-productive species dominate in the mixed plots (positive selection) or when species perform better in mixture than in monoculture because of positive complementarity (Loreau M. & Hector. A., 2001).

$$PH_{exp} = \sum_i^N p_i \; x \; PH_i \qquad (2.1)$$

$$NDE = PH_O - \; PH_{exp} \qquad (2.2)$$

2.6 Data Analysis

Different models to predict the alpha diversity and the productivity were made and evaluated. To determine which variables should be used in the model to predict the SR and plant height, the correlation between all the different variables was evaluated (Appendix XVI). When different variables had a correlation higher than 0.7, only one of them was used. Next, the correlation between the SR and the remaining variables was assessed. The variables with a correlation lower than 0.1 were not used either, because it would only overcomplicate the model. The same variable selection was applied for the plant height models. All data was standardized using the vegan package (Oksanen et al., 2020).

Four different models were made to predict SR: one with only spectral data (formula 2.3), one with only spectral heterogeneity data (formula 2.4), one with only plant height data (formula 2.5) and the last one combining spectral and plant height data (formula 2.6).

$$SR \sim RE + Blue_{cv} + NIR_{cv} + NDVI_{cv} + (1 \mid site) + (1 \mid field) \quad (2.3)$$

$$SR \sim Blue_{cv} + NIR_{cv} + NDVI_{cv} + (1 \mid site) + (1 \mid field) \quad (2.4)$$

$$SR \sim PH_{O\,sd} + (1 \mid site) + (1 \mid field) \quad (2.5)$$

$$SR \sim RE + Blue_{cv} + NIR_{cv} + NDVI_{cv} + PH_{O\,sd} + (1 \mid site) + (1 \mid field) \quad (2.6)$$

A mixed Poisson regression model was used because the response variable in question (species richness) is count data. Both the site and the flight mission were included as random effects to take the hierarchical nature of the data into account. To start, this was done using the lme4 package (Bates et al., 2015). However, that always resulted in singularity problems even when simplifying the models. When a fit is singular, a model result is achieved but there is a high chance that it is a false positive. As a solution, Bayesian modelling was applied using the brms package to fit the abovementioned models (Bürkner, 2017). The number of cores and the number of Markov chains were both set at two and the total number of iterations per chain was set at 30,000. After the fit, it was checked if model convergence was achieved: Rhat needs to equal one and the effective sample size needs to be large enough (>1,000) for each parameter.

The same modelling method as described above was used to model the productivity. On the one hand, the observed plant height was modelled in function of spectral data (formula 2.7) and on the other hand in function of species richness (formula 2.8). Since the plant height is not count data, a Gaussian distribution was used instead of a Poisson distribution.

$$PH_O \sim Blue + RE + NIR_{cv} + NDVI + (1 \mid site) + (1 \mid field) \quad (2.7)$$

$$PH_O \sim SR + (1 \mid site) + (1 \mid field) \quad (2.8)$$

After the fits, the models were evaluated using the DHARMa package (Hartig, 2022). In the case of overdispersion, which was only applicable for the models to predict SR, the model fit was repeated but with a negative binomial distribution instead of a Poisson distribution. Finally, the results of the complex mixed models were also compared with more simple (generalised) linear models to see if the coefficient estimates were similar.

The Kruskal-Wallis test with a significance level of 5% was performed per site to determine if there was a significant difference in NDE between plots with a different SR. This non-parametric test was used because the assumptions of normality were not met since the observations were not independent. When a significant difference was observed, the Dunn's post hoc test with Benjamini-Hochberg adjustment was conducted using the FSA package to identify which SR groups were significantly different from one another (Ogle et al., 2021). The results were visualised with boxplots using the rcompanion package to add letters on top of the boxplots to show significant differences (Mangiafico, 2021).

3 Results

3.1 MAPEO-preprocessed Data

The results across the different flight missions all appear to be similar over the four sites, therefore the results of only one randomly chosen flight mission will be presented here. The chosen flight mission is situated in Zedelgem and contains plots 5 – 7 and plots 13 – 18 (Figure 3-1). The results of the other flight missions can be found in appendix.

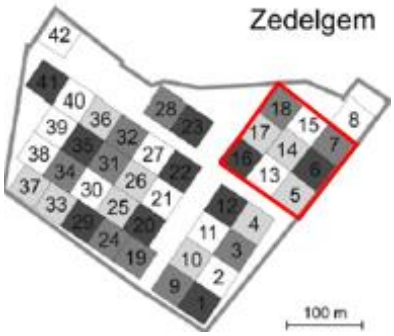

Figure 3-1 A graphic representation of the FORBIO site in Zedelgem. The red contour line indicates the flight mission for which results will be presented (modified from Verheyen et al., 2013).

After MAPEO pre-processing, a reflection raster with seven different bands is obtained: blue, green, red, red edge, near-infrared, longwave infrared and alpha. The range of each of the bands is between 0 and 65535 (Figure 3-3). This is because the alpha band, used for image visualisation has a value of 65535 and the other bands are not yet corrected for it. The terrain height varies between 50 and 65 m and the surface height between 50 and 75 m (Figure 3-2). The NDVI appears to be relatively uniform and has values between 0 and 1 (Figure 3-4).

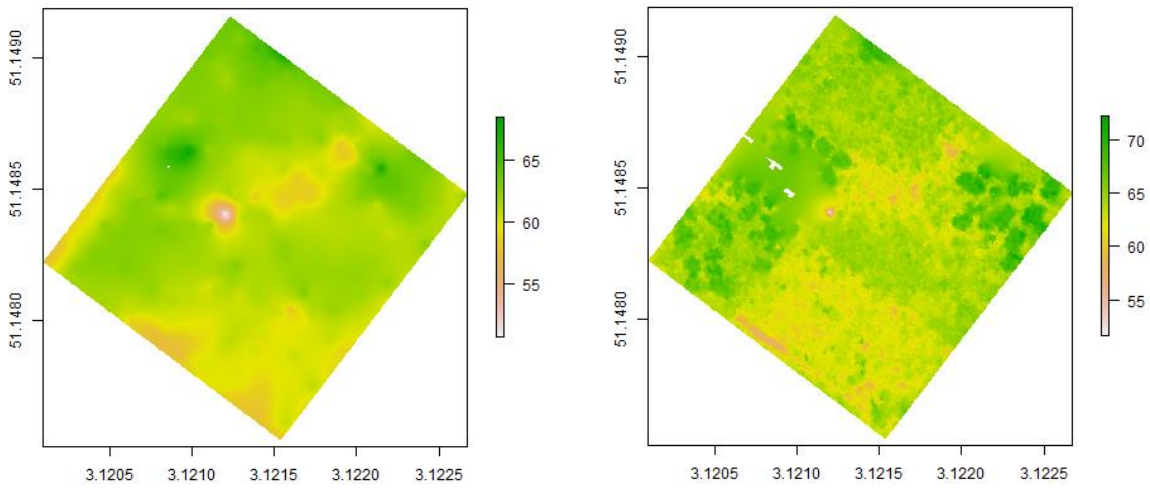

Figure 3-2 DTM (left) and DSM (right) in meters of one show case flight mission at the FORBIO site in Zedelgem.

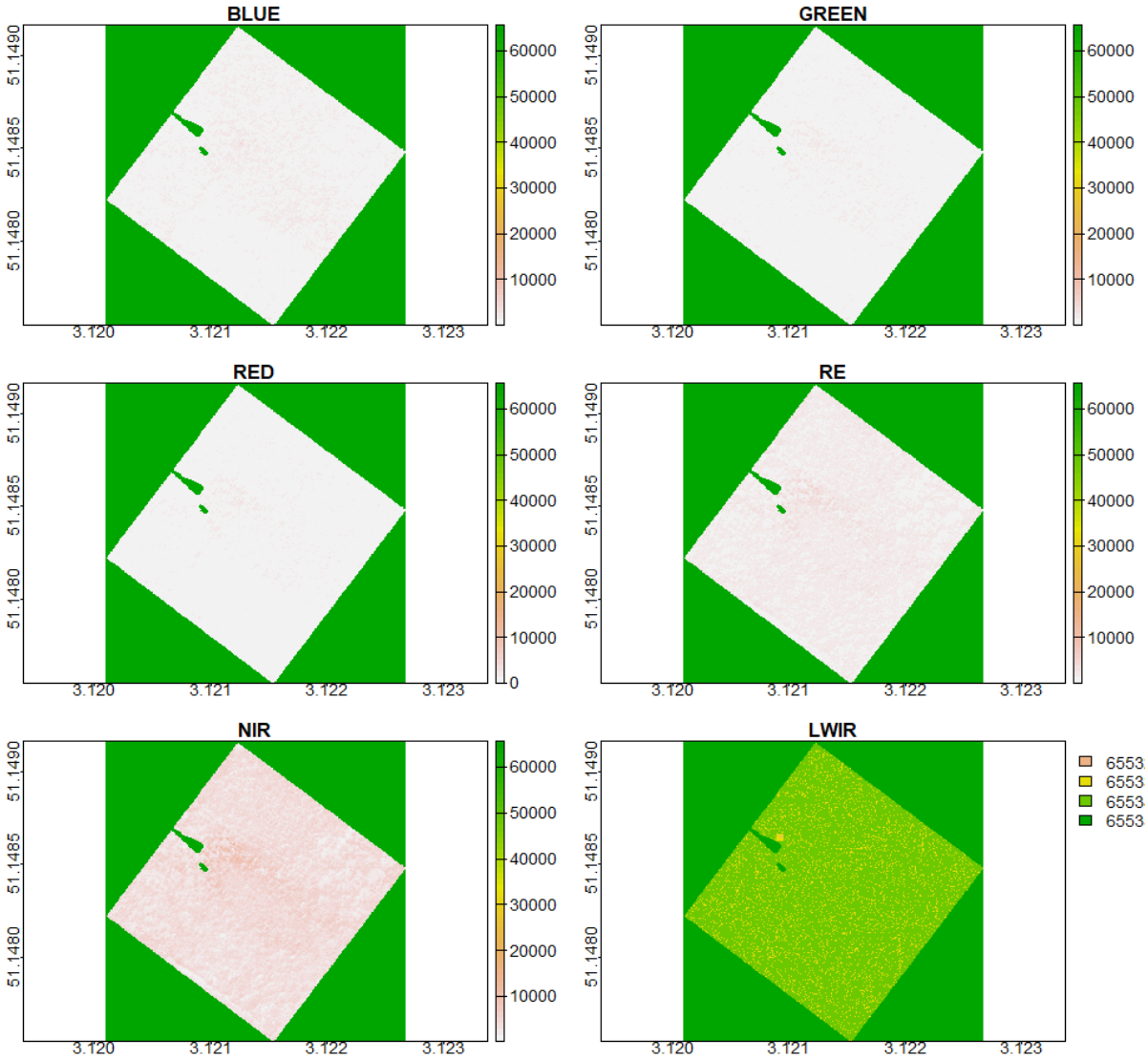

Figure 3-3 Reflectance data of one show case flight mission at the FORBIO site in Zedelgem. Six different bands are presented from left to right: blue, green, red, red edge (RE), near-infrared (NIR), longwave infrared (LWIR).

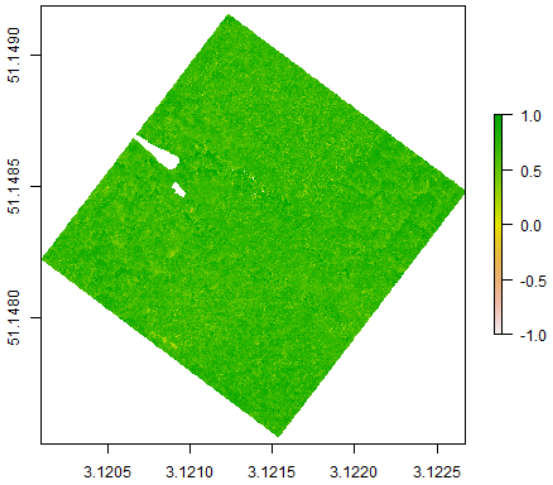

Figure 3-4 NDVI of one show case flight mission at the FORBIO site in Zedelgem.

3.2 Extracted Raster Data per Plot

The new plot sizes of the FORBIO site in Zedelgem are 34 m x 34 m compared to the original plot sizes of 42 m x 42 m (Figure 3-5). Applying these new plots to the DTM of Flanders, results in terrain height between 11 m and 16 m, with higher altitudes in the northeast and lower in the west part of the site (Figure 3-6). The mask layer derived from the NDVI, has zero values for one gap at the west side and some small spots spread over the different plots (Figure 3-7).

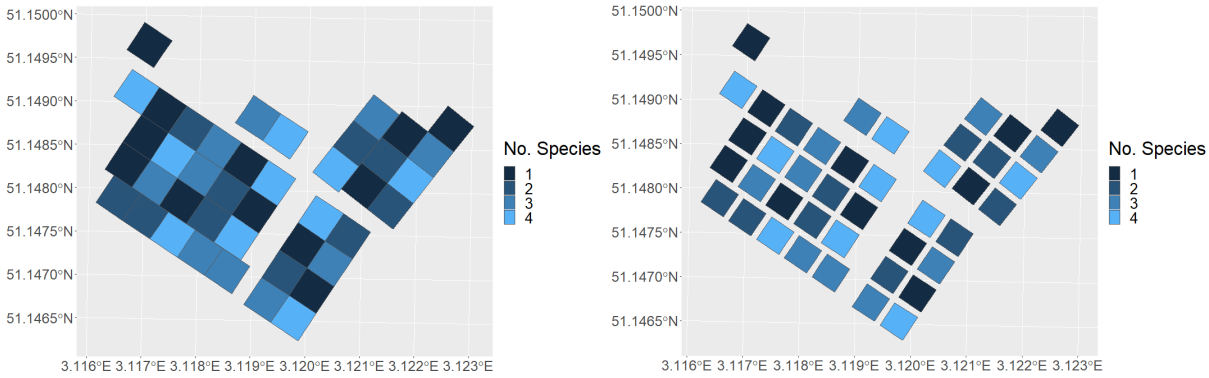

Figure 3-5 Plots of the FORBIO experiment in Zedelgem with the colour representing the number of species. On the left the original plot sizes are given and on the right the plot sizes reduced by 4 m at each side.

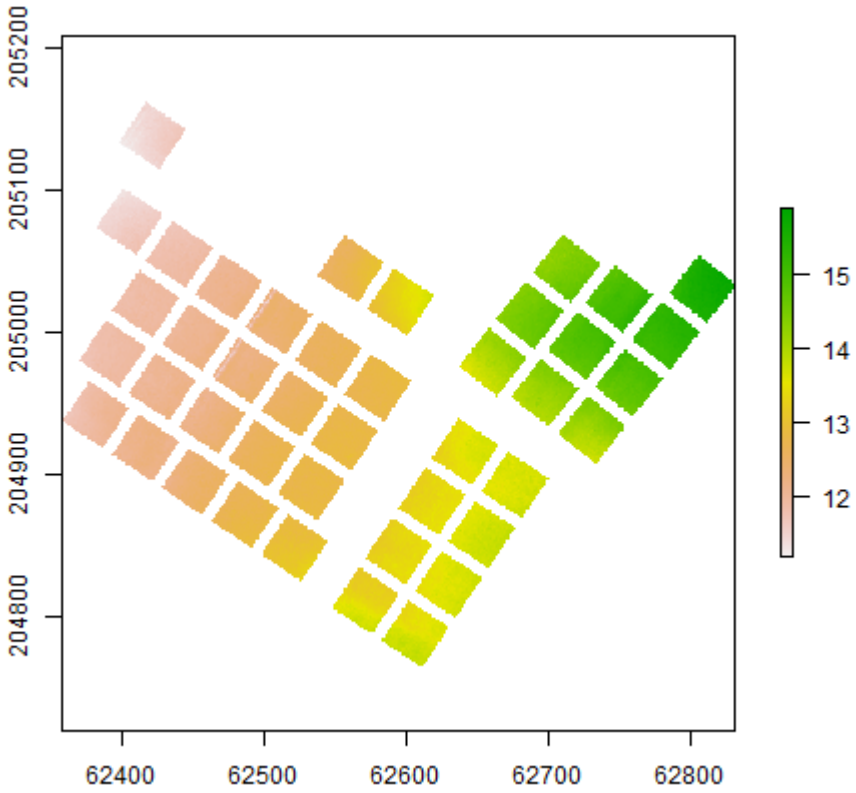

Figure 3-6 DTM in meters of the FORBIO site in Zedelgem.

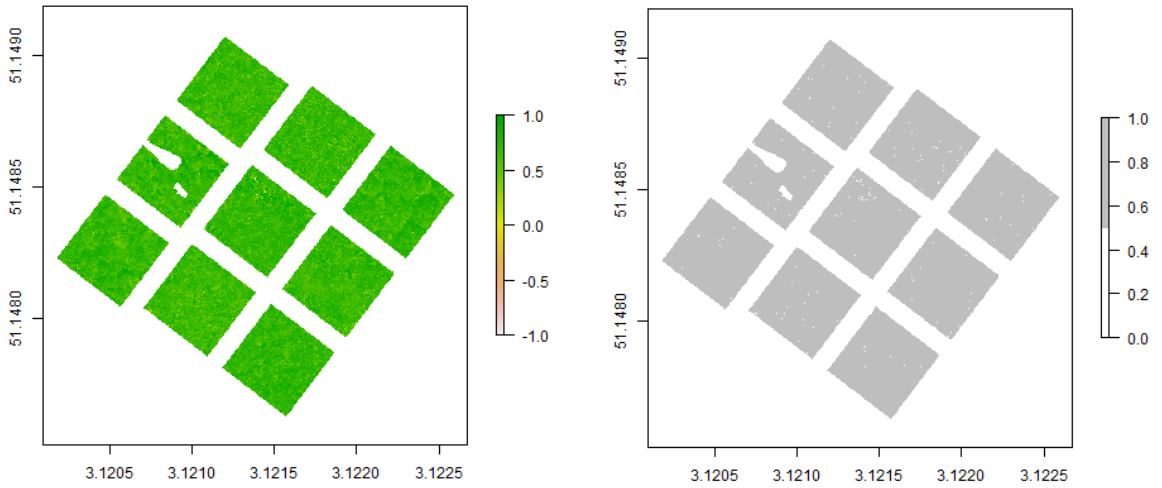

Figure 3-7 A mask layer (right) derived from the NDVI layer (left) where values are lower than 0.3. This is the result of one show case flight mission at the FORBIO site in Zedelgem.

The plant height derived from the DTM of Flanders and the MAPEO DSM ranges between 45 m and 55 m (Figure 3-8). The corrected plant height therefore ranges between 6 and 16 m. After clipping with the reduced plot sizes, correcting for the alpha band and applying the mask layer, more clear variations in the different reflectance bands are visible (Figure 3-9).

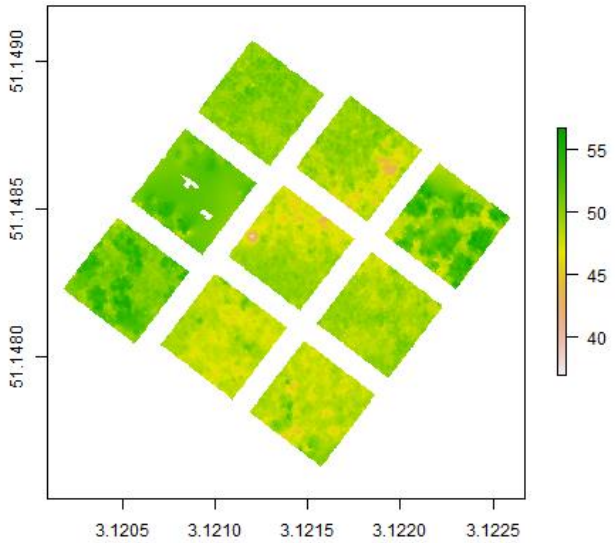

Figure 3-8 Plant height in meters of one show case flight mission at the FORBIO site in Zedelgem.

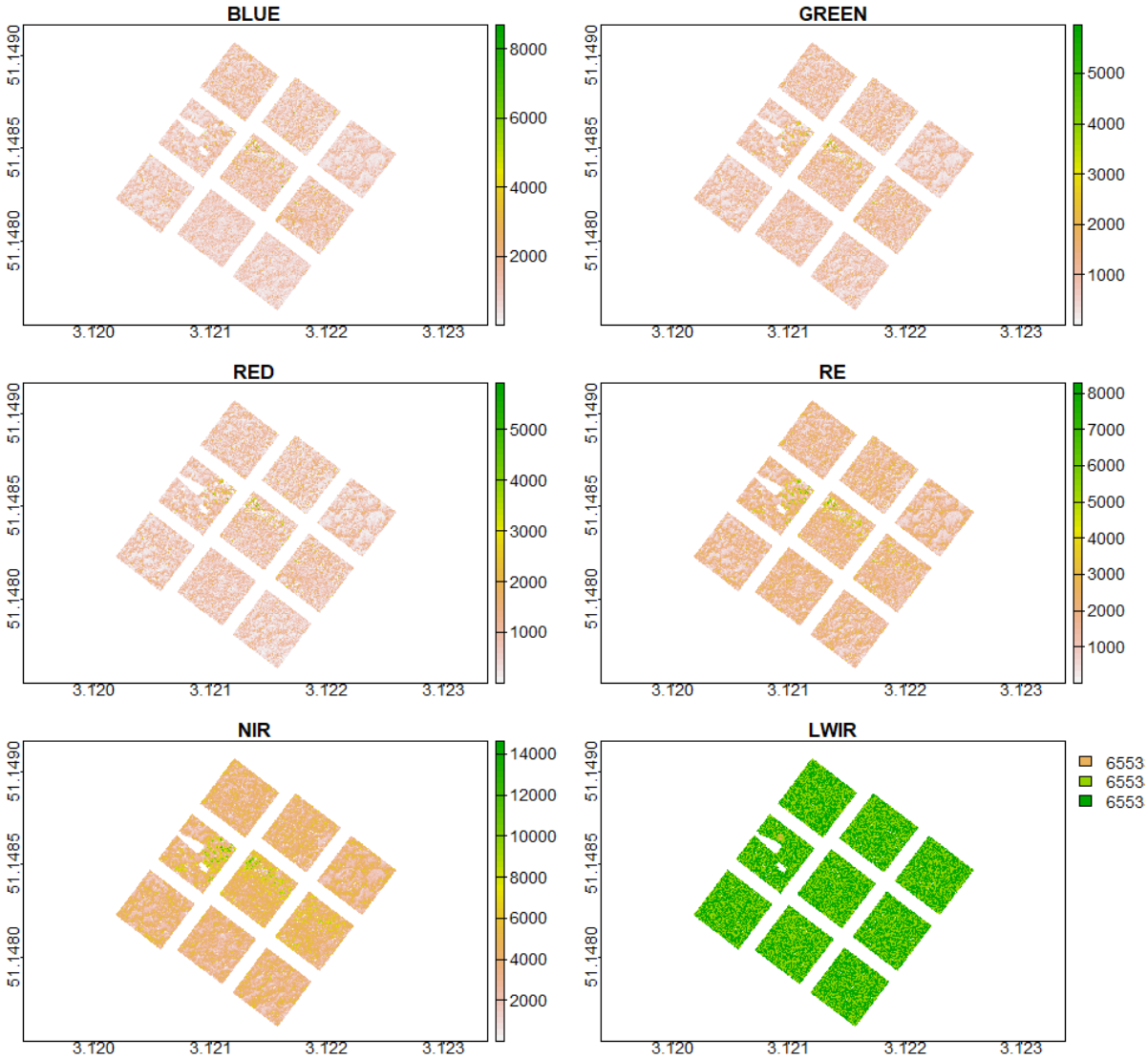

Figure 3-9 Reflectance data after clipping with size-reduced plots and correcting for the alpha band. This is the result of one show case flight mission at the FORBIO site in Zedelgem. Six different bands are presented from left to right: blue, green, red, red edge, near-infrared, longwave infrared.

The mean of the red, green and blue reflectance bands per plot range between 500 and 1200 with an sd between 400 and 900 (Table 3-1). The RE and the NIR generally have a higher mean per plot and therefore a higher sd as well. For every plot, the LWIR has a value of 65535 ± 0.5.

Table 3-1 For the plots of one show case flight mission at the FORBIO site in Zedelgem, represented by plot ID, the number of species and the number of trees per species are given.

Plot ID	No. species	No. common beech	No. pedunculate oak	No. silver birch	No. small-leaved lime	No. Scots pine	Total No. trees
5	2	398	0	0	386	0	784
6	4	189	199	0	204	192	784
7	3	0	261	259	264	0	784
13	1	0	0	0	784	0	784
14	2	384	400	0	0	0	784
15	1	0	784	0	0	0	784
16	4	197	192	190	0	205	784
17	2	0	384	400	0	0	784
18	3	0	259	0	264	261	784

Table 3-2 For the plots of one show case flight mission at the FORBIO site in Zedelgem, represented by plot ID, the mean and standard deviation (sd) of different reflectance bands are given: blue, green, red, red edge (RE), near infrared (NIR) and longwave infrared (LWIR). These values are a result after clipping with the reduced plot sizes, correcting for the alpha band and applying the mask layer to eliminate dead or unhealthy vegetation pixels.

Plot ID	Blue	Green	Red	RE	NIR	LWIR	Blue sd	Green sd	Red sd	RE sd	NIR sd	LWIR sd
5	762	661	563	1440	3373	65535	496	440	406	781	1331	0.50
6	1205	877	784	1627	4190	65535	792	544	531	859	1558	0.50
7	766	612	583	1333	3420	65535	547	432	453	779	1440	0.50
13	806	706	651	1575	3268	65535	478	434	415	767	1227	0.50
14	1157	916	812	1812	4611	65535	820	609	603	1016	1760	0.50
15	985	782	699	1539	3617	65535	727	529	536	852	1418	0.50
16	844	655	619	1362	3396	65535	598	447	459	760	1388	0.50
17	927	774	762	1708	4129	65535	679	576	581	1044	2052	0.51
18	1069	771	689	1441	3522	65535	733	505	486	789	1368	0.50

Table 3-3 For the plots of one show case flight mission at the FORBIO site in Zedelgem, represented by plot ID, the correlation of variance (cv) of different reflectance bands are given: blue, green, red, red edge (RE), near infrared (NIR) and longwave infrared (LWIR). The mean, standard deviation (sd) and cv of the NDVI and the corrected plant height (PH) are presented as well. These values are a result after clipping with the reduced plot sizes, correcting for the alpha band and applying the mask layer to eliminate dead or unhealthy vegetation pixels.

Plot ID	Blue cv	Green cv	Red cv	RE cv	NIR cv	LWIR cv	NDVI	NDVI sd	NDVI cv	PH	PH sd	PH cv
5	0.65	0.66	0.72	0.54	0.39	0.00	0.74	0.12	0.16	9.42	1.06	0.11
6	0.66	0.62	0.68	0.53	0.37	0.00	0.71	0.12	0.17	10.20	0.87	0.08
7	0.71	0.71	0.78	0.58	0.42	0.00	0.74	0.12	0.16	12.33	2.15	0.17
13	0.59	0.62	0.64	0.49	0.38	0.00	0.69	0.12	0.18	9.15	0.88	0.10
14	0.71	0.66	0.74	0.56	0.38	0.00	0.73	0.13	0.18	9.46	1.43	0.15
15	0.74	0.68	0.77	0.55	0.39	0.00	0.71	0.14	0.19	9.80	1.45	0.15
16	0.71	0.68	0.74	0.56	0.41	0.00	0.72	0.13	0.17	12.77	1.50	0.12
17	0.73	0.74	0.76	0.61	0.50	0.00	0.72	0.13	0.19	12.67	0.94	0.07
18	0.69	0.66	0.71	0.55	0.39	0.00	0.70	0.12	0.17	11.21	0.81	0.07

3.3 Species Richness and Productivity Models

The model to predict SR based on spectral data has a coefficient of determination (R^2) value of 0.16 and the only significant variable is the intercept. The intercepts also significantly differ across the different sites and flight missions (Table 3-4). When only using spectral heterogeneity data, i.e. cv of different bands, the R^2-value of the model decreases to 0.13. Again, nothing but the intercept is significant (Table 3-4). The model to predict SR based on the variation in plant height has a higher R^2-value of 0.26. Besides the intercept, the sd of the observed plant height is significant as well and has an effect size of 0.22 (Table 3-4). The combined model has the highest R^2-values of the models to predict the species richness (R^2-value = 0.33). Only the intercept and the sd of the observed plant height with an effect size of 0.21 are significant (Table 3-4).

Table 3-4 Results of Bayesian generalised linear models with negative binomial distribution to predict the species richness. The estimate, estimate error, lower 95% credible interval, upper 95% credible interval and Rhat are given per variable.

Spectral model						
		Estimate	Error	l-95% CI	u-95% CI	Rhat
Group level effects: sd intercept	Flight mission	0.14	0.11	0.01	0.41	1.00
	Site	0.23	0.28	0.01	0.98	1.00
Population level effects	Intercept	0.86	0.19	0.48	1.22	1.00
	RE	-0.09	0.09	-0.27	0.08	1.00
	Blue cv	0.16	0.10	-0.03	0.37	1.00
	NIR cv	-0.05	0.12	-0.29	0.19	1.00
	NDVI cv	-0.04	0.11	-0.27	0.15	1.00
Spectral heterogeneity model						
		Estimate	Error	l-95% CI	u-95% CI	Rhat
Group level effects: sd intercept	Flight mission	0.11	0.09	0.00	0.35	1.00
	Site	0.25	0.36	0.01	1.00	1.00
Population level effects	Intercept	0.87	0.19	0.47	1.23	1.00
	Blue cv	0.15	0.10	-0.04	0.36	1.00
	NIR cv	-0.02	0.11	-0.25	0.21	1.00
	NDVI cv	-0.05	0.10	-0.27	0.14	1.00
Plant height model						
		Estimate	Error	l-95% CI	u-95% CI	Rhat
Group level effects: sd intercept	Flight mission	0.08	0.06	0.00	0.24	1.00
	Site	0.21	0.25	0.01	0.85	1.00
Population level effects	Intercept	0.84	0.17	0.50	1.15	1.00
	PH_O sd	0.22	0.06	0.11	0.34	1.00
Combined model						
		Estimate	Error	l-95% CI	u-95% CI	Rhat
Group level effects: sd intercept	Flight mission	0.11	0.09	0.00	0.33	1.00
	Site	0.31	0.39	0.01	1.27	1.00
Population level effects	Intercept	0.82	0.24	0.34	1.27	1.00
	RE	-0.04	0.08	-0.22	0.12	1.00
	Blue cv	0.08	0.11	-0.13	0.30	1.00
	NIR cv	-0.03	0.13	-0.29	0.21	1.00
	NDVI cv	-0.01	0.11	-0.24	0.18	1.00
	PH_O sd	0.21	0.06	0.09	0.34	1.00

The model to predict the plant height based on spectral data has an R^2-value of 0.72. Two different variables are significant: the RE band and the NDVI, with effect sizes of respectively -0.42 and 0.43 (Table 3-5). When modelling the plant height solely based on SR, the R^2-value decreases to 0.69. The SR is the only significant variable and has an effect size of 0.11 (Table 3-5).

Table 3-5 Results of Bayesian linear models with Gaussian distribution to predict the plant height. The estimate, estimate error, lower 95% credible interval, upper 95% credible interval and Rhat are given per variable.

Spectral model						
		Estimate	Error	l-95% CI	u-95% CI	Rhat
Group level effects: sd intercept	Flight mission	0.37	0.18	0.09	0.79	1.00
	Site	1.48	0.80	0.57	3.53	1.00
Population level effects	Intercept	0.07	0.75	-1.45	1.60	1.00
	Blue	0.17	0.13	-0.09	0.42	1.00
	RE	-0.42	0.15	-0.72	-0.13	1.00
	NIR cv	0.14	0.12	-0.09	0.37	1.00
	NDVI	0.43	0.19	0.02	0.61	1.00
Species Richness model						
		Estimate	Error	l-95% CI	u-95% CI	Rhat
Group level effects: sd intercept	Flight mission	0.29	0.13	0.07	0.59	1.00
	Site	1.30	0.74	0.51	3.20	1.00
Population level effects	Intercept	-0.22	0.68	-1.58	1.17	1.00
	SR	0.11	0.05	0.02	0.20	1.00

In 80% of all the mixed plots, a positive NDE is observed. When looking per site, this percentage is higher in Zedelgem (97%) and lower in Hechtel-Eksel and Gedinne (70% and 72%). However, the NDE shows no significant difference with increasing SR at the Hechtel-Eksel site (p-value = 0.24) and at the Gedinne site (p-value = 0.28; Figure 3-10). There is more variation present in the Gedinne data set. At the Zedelgem site, the NDE significantly differs between plots with a different SR (p-value < 0.01). Plots with three or four species have a significant higher NDE compared to plots with one species. The NDE in plots with more than one species do not significantly differ from one another (Figure 3-11).

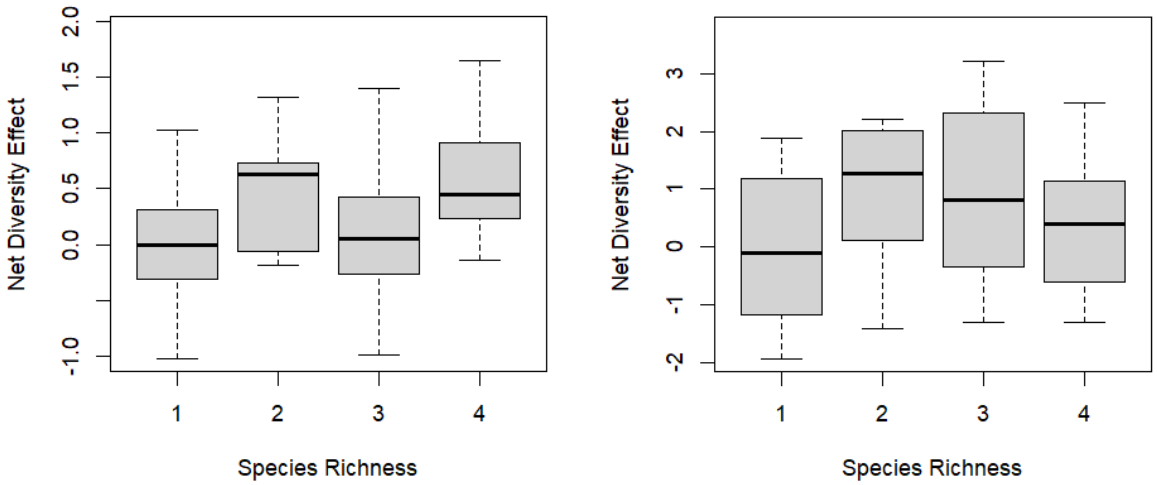

Figure 3-10 Net diversity effect per species richness of the FORBIO site in Hechtel-Eksel (left) and Gedinne (right).

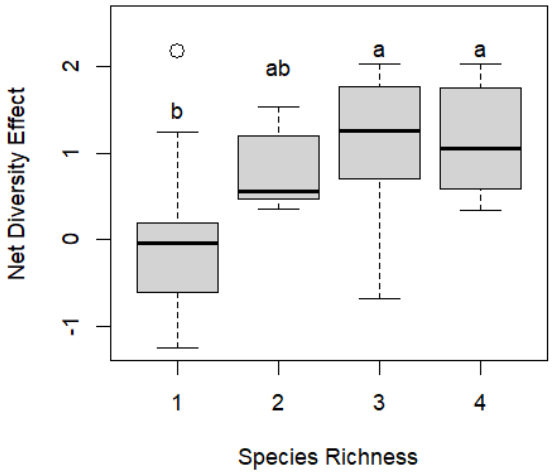

Figure 3-11 Net diversity effect (NE) per species richness (SR) of the FORBIO site in Zedelgem. Different letters above the boxplots show that the SR have a significantly different NDE according to Dunn's post hoc test.

4 Discussion

4.1 Spectral Diversity is a Weak Predictor of Tree Species Diversity

In this study, we tried to predict tree species richness on the one hand and tree productivity on the other hand based on collected multispectral drone data. We evaluated which parameters were best to be included in the models and how they could be improved. A pipeline of the steps of collecting, processing and analysing drone data was documented during this study and possible improvements for future research will be indicated in this discussion as well.

The models to predict species richness are not well performing. They all have a weak (0.20 – 0.39) or very weak (< 0.20) R^2-value. An explanation for that can be that a spectral signature is a representation of the functional characteristics more than the species characteristics, so that accordingly functional diversity will be evaluated rather than species diversity (Tilman, 2001). Certain functional traits (e.g. specific leaf area, leaf nitrogen content…) can be measured in situ to compare if spectral models are better in predicting those traits than the species itself. By performing flights during different seasons, tree phenology can also be taken into account which can improve the models to predict species richness (Madonsela et al., 2021). It looks like longwave infrared radiation is not useful to predict species richness since it results in images with the same mean and standard deviation for each plot. However, it should be noted that the resolution of this band is lower, which makes the variable less reliable than the others.

Including a vertical dimension, i.e. plant height data, significantly increases the model performance. This confirms the results of other studies (Gini et al., 2018; Peng et al., 2021). The positive effect size indicates that the higher the variation in plant height, the higher the species richness. The variation in vertical tree structure both in even-aged and uneven-aged stands is therefore a good indicator of local biodiversity (Peng et al., 2021). For that reason, it is important to always include a vertical component in models to predict species diversity and maybe this is even more required than spectral data. The R^2-values of the combined model with spectral data and the plant height model without spectral data to predict species richness do not differ much. Moreover, in the combined model, the standard deviation of the plant height was the only significant variable, confirming its importance.

Improving the accuracy of the plant height measurements will probably also improve the model quality. This can be done in different ways. First, collecting digital surface model LiDAR data with cm spatial resolution would give a very accurate representation of the tree structures but these sensors are very costly. Another possibility is to execute double grid flight missions instead of single grid missions. This results in a more accurate point cloud image from which plant height can be extracted but the flight and processing time will increase which is not always a better option because of reasons that will be explained in section 4.4. A third way to improve plant height data is flying during two different seasons over the same site. During early spring with leaf-off conditions it is possible to generate an accurate digital terrain model, while in summer an accurate digital surface model can be obtained. Combining both will result in a more accurate canopy height model (Nasiri et al., 2021).

4.2 Tree Productivity can be Predicted by Spectral Data

UAS-based tree height data was used as proxy for productivity in this study. The model to predict tree productivity based on spectral data has a strong accuracy (R^2-value = 0.72). Productivity can be accurately predicted by functional traits (Van de Peer et al., 2018). Since spectral data is related to functional characteristics, it makes sense that productivity can be predicted based on spectral data. In the developed model, the NDVI has a significant large positive effect on the plant height. A possible explanation is that the NDVI is inversely correlated with physiological stress and positively correlated with photosynthetic activity (Dash et al., 2018; Wang et al., 2004). Therefore, an increased NDVI generally relates to higher productivity. According to the model, a higher red edge band value correlates to a decreased plant height. This could be explained by the relation between red edge reflectance and tree stress (Masaitis et al., 2013). Stressed trees will be less productive compared to healthy trees. Some studies also indicate that red edge reflectance is related to the leaf area index, which in turn is correlated with tree productivity (Arias et al., 2007; C. Wang, 2021).

4.3 UAS-based Plant Height Data Confirms the Biodiversity-Productivity Hypothesis

The model to predict tree productivity based on species richness confirms the biodiversity-productivity hypothesis: higher species richness results in higher productivity. On contrary, the net diversity effect, which compares the observed yield

with the expected yield, shows no significant increase with increasing species richness at each FORBIO site. However, in 80% of the mixed plots a positive net diversity effect is observed proving overyielding in polycultures. The study performed by Van de Peer et al. (2018) at the FORBIO sites in Zedelgem and Gedinne six years after planting showed similar results: a positive net diversity effect in 83% of the mixed plots. Their results were based on in situ tree diameter and height measurements.

At the Hechtel-Eksel and Gedinne FORBIO sites, the observed net diversity effect in monocultures is not significantly higher than in polycultures . Compared to Zedelgem, where the plots with more than two species have a significant higher net diversity effect, the site in Hechtel-Eksel was established two years later. This could be an explanation why no significant overyielding as in Zedelgem is present yet. It takes several years before species can benefit from complementarity, which leads to higher productivity. However, in high-density plantations, the higher productivity in mixtures compared to monocultures could already be visible after a few years (< five years; Cardinale et al., 2007). Another reason for the observed non-significant net diversity effect could be the poorer sandy soil present in Hechtel-Eksel, compared to a richer loamy soil in Zedelgem. The accuracy of the UAS-based plant height measurements as predictor for tree productivity could also be a possible explanation. However, this accuracy issue could be solved by improving the plant height model generation as discussed in previous section.

The two FORBIO sites in Zedelgem and Gedinne are established in the same year. However, in Gedinne there is no significant higher net diversity effect in mixed-species plots. The variability in net diversity effect is also larger in Gedinne than at the other two sites. The reason for that could be that the Gedinne FORBIO experiment consists of two subsites with some minor differences in soil conditions. The climatic conditions in Gedinne are harsher compared to Zedelgem. Therefore, fast-growing species that are well adapted to these harsh environmental conditions in Gedinne (e.g. Douglas fir, Japanese larch) have a competitive advantage over other species (Van de Peer et al., 2018). The competitive dominance of certain species reducing the performance of others at the Gedinne site can be an explanation for the lower, non-significant net diversity effect.

In Zedelgem, the mild climate and the high post-agricultural nutrient availability caused the tree species to grow effortless and the species benefited from facilitation rather

than being held back by dominance resulting in higher productivity in mixtures (Van de Peer et al., 2018). These differences point out the context-dependency of the biodiversity-productivity relationship. In Zedelgem, higher levels of species richness did not significantly increase the net diversity effect, similarly as observed in the study of Van de Peer et al. (Van de Peer et al., 2018).

4.4 Further Improving Drone Data Collection

For biodiversity studies, drones have numerous advantages compared to other remote sensing platforms and costly, labour-intensive field surveys. However, this study made it clear that collecting drone data goes hand in hand with a lot of uncertainty as well. First, flight restriction geo-zones pose a limitation on where you can fly. This limits the area where and when you can do research. In case of helicopter training areas, it is announced only one day in advance if they become active. This requires a good relationship with the stakeholders, such as the landowners, as they need to be flexible in giving permission with the date and time of flight missions changing more than once. Collecting data around solar noon will give the best results because less shadow is present in the canopy, but matching this benefit with flight restricted time frames can be challenging.

The weather is undoubtedly a limiting factor in UAS-based studies. In case of rain, even a limited amount, your flights need to be postponed. In countries like Belgium, the weather is often very unpredictable, which again makes flight planning difficult. Also, when the weather changes during the flight mission, the mission needs to be aborted and may be repeated later or on another day, which makes the variability between different flight missions at the same location larger. Small gusts of wind can suddenly rise, which significantly decrease the accuracy of the multispectral data. For example, during the last flight missions in Gedinne, the wind gradually came up – staying within acceptable ranges – which is probably the cause of some unprocessed parts during the MAPEO pre-processing. The DLS 2 sensor, which allows flying under non-constant light conditions, is a big improvement in creating less uncertainty. This widens the options for possible flight executions.

It is better to make the flight mission plans in advance, based on the exact perimeter of the region of interest, than doing this in the field such as done during this study. This will ensure an exact overlap with the field data during processing. For example, in

Hechtel-Eksel, one flight mission plan was drawn incorrectly whereby two plots needed to be excluded for further analysis. In this case, it was still quite easy to distinguish the experiment from the surrounding vegetation on an aerial map, but when the vegetation grows, this will become harder and thus more important to make the flight mission plans beforehand. However, it is still very important to doublecheck everything in the field because small adaptations to the flight mission plans could be required e.g. to avoid interaction with large trees, power lines etc.

Another improvement that can be made, is increasing the side and front overlap from 75% to 85%. The quality checks during the MAPEO pre-processing indicate that for almost every flight mission the real overlap was too low, at some points even lower than 65%. The real overlap appears to be inhomogeneous during the entire flight – despite the fixed distance interval setting – resulting in some pixels with an overlap being lower than the pre-programmed one. This reduces the quality of the images significantly and even creates some data gaps. Studies prove that overlap settings are usually the variable with the largest effect on the processing quality (de Lima et al., 2021; Ottoy et al., 2022).

However, the trade-off between image resolution and computing power needed to process the images always needs to be considered. Increasing the overlap by a few percentages, can in fact increase the computing time in orders of magnitude when generating for example a digital surface model (Torres-Sánchez et al., 2018). When increasing the overlap, the flight altitude can be enlarged as compensation. In that way, the flight time will not be longer than the battery power can provide and the data quantity to be processed will still be within the acceptable range. Some studies have evaluated the effect of different processing parameters for photogrammetry (de Lima et al., 2021; Ottoy et al., 2022; Young et al., 2022). The chosen altitude, overlap, pitch and even the software all influence the result. However, few studies on optimizing the parameters regarding UAS-based forest biodiversity studies have been performed up to now.

Measuring some ground control points in the field will improve the data quality as well. Even though the drone is connected to the RTK network, this will still enlarge the precision. As a result, less size reduction of the plots will be needed during the data processing and therefore more data can be used. Flying over forest ecosystems is harder than over agricultural fields. Therefore, if you just obtained a theoretical pilot

license, I would highly recommend having you assisted by an experienced pilot in more difficult environments such as present in this study to ensure safety.

MAPEO uses WGS84+EGM96 as standard CRS for pre-processing data from DJI multispectral sensors. However, our original input data had another CRS, i.e. WGS84, which caused incorrect, higher values in the digital surface models and digital terrain models. To avoid such problems, this always needs to be checked beforehand. However, our applied correction did not influence the final results because all pixels were treated equally.

5 Conclusion

Collecting UAS data for forest monitoring applications has numerous advantages because of its low cost and high flexibility. However, UAS-based studies have also some disadvantages since they are subjected to uncertainties concerning weather and geo zone flight restrictions. For achieving the best result, a strict pipeline needs to be followed in collecting and processing drone data. Further research is advised to optimize the parameters for UAS-based forest biodiversity studies.

Models predicting tree species richness based on spectral data have low R^2-values. Adding a structural component significantly improves the model accuracy. Based on spectral diversity, it is hard to predict species diversity, since spectral diversity is rather related to functional diversity. In general, UAS applications have the potential to monitor tree diversity when combined with further research including parameter optimization and assessing season variability for long-term monitoring applications. However, direct monitoring of tree species diversity based on UAS data will always have limitations regarding biodiversity conservation since the ecological importance or rareness of species is not considered.

Spectral data can be used to model tree species productivity with high accuracy. The productivity-diversity hypothesis can also be confirmed based on UAS data. To evaluate its accuracy, plant height data should be collected in situ and compared with the results found in this study. Differences in net diversity effects between the different FORBIO sites indicate the context-dependency of overyielding in mixtures. Therefore, further research assessing the concrete mechanisms causing these differences is required.

6 References

AgEagle Sensor Systems Inc. (2021). *Altum - MicaSense*. https://micasense.com/es/altum/

Agentschap Digitaal Vlaanderen. (2014). *Digitaal Hoogtemodel Vlaanderen II, DTM, raster, 1 m. Version dataset: 2014.01*. https://www.geopunt.be/

Arias, D., Calvo-Alvarado, J., & Dohrenbusch, A. (2007). Calibration of LAI-2000 to estimate leaf area index (LAI) and assessment of its relationship with stand productivity in six native and introduced tree species in Costa Rica. *Forest Ecology and Management*, *247*(1–3), 185–193. https://doi.org/10.1016/j.foreco.2007.04.039

Bánki, O., Roskov, Y., Döring, M., Ower, G., Vandepitte, L., Hobern, D., Remsen, D., Schalk, P., DeWalt, R. E., Keping, M., Miller, J., Orrell, T., Aalbu, R., Adlard, R., Adriaenssens, E. M., Aedo, C., Aescht, E., Akkari, N., Alfenas-Zerbini, P., … von Konrat, M. (2022). Catalogue of Life Checklist (Version 2022-04-26). *Catalogue of Life*. https://doi.org/https://doi.org/10.48580/dfpk

Barnosky, A. D., Matzke, N., Tomiya, S., Wogan, G. O. U., Swartz, B., Quental, T. B., Marshall, C., McGuire, J. L., Lindsey, E. L., Maguire, K. C., Mersey, B., & Ferrer, E. A. (2011). Has the Earth's sixth mass extinction already arrived? *Nature*, *471*(7336), 51–57. https://doi.org/10.1038/nature09678

Bates, D., Mächler, M., Bolker, B., & Walker, S. (2015). Fitting Linear Mixed-Effects Models Using {lme4}. *Journal of Statistical Software*, *67*(1), 1–48. https://doi.org/10.18637/jss.v067.i01

Bürkner, P.-C. (2017). {brms}: An {R} Package for {Bayesian} Multilevel Models Using {Stan}. *Journal of Statistical Software*, *80*(1), 1–28. https://doi.org/10.18637/jss.v080.i01

Candiago, S., Remondino, F., De Giglio, M., Dubbini, M., & Gattelli, M. (2015). Evaluating multispectral images and vegetation indices for precision farming applications from UAV images. *Remote Sensing*, *7*(4), 4026–4047. https://doi.org/10.3390/rs70404026

Cardinale, B. J., Duffy, J. E., Gonzalez, A., Hooper, D. U., Perrings, C., Venail, P.,

Narwani, A., MacE, G. M., Tilman, D., Wardle, D. A., Kinzig, A. P., Daily, G. C., Loreau, M., Grace, J. B., Larigauderie, A., Srivastava, D. S., & Naeem, S. (2012). Biodiversity loss and its impact on humanity. *Nature*, *486*(7401), 59–67. https://doi.org/10.1038/nature11148

Cardinale, B. J., Wright, J. P., Cadotte, M. W., Carroll, I. T., Hector, A., Srivastava, D. S., Loreau, M., & Weis, J. J. (2007). Impacts of plant diversity on biomass production increase through time because of species complementarity. *Proceedings of the National Academy of Sciences of the United States of America*, *104*(46), 18123–18128. https://doi.org/10.1073/pnas.0709069104

Ceballos, G., García, A., & Ehrlich, P. R. (2010). The Sixth Extinction Crisis Loss of Animal Populations and Species. *Journal of Cosmology*, *8*(November 2009), 1821–1831.

Chabot, D. (2018). Trends in drone research and applications as the journal of unmanned vehicle systems turns five. *Journal of Unmanned Vehicle Systems*, *6*(1), Vi–xv. https://doi.org/10.1139/juvs-2018-0005

Daniel Baston. (2022). *exactextractr: Fast Extraction from Raster Datasets using Polygons*. https://cran.r-project.org/package=exactextractr

Dash, J. P., Pearse, G. D., & Watt, M. S. (2018). UAV multispectral imagery can complement satellite data for monitoring forest health. *Remote Sensing*, *10*(8), 1–22. https://doi.org/10.3390/rs10081216

de Lima, R. S., Lang, M., Burnside, N. G., Peciña, M. V., Arumäe, T., Laarmann, D., Ward, R. D., Vain, A., & Sepp, K. (2021). An evaluation of the effects of uas flight parameters on digital aerial photogrammetry processing and dense-cloud production quality in a scots pine forest. *Remote Sensing*, *13*(6), 3–5. https://doi.org/10.3390/rs13061121

De Muynck, E. (2018). *Frankrijk wil ontbossingen tegengaan: 'Een derde van de were... - De Standaard*. http://www.standaard.be/cnt/dmf20181116_03949654

Díaz-Delgado, R., Ónodi, G., Kröel-Dulay, G., & Kertész, M. (2019). Enhancement of ecological field experimental research by means of UAV multispectral sensing. *Drones*, *3*(1), 1–15. https://doi.org/10.3390/drones3010007

DJI. (2019). *MATRICE 200 SERIES V2 User Manual*. https://www.dji.com/uk/matrice-200-series-v2/info

EASA. (2021). *Specific Category - Civil Drones*. European Aviation Safety Agency (EASA). https://www.easa.europa.eu/domains/civil-drones/drones-regulatory-framework-background/open-category-civil-drones#group-easa-related-content

FAO. (1999). *Agricultural Biodiversity, Multifunctional Character of Agriculture and Land Conference, Background Paper 1*.

Franklin, S. E., & Ahmed, O. S. (2018). Deciduous tree species classification using object-based analysis and machine learning with unmanned aerial vehicle multispectral data. *International Journal of Remote Sensing*, *39*(15–16), 5236–5245. https://doi.org/10.1080/01431161.2017.1363442

Gholizadeh, H., Gamon, J. A., Helzer, C. J., & Cavender-Bares, J. (2020). Multi-temporal assessment of grassland α- and β-diversity using hyperspectral imaging. *Ecological Applications*, *30*(7), 1–13. https://doi.org/10.1002/eap.2145

Gini, R., Sona, G., Ronchetti, G., Passoni, D., & Pinto, L. (2018). Improving tree species classification using UAS multispectral images and texture measures. *ISPRS International Journal of Geo-Information*, *7*(8). https://doi.org/10.3390/ijgi7080315

González-Jaramillo, V., Fries, A., & Bendix, J. (2019). AGB estimation in a tropical mountain forest (TMF) by means of RGB and multispectral images using an unmanned aerial vehicle (UAV). *Remote Sensing*, *11*(12), 1–22. https://doi.org/10.3390/rs11121413

Govender, M., Chetty, K., & Bulcock, H. (2007). A review of hyperspectral remote sensing and its application in vegetation and water resource studies. *Water SA*, *33*(2), 145–151. https://doi.org/10.4314/wsa.v33i2.49049

Haines-Young, R., & Potschin, M. (2010). The links between biodiversity, ecosystem services and human well-being. In *Ecosystem Ecology: a new synthesis* (1st ed., pp. 110–139).

Hartig, F. (2022). *DHARMa: Residual Diagnostics for Hierarchical (Multi-Level / Mixed) Regression Models. R package version 0.4.5*. https://cran.r-

project.org/package=DHARMa

Hijmans, R. J. (2022a). *raster: Geographic Data Analysis and Modeling. R package version 3.5-15.* https://cran.r-project.org/package=raster

Hijmans, R. J. (2022b). *terra: Spatial Data Analysis. R package version 1.5-21.* https://cran.r-project.org/package=terra

Huete, A. R. (2004). Remote Sensing for Environmental Monitoring. In *Environmental Monitoring and Characterization*. Elsevier, Inc. https://doi.org/10.1016/B978-0-12-064477-3.50013-8

IPBES. (2019). *IPBES Global Assessment Summary for Policymakers*. https://ipbes.net/system/tdf/ipbes_global_assessment_report_summary_for_policymakers.pdf?file=1&type=node&id=35329

IUCN. (2022). *The IUCN Red List of Threatened Species*.

Jing, X., Muys, B., Bruelheide, H., Desie, E., Hättenschwiler, S., Jactel, H., Jaroszewicz, B., Kardol, P., Ratcliffe, S., Scherer-Lorenzen, M., Selvi, F., Vancampenhout, K., van der Plas, F., Verheyen, K., Vesterdal, L., Zuo, J., & Van Meerbeek, K. (2021). Above- and below-ground complementarity rather than selection drive tree diversity–productivity relationships in European forests. *Functional Ecology*, *35*(8), 1756–1767. https://doi.org/10.1111/1365-2435.13825

Jones, H. G., & Vaughan, R. A. (2010). *Remote sensing of vegetation: Principles, techniques, and applications*. Oxford University Press.

Khorram, S., Koch, F. H., van der Wiele, C. F., & Nelson, S. A. C. (2012). Introduction. In *Remote Sensing* (pp. 1–15). Springer US, Boston, MA. https://doi.org/10.1007/978-1-4614-3103-9_1

Kirkaya, A. (2020). Smart Farming- Precision Agriculture Technologies and Practices. *Journal of Scientific Perspectives*, *4*(2), 123–136. https://doi.org/10.26900/jsp.4.010

Koh, L. P., Dunn, R. R., Sodhi, N. S., Colwell, R. K., Proctor, H. C., & Smith, V. S. (2004). Species coextinctions and the biodiversity crisis. *Science*, *305*(5690), 1632–1634. https://doi.org/10.1126/science.1101101

Loreau M., & Hector. A. (2001). Partitioning selection and complementarity in biodiversity experiments. *Nature*, *412*(6842), 72–76. http://www.biology.mcgill.ca/faculty/loreau/

Madonsela, S., Cho, M. A., Ramoelo, A., & Mutanga, O. (2021). Investigating the relationship between tree species diversity and landsat-8 spectral heterogeneity across multiple phenological stages. *Remote Sensing*, *13*(13). https://doi.org/10.3390/rs13132467

Mangiafico, S. (2021). *rcompanion: Functions to Support Extension Education Program Evaluation. R package version 2.4.6*. https://cran.r-project.org/package=rcompanion

Masaitis, G., Mozgeris, G., & Augustaitis, A. (2013). Spectral reflectance properties of healthy and stressed coniferous trees. *IForest*, *6*(JANUARY 2013), 30–36. https://doi.org/10.3832/ifor0709-006

Micasense Inc. (2020). *Downwelling Light Sensor 2 (DLS 2) Integration Guide*. *2*(Dls 2), 1–17.

Micasense Inc. (2021). *User Guide for MicaSense Sensors*. *January*.

Millennium Ecosystem Assessment. (2005). *Ecosystems and Human Well-being: Biodiversity Synthesis*.

Möckel, T., Dalmayne, J., Schmid, B. C., Prentice, H. C., & Hall, K. (2016). Airborne hyperspectral data predict fine-scale plant species diversity in grazed dry grasslands. *Remote Sensing*, *8*(2), 1–19. https://doi.org/10.3390/rs8020133

Mora, C., Tittensor, D. P., Adl, S., Simpson, A. G. B., & Worm, B. (2011). How many species are there on earth and in the ocean? *PLoS Biology*, *9*(8), 1–8. https://doi.org/10.1371/journal.pbio.1001127

Nasiri, V., Darvishsefat, A. A., Arefi, H., Pierrot-Deseilligny, M., Namiranian, M., & Le Bris, A. (2021). Unmanned aerial vehicles (Uav)-based canopy height modeling under leaf-on and leaf-off conditions for determining tree height and crown diameter (case study: Hyrcanian mixed forest). *Canadian Journal of Forest Research*, *51*(7), 962–971. https://doi.org/10.1139/cjfr-2020-0125

Ogle, D. H., Doll, J. C., Wheeler, P., & Dinno, A. (2021). *FSA: Fisheries Stock Analysis.*

R package version 0.9.1. https://github.com/droglenc/FSA

Oksanen, J., Blanchet, F. G., Friendly, M., Kindt, R., Legendre, P., McGlinn, D., Minchin, P. R., O'Hara, R. B., Simpson, G. L., Solymos, P., Stevens, M. H. H., Szoecs, E., & Wagner, H. (2020). *vegan: Community Ecology Package. R package version 2.5-7*. https://cran.r-project.org/package=vegan

Oliver, T. H., Heard, M. S., Isaac, N. J. B., Roy, D. B., Procter, D., Eigenbrod, F., Freckleton, R., Hector, A., Orme, C. D. L., Petchey, O. L., Proença, V., Raffaelli, D., Suttle, K. B., Mace, G. M., Martín-López, B., Woodcock, B. A., & Bullock, J. M. (2015). Biodiversity and Resilience of Ecosystem Functions. In *Trends in Ecology and Evolution* (Vol. 30, Issue 11, pp. 673–684). Elsevier Ltd. https://doi.org/10.1016/j.tree.2015.08.009

Ottoy, S., Tziolas, N., Meerbeek, K. Van, Aravidis, I., Tilkin, S., Sismanis, M., Stavrakoudis, D., Gitas, I. Z., Zalidis, G., & Vocht, A. De. (2022). *Effects of Flight and Smoothing Parameters on the Detection of Taxus and Olive Trees with UAV-Borne Imagery*. 2–11.

Pajares, G. (2015). Overview and current status of remote sensing applications based on unmanned aerial vehicles (UAVs). *Photogrammetric Engineering and Remote Sensing*, *81*(4), 281–329. https://doi.org/10.14358/PERS.81.4.281

Pebesma, E. (2018). Simple Features for R: Standardized Support for Spatial Vector Data. *The R Journal*, *10*(1), 439–446. https://doi.org/10.32614/RJ-2018-009

Peng, X., Chen, Z., Chen, Y., Chen, Q., Liu, H., Wang, J., & Li, H. (2021). Modelling of the biodiversity of tropical forests in China based on unmanned aerial vehicle multispectral and light detection and ranging data. *International Journal of Remote Sensing*, *42*(23), 8858–8877. https://doi.org/10.1080/01431161.2021.1954714

Peng, Y., Fan, M., Bai, L., Sang, W., Feng, J., Zhao, Z., & Tao, Z. (2019). Identification of the best hyperspectral indices in estimating plant species richness in sandy grasslands. *Remote Sensing*, *11*(5). https://doi.org/10.3390/rs11050588

R Core Team. (2022). *R: A Language and Environment for Statistical Computing. R Foundation for Statistical Computing, Vienna, Austria*. https://www.r-project.org/

Rampino, M. R., & Shen, S. Z. (2021). The end-Guadalupian (259.8 Ma) biodiversity

crisis: the sixth major mass extinction? *Historical Biology*, *33*(5), 716–722. https://doi.org/10.1080/08912963.2019.1658096

Roberts, L., Hassan, A., Elamer, A., & Nandy, M. (2021). Biodiversity and extinction accounting for sustainable development: A systematic literature review and future research directions. *Business Strategy and the Environment*, *30*(1), 705–720. https://doi.org/10.1002/bse.2649

Rocchini, D., Bacaro, G., Chirici, G., Da Re, D., Feilhauer, H., Foody, G. M., Galluzzi, M., Garzon-Lopez, C. X., Gillespie, T. W., He, K. S., Lenoir, J., Marcantonio, M., Nagendra, H., Ricotta, C., Rommel, E., Schmidtlein, S., Skidmore, A. K., Van De Kerchove, R., Wegmann, M., & Rugani, B. (2018). Remotely sensed spatial heterogeneity as an exploratory tool for taxonomic and functional diversity study. *Ecological Indicators*, *85*(June 2017), 983–990. https://doi.org/10.1016/j.ecolind.2017.09.055

Rocchini, D., Ricotta, C., & Chiarucci, A. (2007). Using satellite imagery to assess plant species richness: The role of multispectral systems. *Applied Vegetation Science*, *10*(3), 325–331. https://doi.org/10.1111/j.1654-109X.2007.tb00431.x

Rull, V. (2022). Biodiversity crisis or sixth mass extinction? *EMBO Reports*, *23*(1), 1–4. https://doi.org/10.15252/embr.202154193

Sax, D. F., & Gaines, S. D. (2003). Species diversity: From global decreases to local increases. *Trends in Ecology and Evolution*, *18*(11), 561–566. https://doi.org/10.1016/S0169-5347(03)00224-6

Schwartz, M. W., Brigham, C. A., Hoeksema, J. D., Lyons, K. G., Mills, M. H., & Van Mantgem, P. J. (2000). Linking biodiversity to ecosystem function: Implications for conservation ecology. *Oecologia*, *122*(3), 297–305. https://doi.org/10.1007/s004420050035

Service public de Wallonie. (2014). *Relief de la Wallonie - Modèle Numérique de Terrain (MNT) 2013-2014*. https://geoportail.wallonie.be/

Shaw, G. A., & Burke, H. K. (2003). Spectral Imaging for Remote sensing. *Lincoln Laboratory Journal*, *14*(1), 3–28.

Singh, J. S. (2002). The biodiversity crisis: A multifaceted review. *Current Science*,

82(6), 638–647.

Skeyes. (2021). *Droneguide Viewer*. https://map.droneguide.be/

Tilman, D. (2001). Functional diversity. In S. A. Levin (Ed.), *Encyclopedia of biodiversity* (pp. 109–120). Academic Press.

Tilman, D., Isbell, F., & Cowles, J. M. (2014). Biodiversity and ecosystem functioning. *Annual Review of Ecology, Evolution, and Systematics*, *45*, 471–493. https://doi.org/10.1146/annurev-ecolsys-120213-091917

Toivonen, J., Korhonen, L., Kukkonen, M., Kotivuori, E., Maltamo, M., & Packalen, P. (2021). Transferability of ALS-based forest attribute models when predicting with drone-based image point cloud data. *International Journal of Applied Earth Observation and Geoinformation*, *103*, 102484. https://doi.org/10.1016/j.jag.2021.102484

Torres-Sánchez, J., López-Granados, F., Borra-Serrano, I., & Manuel Peña, J. (2018). Assessing UAV-collected image overlap influence on computation time and digital surface model accuracy in olive orchards. *Precision Agriculture*, *19*(1), 115–133. https://doi.org/10.1007/s11119-017-9502-0

Toth, C., & Jóźków, G. (2016). Remote sensing platforms and sensors: A survey. *ISPRS Journal of Photogrammetry and Remote Sensing*, *115*, 22–36. https://doi.org/10.1016/j.isprsjprs.2015.10.004

Tsiamis, N., Efthymiou, L., & Tsagarakis, K. P. (2019). A comparative analysis of the legislation evolution for drone use in oecd countries. *Drones*, *3*(4), 1–15. https://doi.org/10.3390/drones3040075

Van de Peer, T., Verheyen, K., Ponette, Q., Setiawan, N. N., & Muys, B. (2018). Overyielding in young tree plantations is driven by local complementarity and selection effects related to shade tolerance. *Journal of Ecology*, *106*(3), 1096–1105. https://doi.org/10.1111/1365-2745.12839

Vellend, M., Baeten, L., Becker-Scarpitta, A., Boucher-Lalonde, V., McCune, J. L., Messier, J., Myers-Smith, I. H., & Sax, D. F. (2017). Plant Biodiversity Change Across Scales During the Anthropocene. *Annual Review of Plant Biology*, *68*, 563–586. https://doi.org/10.1146/annurev-arplant-042916-040949

Verheyen, K., Ceunen, K., Ampoorter, E., Baeten, L., Bosman, B., Branquart, E., Carnol, M., De Wandeler, H., Grégoire, J. C., Lhoir, P., Muys, B., Setiawan, N. N., Vanhellemont, M., & Ponette, Q. (2013). Assessment of the functional role of tree diversity: The multi-site FORBIO experiment. *Plant Ecology and Evolution*, *146*(1), 26–35. https://doi.org/10.5091/plecevo.2013.803

Wang, C. (2021). At-sensor radiometric correction of a multispectral camera (Rededge) for suas vegetation mapping. *Sensors*, *21*(24). https://doi.org/10.3390/s21248224

Wang, J., Rich, P. M., Price, K. P., & Kettle, W. D. (2004). Relations between NDVI and tree productivity in the central Great Plains. *International Journal of Remote Sensing*, *25*(16), 3127–3138. https://doi.org/10.1080/0143116032000160499

Whittaker, R. J., Willis, K. J., & Field, R. (2001). Scale and species richness: Towards a general, hierarchical theory of species diversity. *Journal of Biogeography*, *28*(4), 453–470. https://doi.org/10.1046/j.1365-2699.2001.00563.x

Wickham, H., François, R., Henry, L., & Müller, K. (2022). *dplyr: A Grammar of Data Manipulation. R package version 1.0.8.* https://cran.r-project.org/package=dplyr

Xu, Z., Shen, X., Cao, L., Coops, N. C., Goodbody, T. R. H., Zhong, T., Zhao, W., Sun, Q., Ba, S., Zhang, Z., & Wu, X. (2020). Tree species classification using UAS-based digital aerial photogrammetry point clouds and multispectral imageries in subtropical natural forests. *International Journal of Applied Earth Observation and Geoinformation*, *92*(July), 102173. https://doi.org/10.1016/j.jag.2020.102173

Young, D. J. N., Koontz, M. J., & Weeks, J. M. (2022). Optimizing aerial imagery collection and processing parameters for drone-based individual tree mapping in structurally complex conifer forests. *Methods in Ecology and Evolution*, *2022*(November 2021), 1447–1463. https://doi.org/10.1111/2041-210X.13860

Zhu, L., Suomalainen, J., Liu, J., Hyyppä, J., Kaartinen, H., & Haggren, H. (2018). A Review: Remote Sensing Sensors. *Multi-Purposeful Application of Geospatial Data*. https://doi.org/10.5772/intechopen.71049

7 Appendices

Appendix I List of species present in the FORBIO sites in Belgium.

Scientific Name	English Name
Betula pendula Roth.	silver birch
Larix kaempferi Sarg.	Japanese larch
Pinus sylvestris L.	Scots pine
Pseudotsuga menziesii (Mirb.) Franco	Douglas fir
Quercus petraea (Mattuschka) Liebl.	sessile oak
Fagus sylvatica L.	common beech
Quercus robur L.	pedunculate oak
Tilia cordata Mill.	small-leaved lime
Acer pseudoplatanus L.	sycamore maple
Larix x eurolepis Henry	hybrid larch

Appendix II Plots of the FORBIO experiment in Hechtel-Eksel (top), Gribelle (middle) and Gouverneurs (bottom) with the colour representing the number of species. On the left the original plot sizes are given and on the right the plot sizes reduced by 4 m at each side

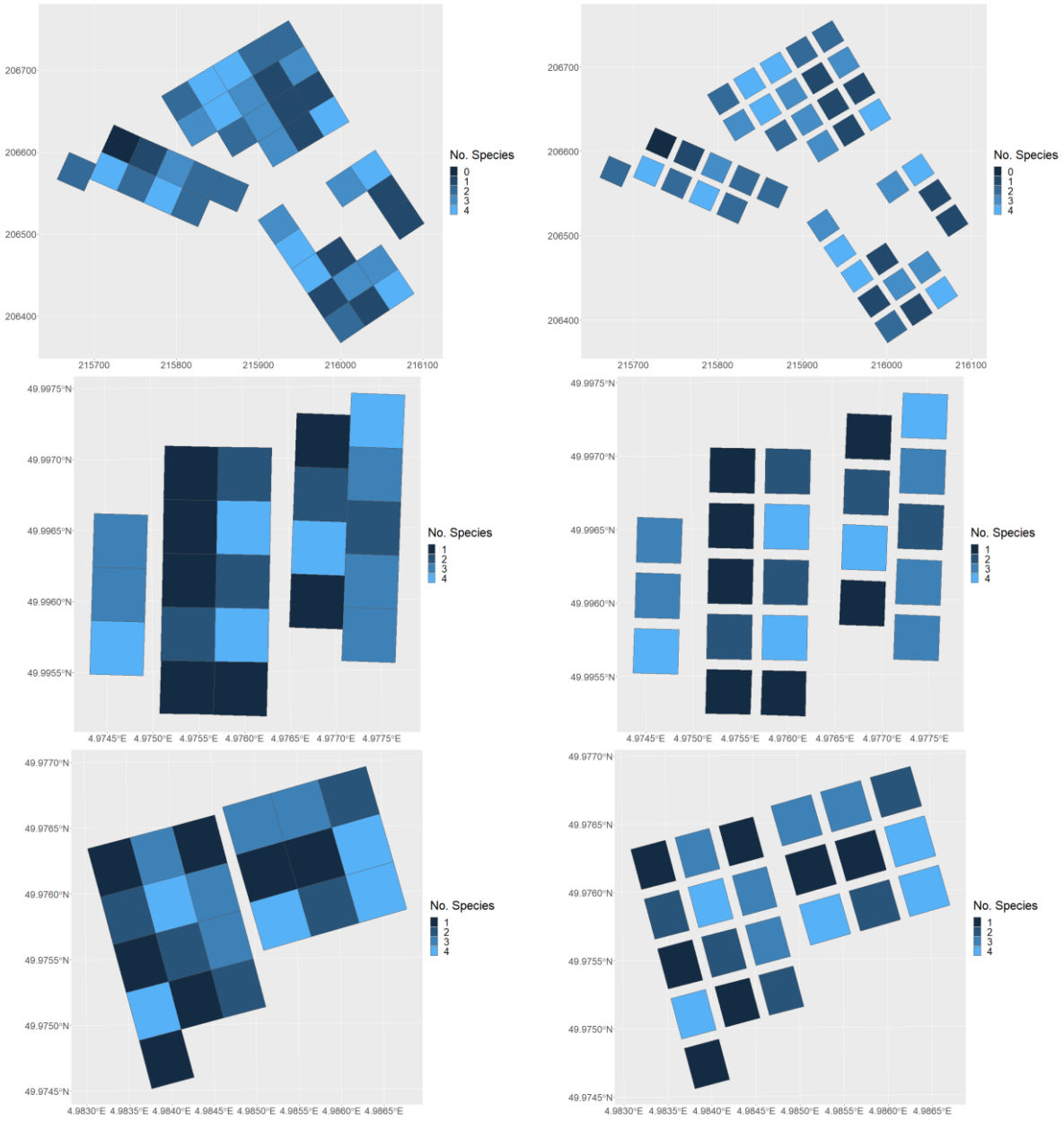

Appendix III Digital Terrain Model in meters of the FORBIO sites is Hechtel-Eksel (top left), Gribelle (top right) and Gouverneus (bottom)

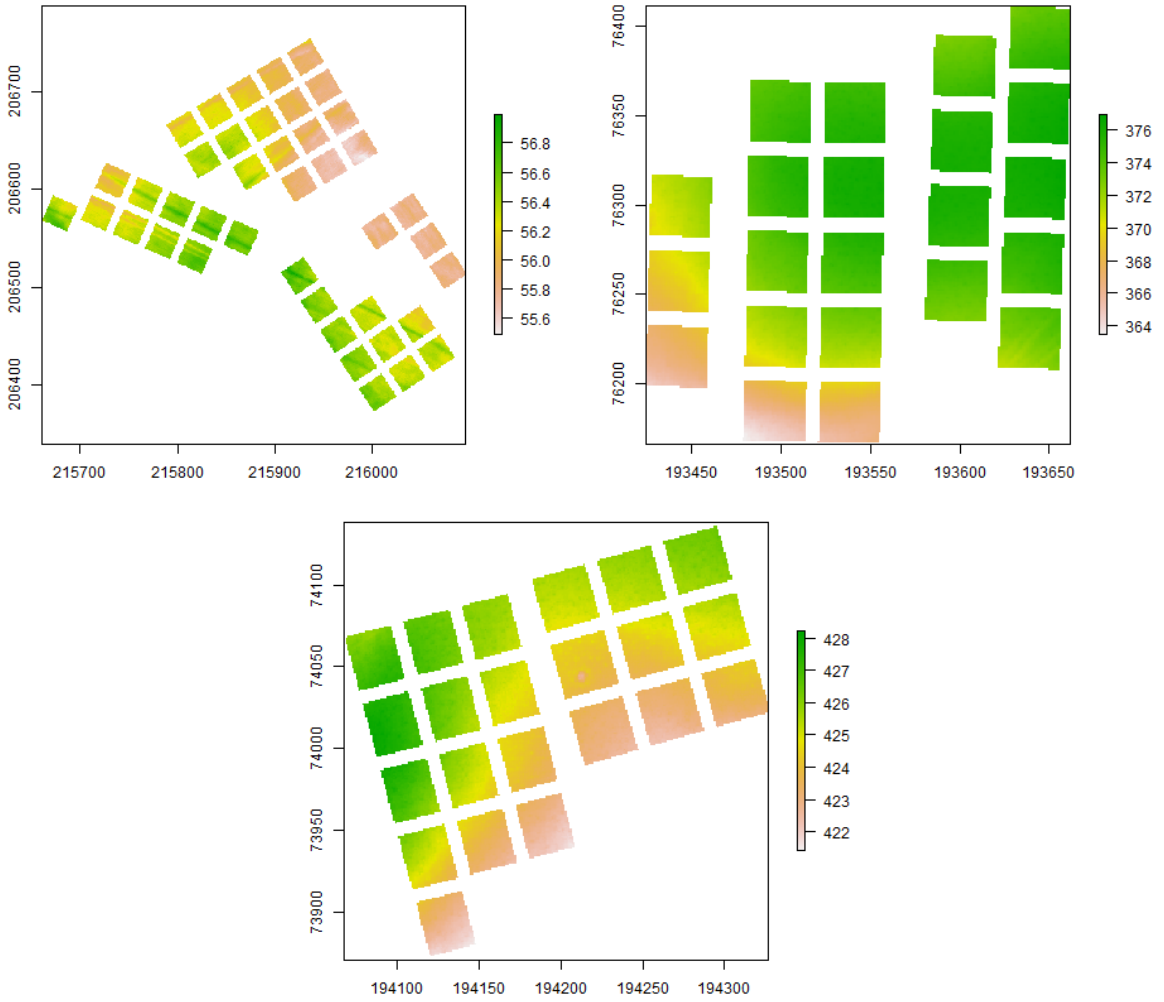

Appendix IV DTM (left) and DSM (right) in meters derived from MAPEO-preprocessed drone data. The results of the four different flight missions over the FORBIO site in Hechtel-Eksel are given (continued next page).

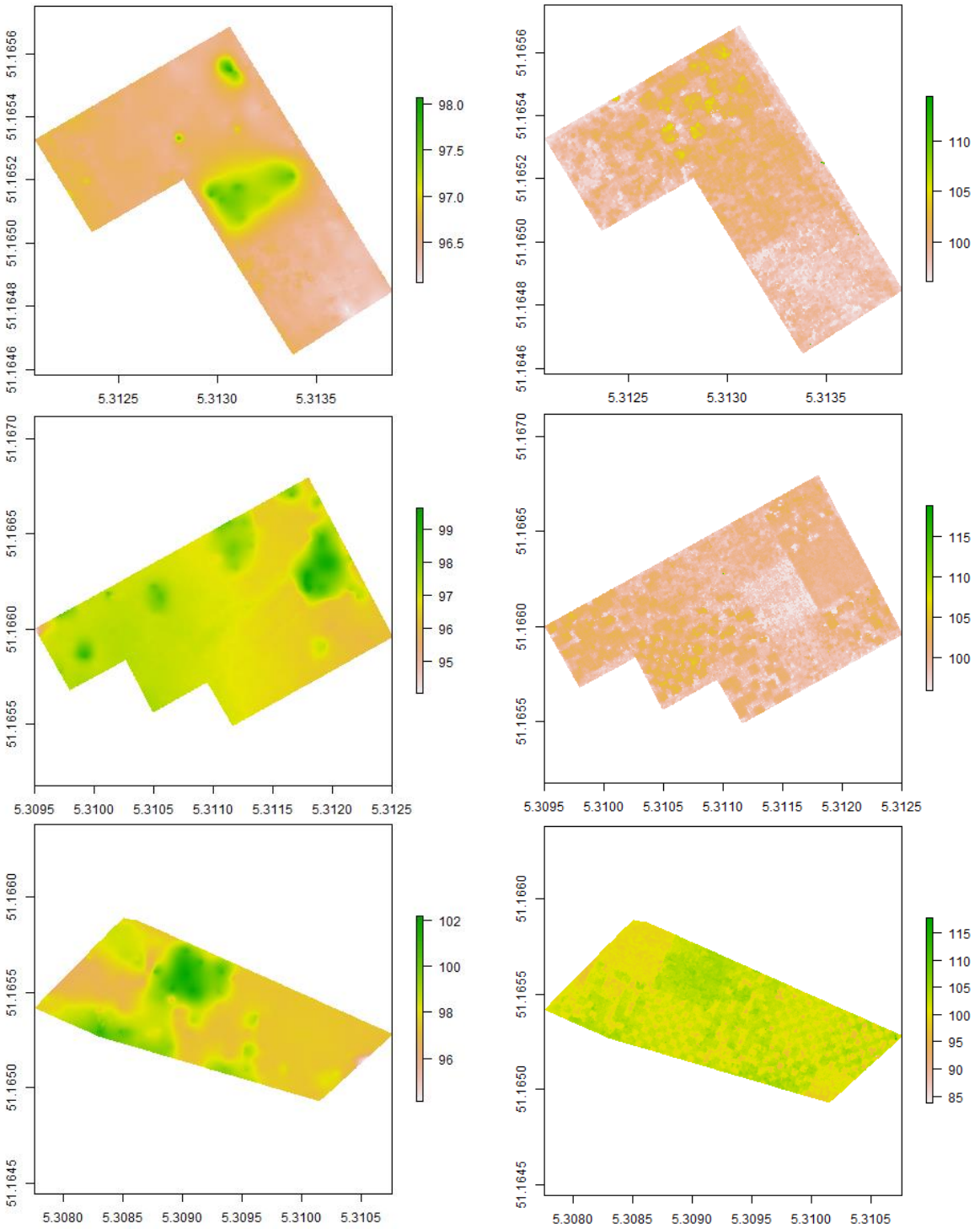

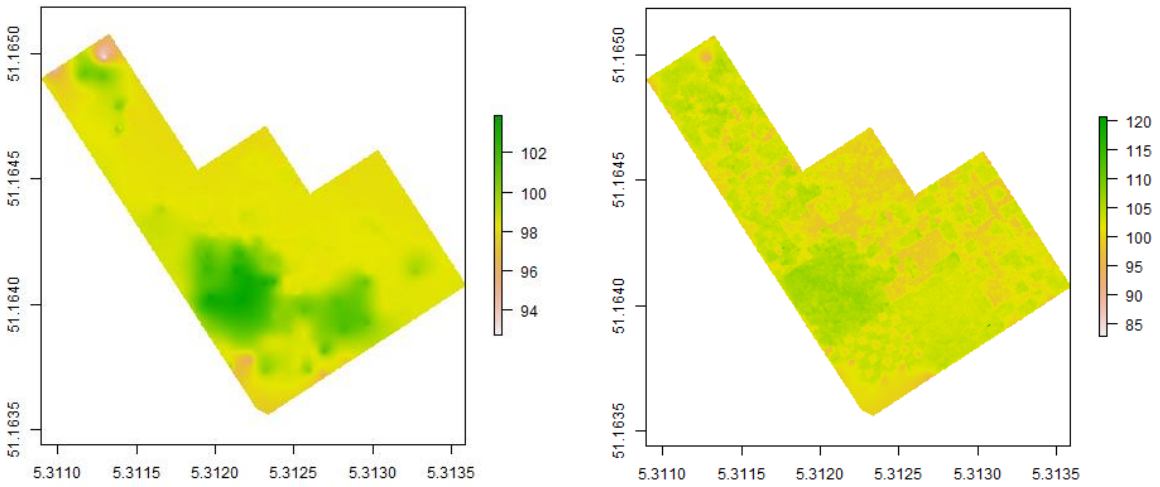

Appendix V Mask layer (right) derived from the NDVI layer (left) where values are lower than 0.3. The results of the four different flight missions over the FORBIO site in Hechtel-Eksel are given (continued next page).

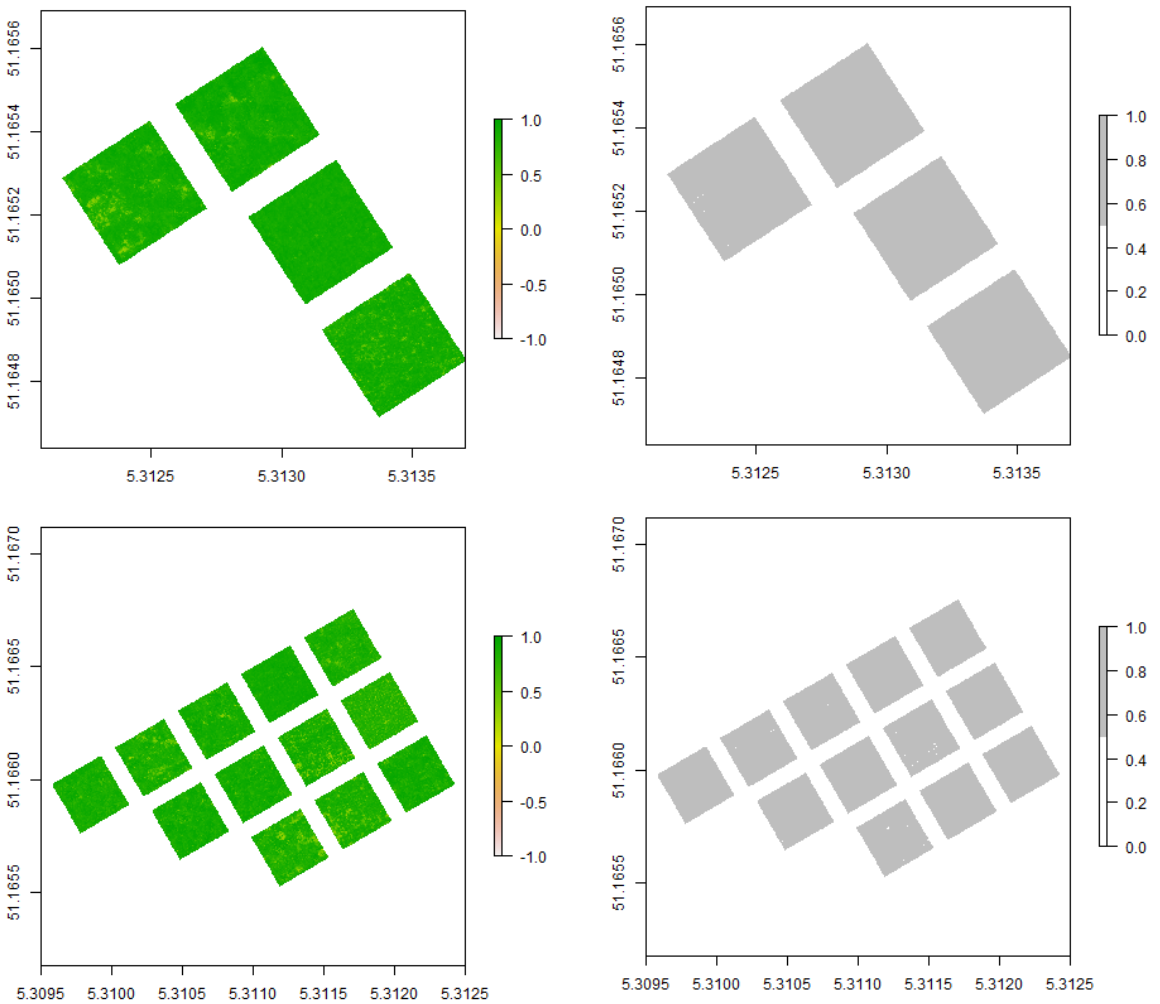

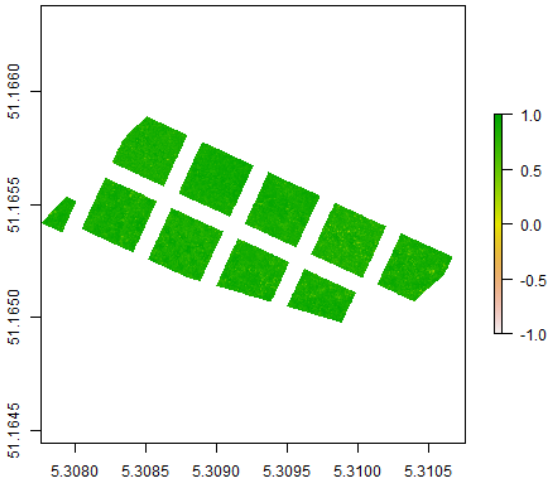
51.1660
51.1655
51.1650
51.1645
5.3080
5.3085
5.3090
5.3095
5.3100
5.3105
1.0
0.5
0.0
-0.5
-1.0

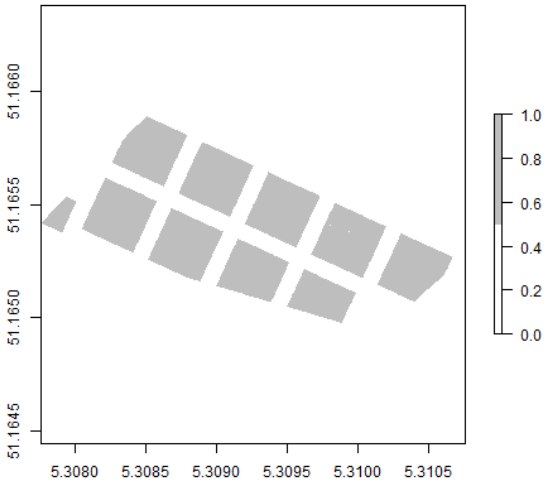
51.1660
51.1655
51.1650
51.1645
5.3080
5.3085
5.3090
5.3095
5.3100
5.3105
1.0
0.8
0.6
0.4
0.2
0.0

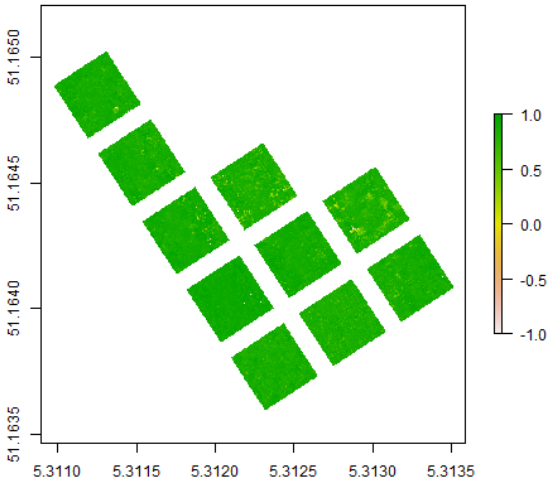
51.1650
51.1645
51.1640
51.1635
5.3110
5.3115
5.3120
5.3125
5.3130
5.3135
1.0
0.5
0.0
-0.5
-1.0

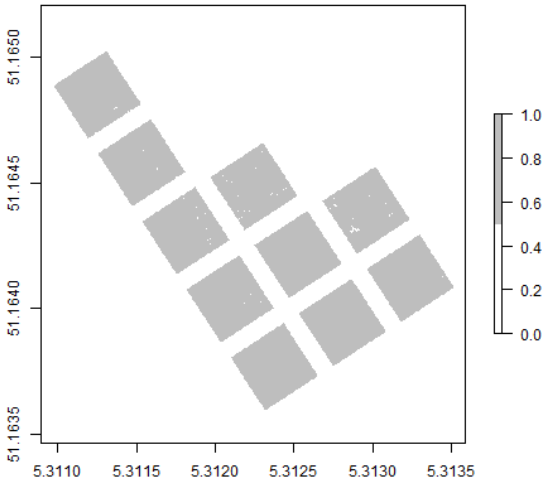
51.1650
51.1645
51.1640
51.1635
5.3110
5.3115
5.3120
5.3125
5.3130
5.3135
1.0
0.8
0.6
0.4
0.2
0.0

Appendix VI Plant height in meters derived by subtracting the DTM of Flanders from the MAPEO-preprocessed DSM result. The results of the four different flight missions over the FORBIO site in Hechtel-Eksel are given.

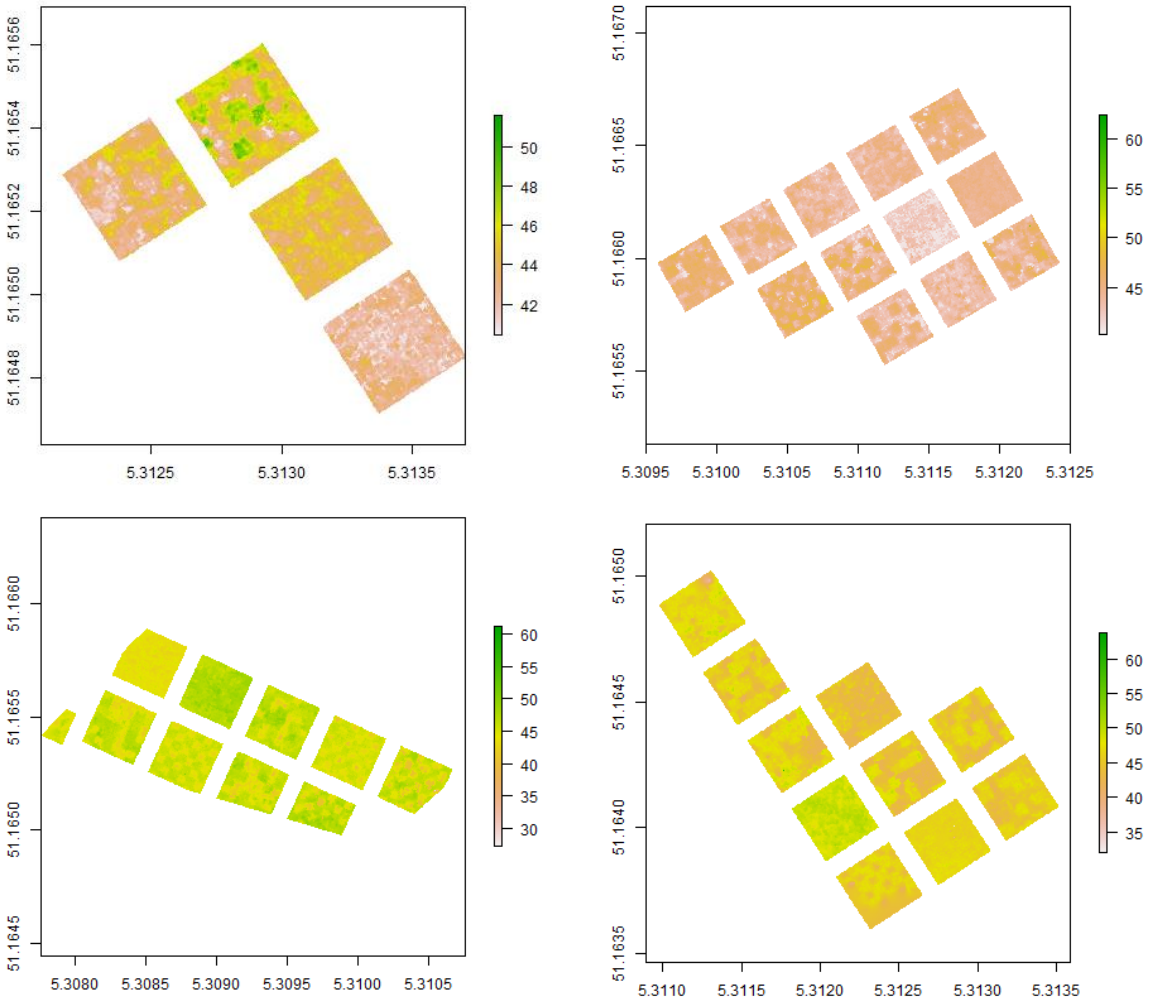

Appendix VII Reflectance drone data after clipping with size-reduced plots of the FORBIO site in Hechtel-Eksel. Six different bands are presented from left to right: blue, green, red, red edge (RE), near-infrared (NIR), longwave infrared (LWIR). The results of the four different flight missions over the FORBIO site in Hechtel-Eksel are given (continued next pages).

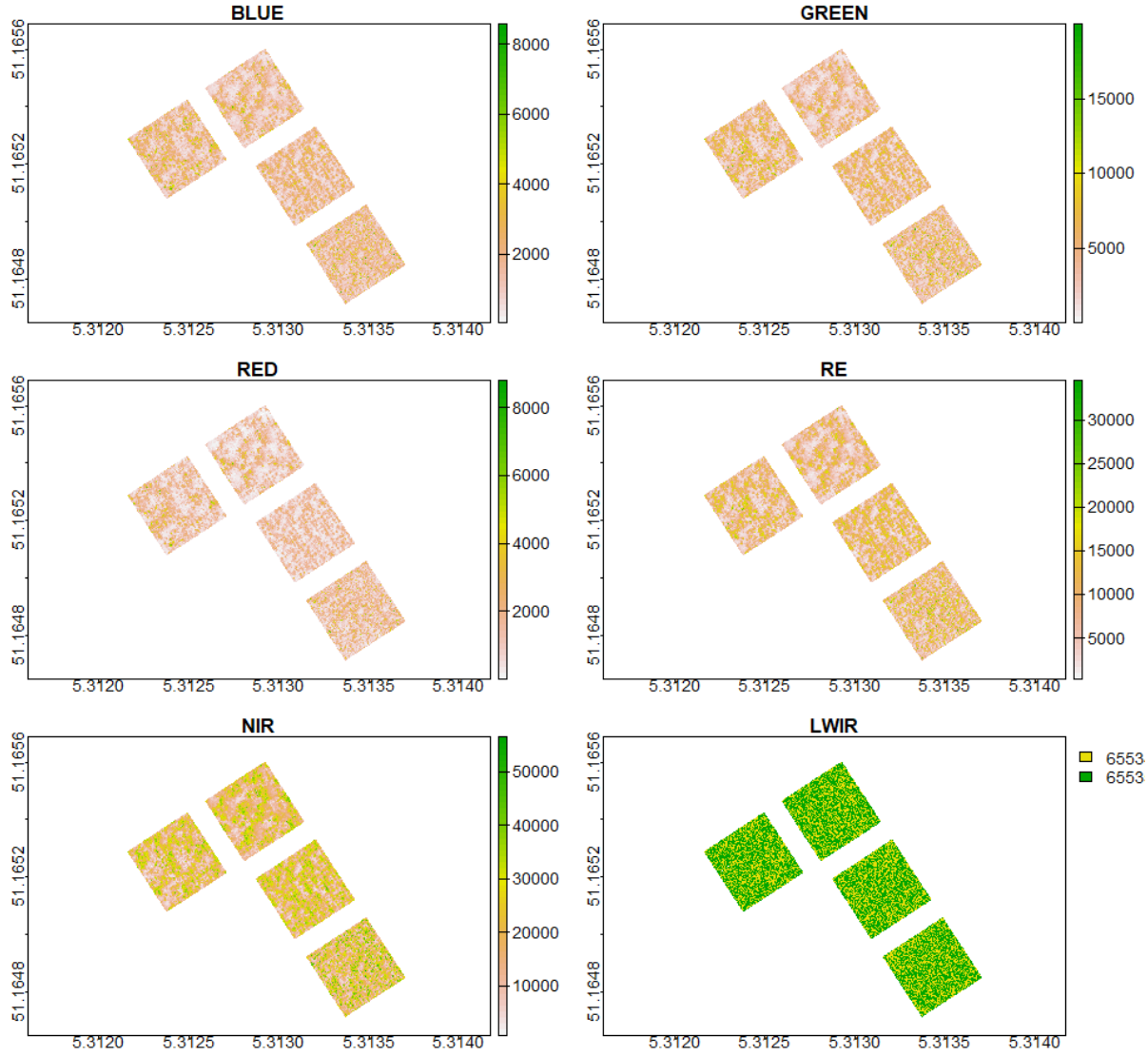

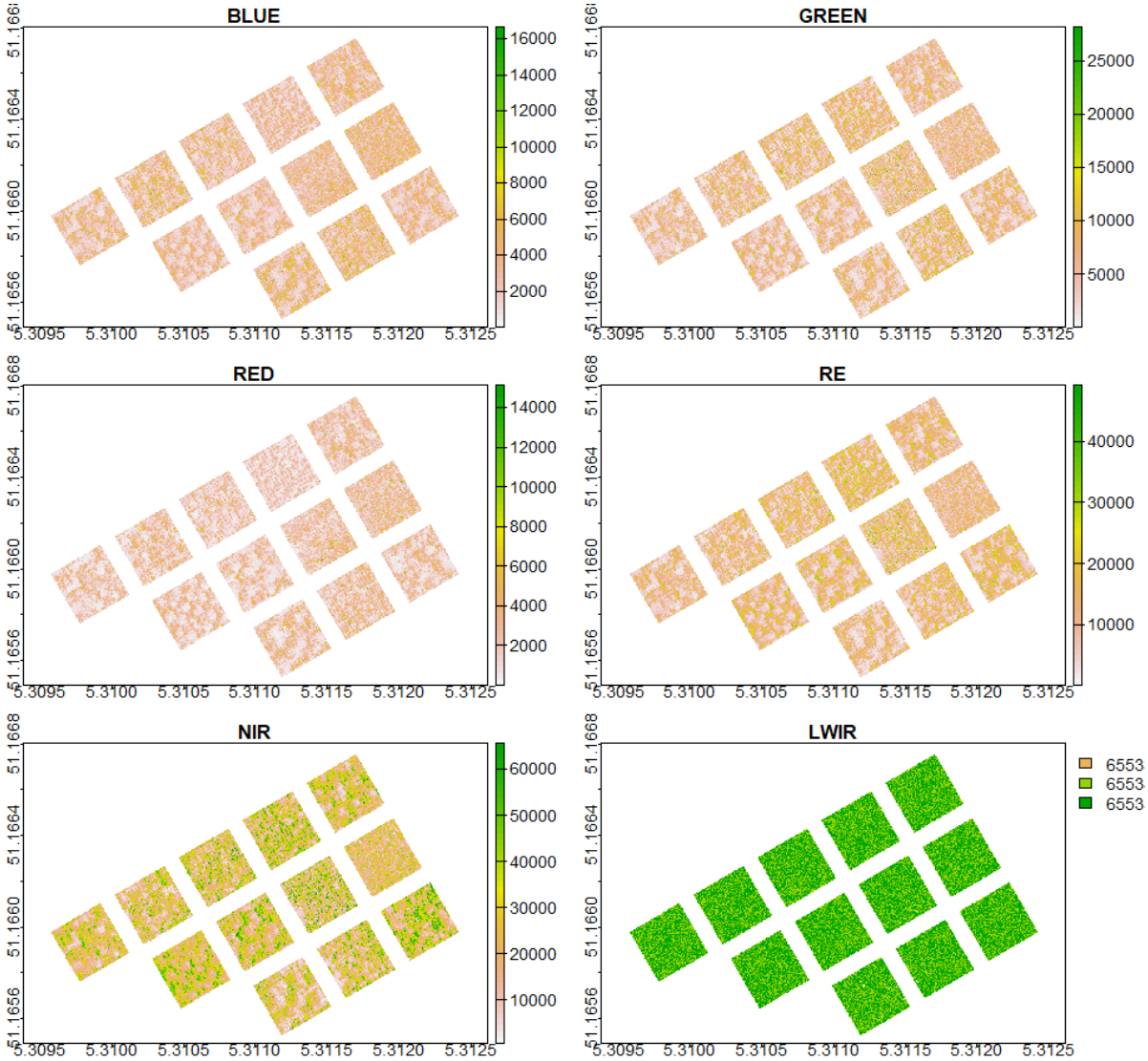
BLUE
GREEN
RED
RE
NIR
LWIR
5.3095 5.3100 5.3105 5.3110 5.3115 5.3120 5.3125
51.1668 51.1664 51.1660 51.1656
16000 14000 12000 10000 8000 6000 4000 2000
25000 20000 15000 10000 5000
14000 12000 10000 8000 6000 4000 2000
40000 30000 20000 10000
60000 50000 40000 30000 20000 10000
6553
6553
6553

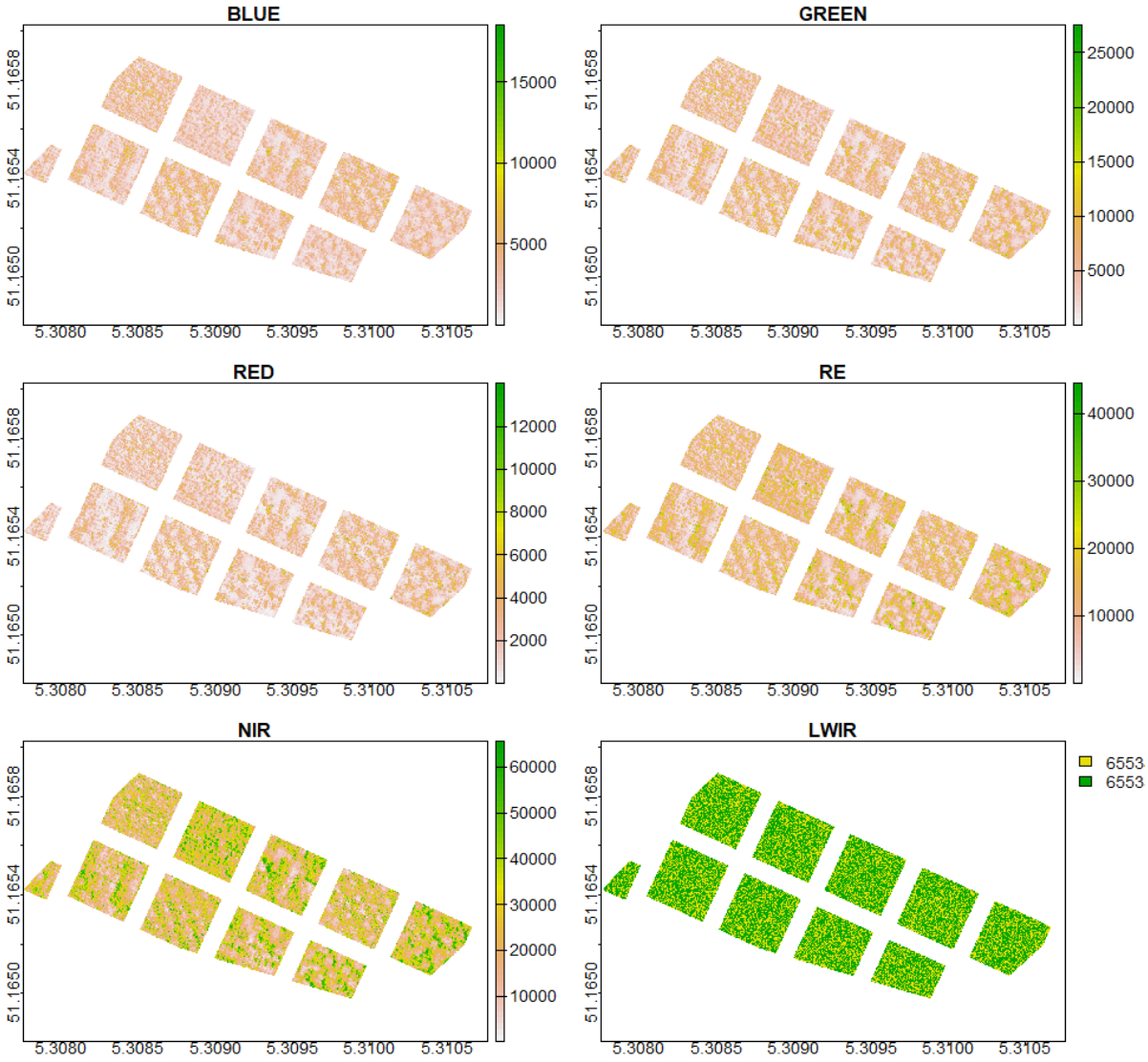
BLUE
GREEN
RED
RE
NIR
LWIR
51.1658
51.1654
51.1650
5.3080
5.3085
5.3090
5.3095
5.3100
5.3105
15000
10000
5000
25000
20000
12000
8000
6000
4000
2000
40000
30000
60000
50000
6553
6553

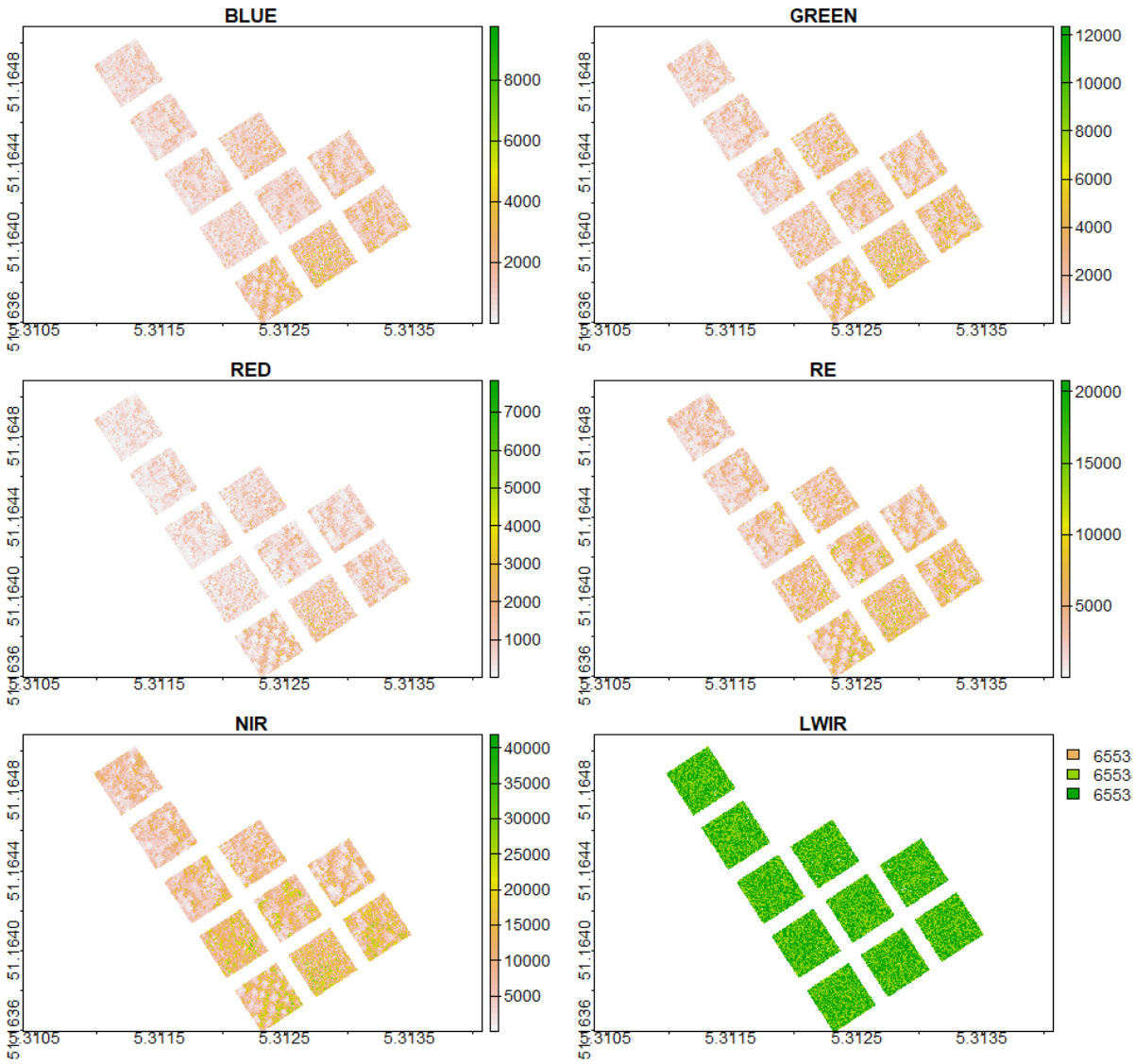
BLUE
GREEN
RED
RE
NIR
LWIR
51.1648
51.1644
51.1640
51.1636
5.3105
5.3115
5.3125
5.3135
8000
6000
4000
2000
12000
10000
7000
5000
1000
20000
15000
40000
35000
30000
25000
6553
6553
6553

Appendix VIII DTM (left) and DSM (right) in meters derived from MAPEO-preprocessed drone data. The results of four different flight missions, the ones not presented in sections 3.1 and 3.2, over the FORBIO site in Zedelgem are given (continued next page).

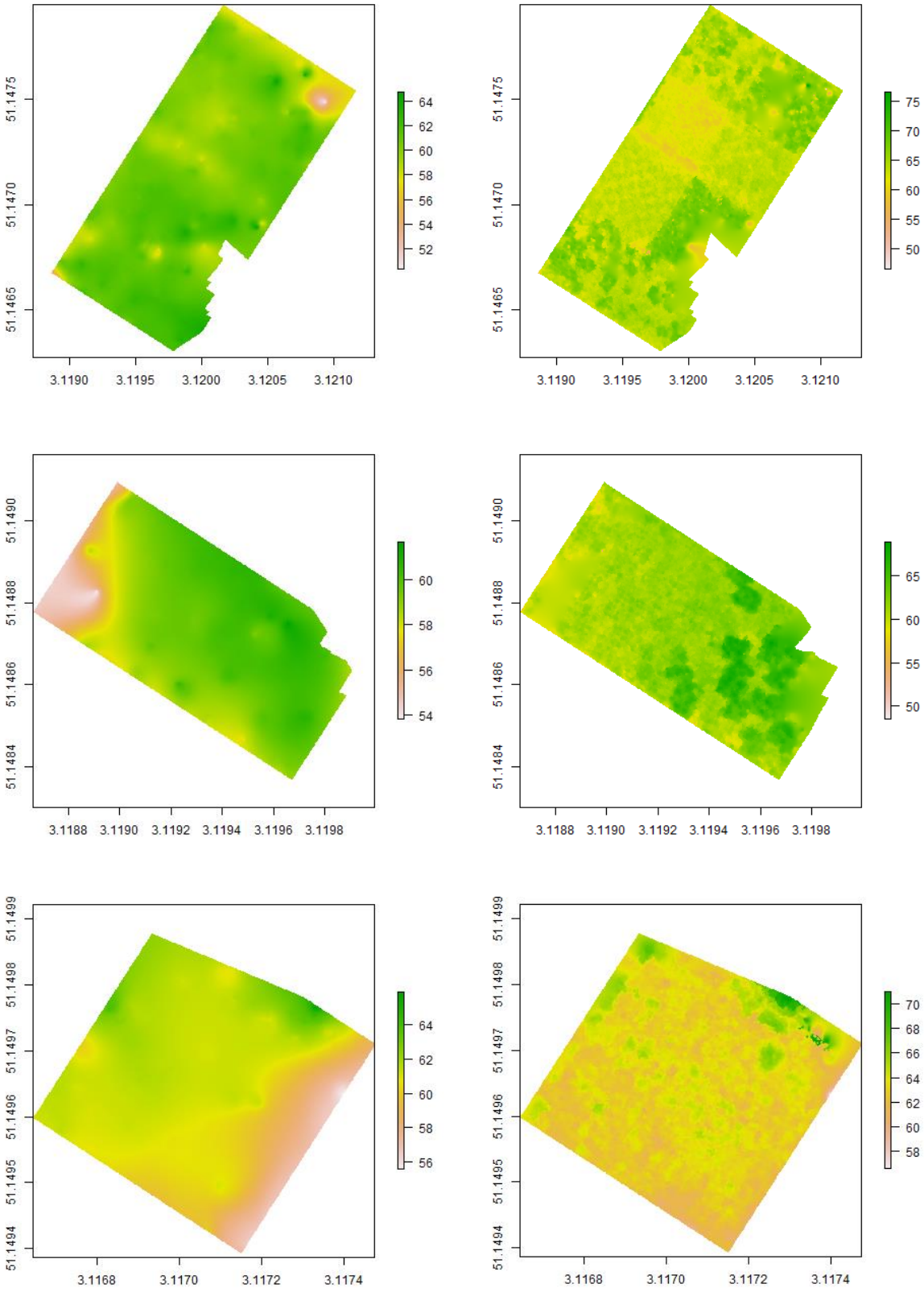

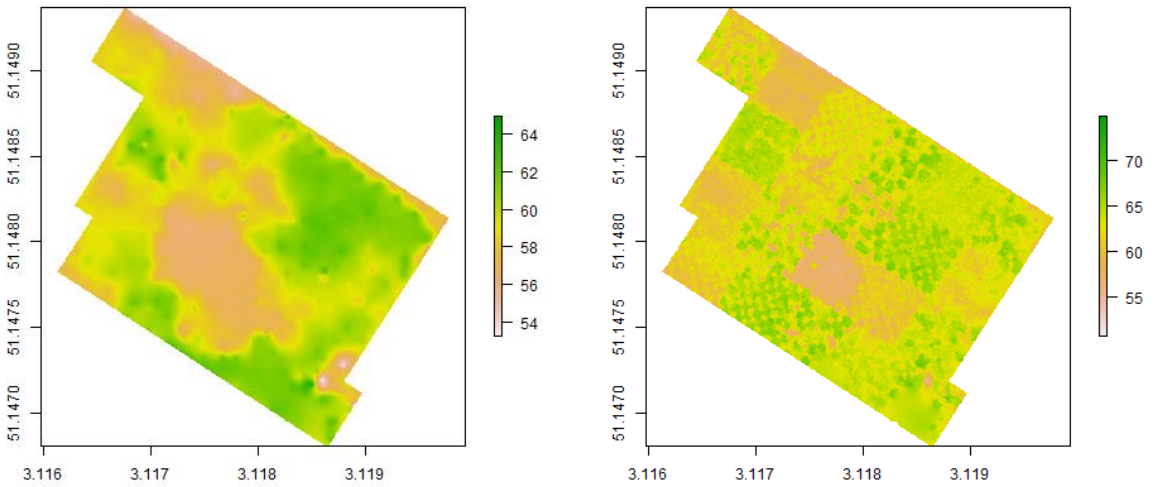

Appendix IX Mask layer (right) derived from the NDVI layer (left) where values are lower than 0.3. The results of four different flight missions, the ones not presented in sections 3.1 and 3.2, over the FORBIO site in Zedelgem are given (continued next page).

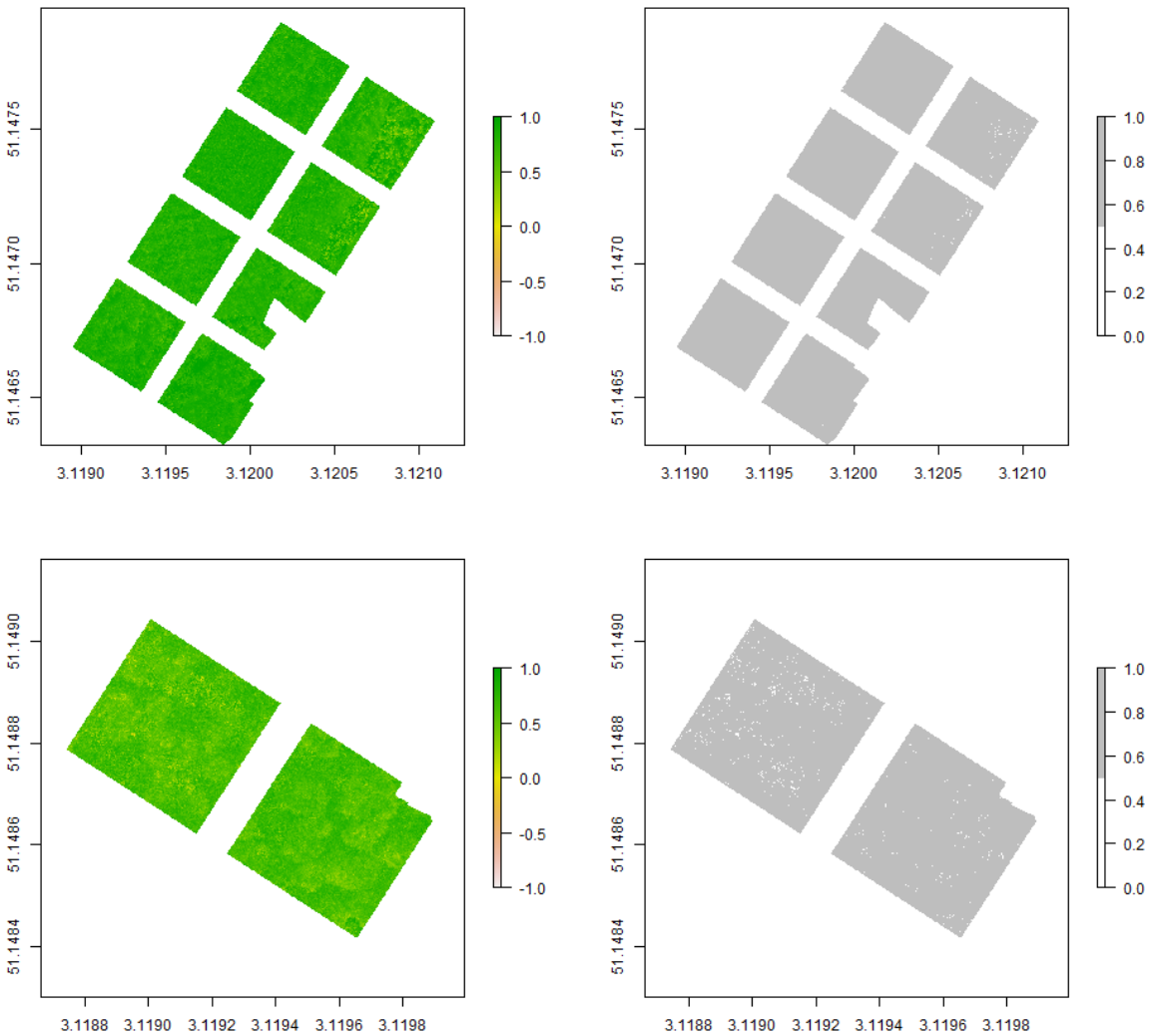

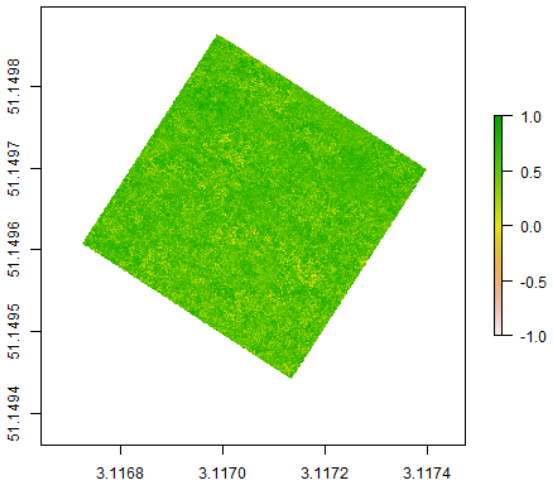
51.1498
51.1497
51.1496
51.1495
51.1494
3.1168
3.1170
3.1172
3.1174
1.0
0.5
0.0
-0.5
-1.0

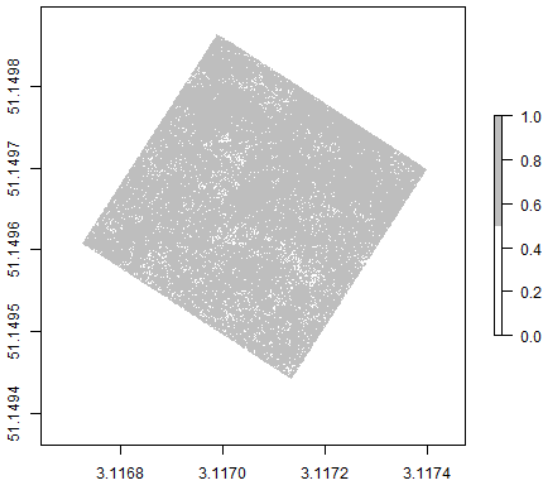
51.1498
51.1497
51.1496
51.1495
51.1494
3.1168
3.1170
3.1172
3.1174
1.0
0.8
0.6
0.4
0.2
0.0

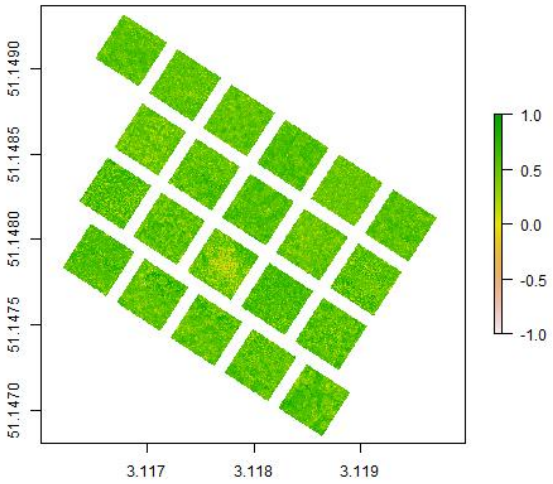
51.1490
51.1485
51.1480
51.1475
51.1470
3.117
3.118
3.119
1.0
0.5
0.0
-0.5
-1.0

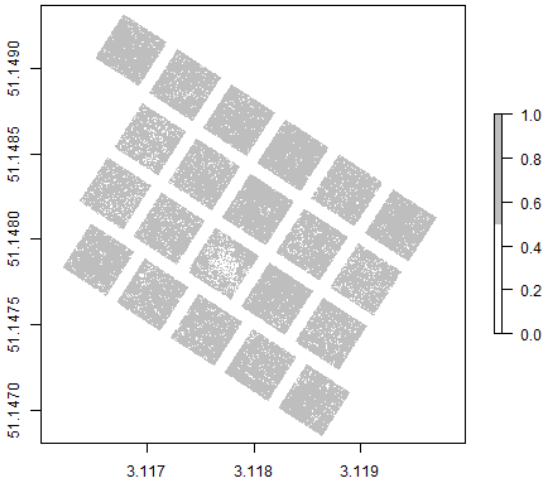
51.1490
51.1485
51.1480
51.1475
51.1470
3.117
3.118
3.119
1.0
0.8
0.6
0.4
0.2
0.0

Appendix X Plant height in meters derived by subtracting the DTM of Flanders from the MAPEO-preprocessed DSM result. The results of four different flight missions, the ones not presented in sections 3.1 and 3.2, over the FORBIO site in Zedelgem are given.

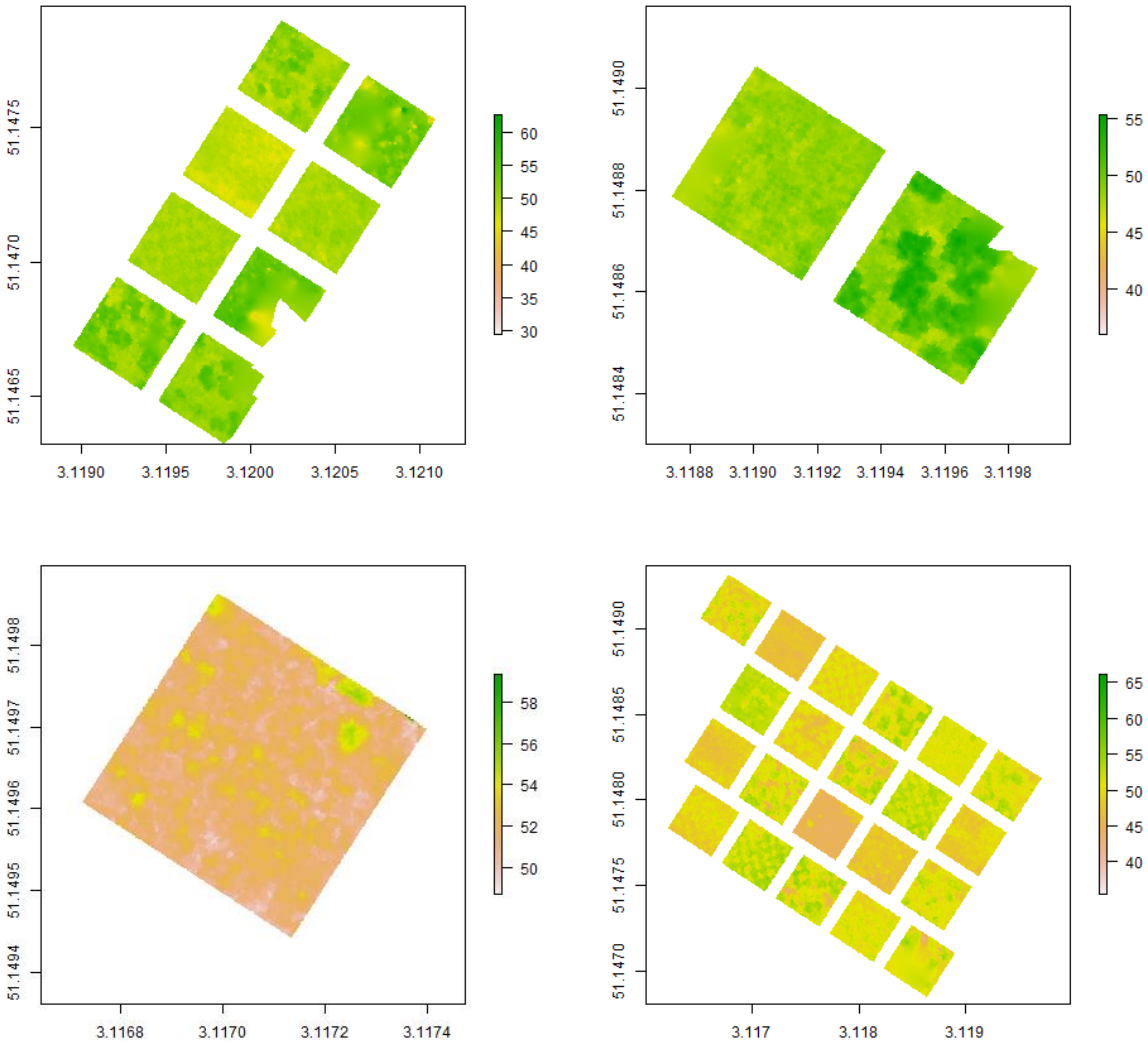

Appendix XI Reflectance drone data after clipping with size-reduced plots of the FORBIO site in Zedelgem. Six different bands are presented from left to right: blue, green, red, red edge (RE), near-infrared (NIR), longwave infrared (LWIR). The results of four different flight missions, the ones not presented in sections 3.1 and 3.2, over the FORBIO site in Zedelgem are given (continued next pages).

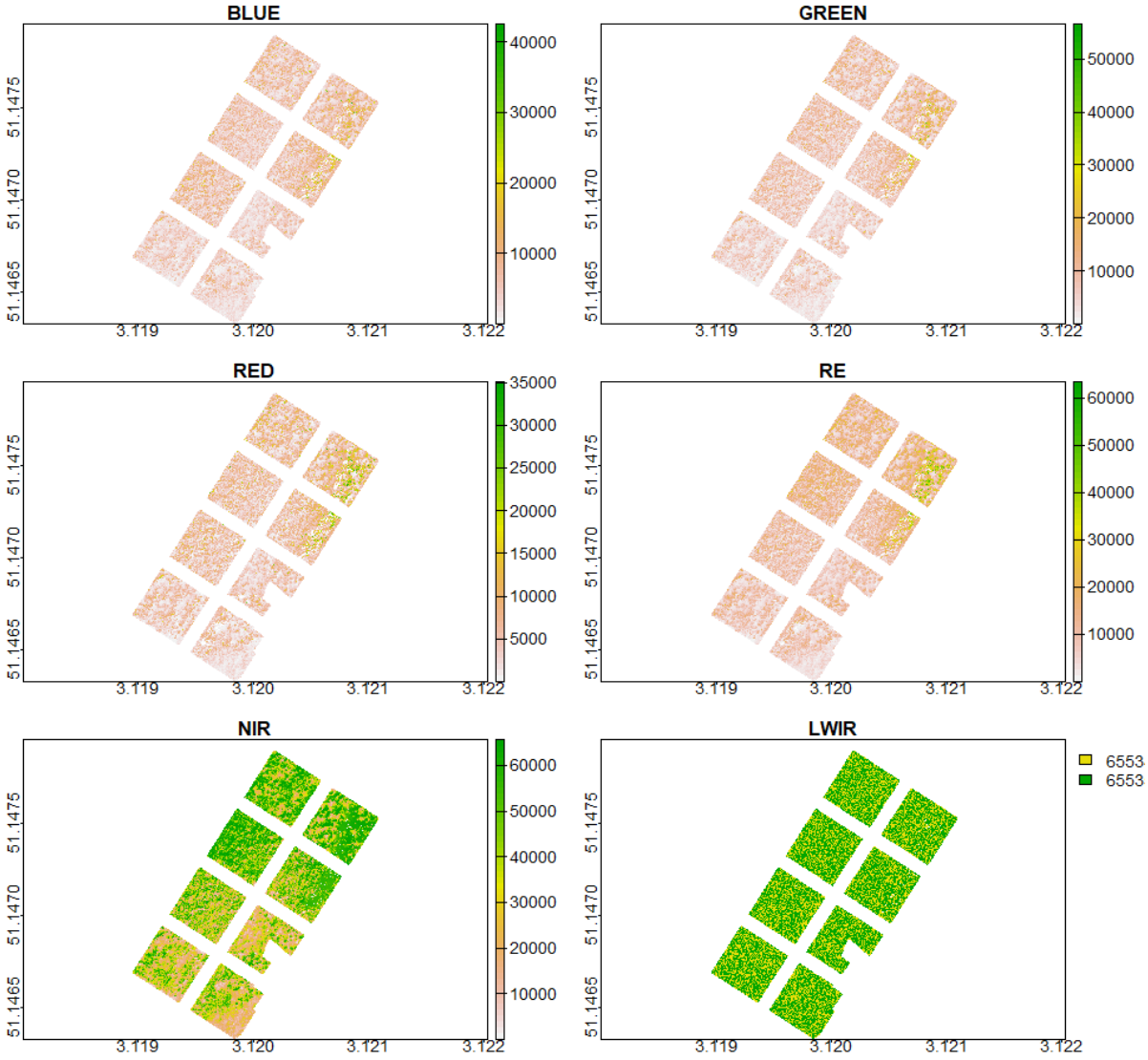

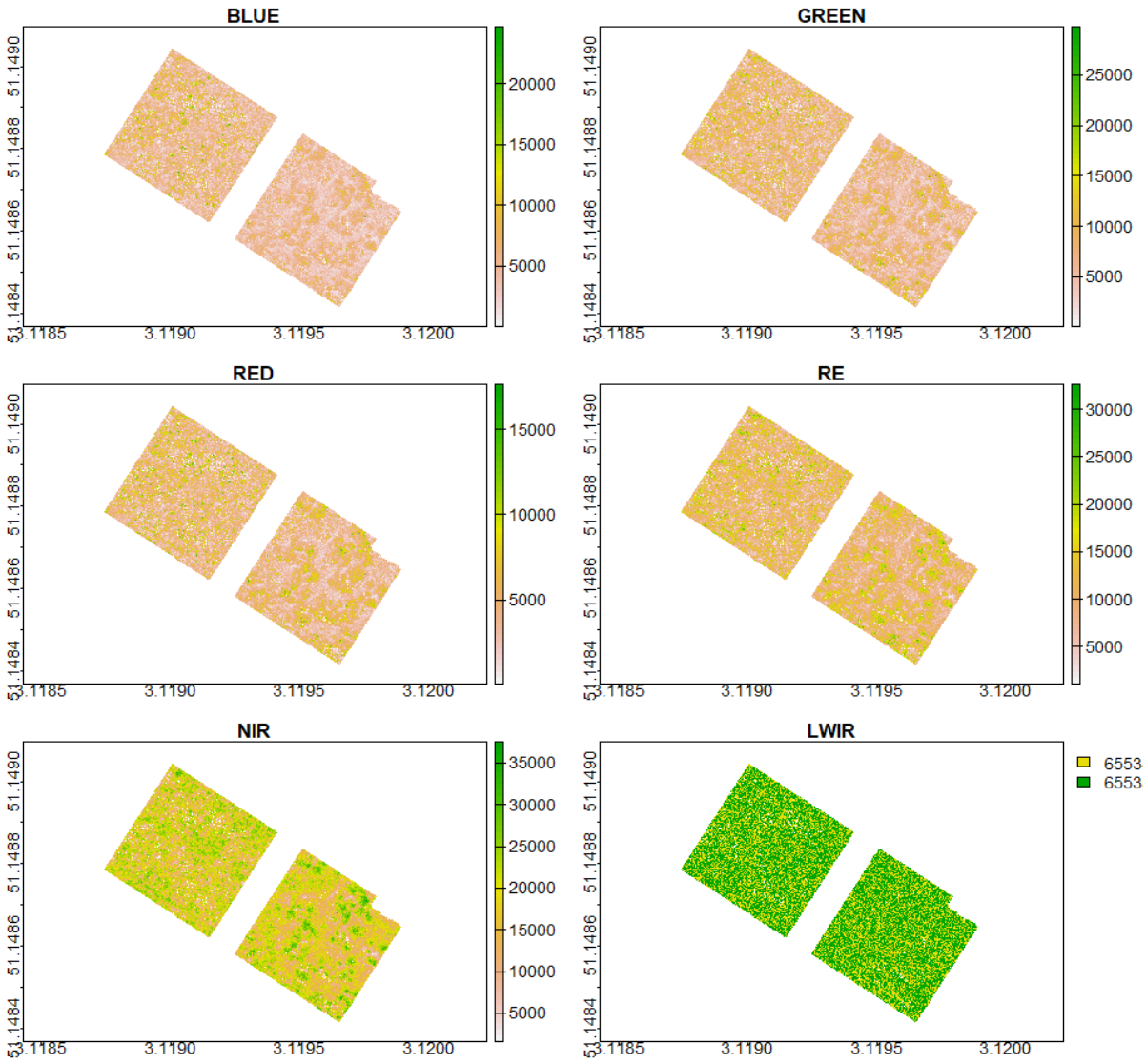
BLUE
GREEN
RED
RE
NIR
LWIR
51.1490
51.1488
51.1486
51.1484
3.1185
3.1190
3.1195
3.1200
20000
15000
10000
5000
25000
30000
35000
6553
6553

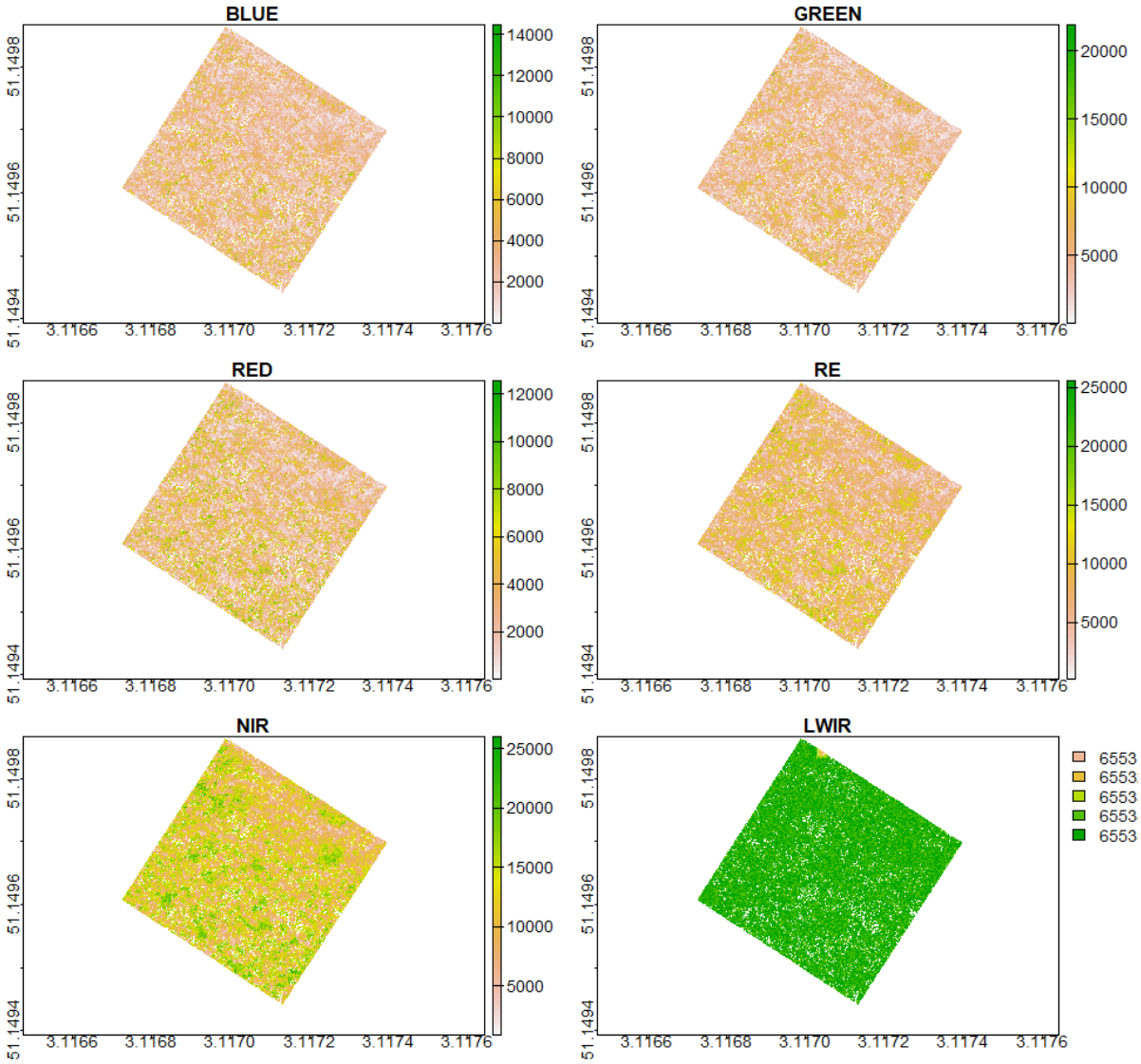
BLUE
GREEN
RED
RE
NIR
LWIR
51.1498
51.1496
51.1494
3.1166
3.1168
3.1170
3.1172
3.1174
3.1176
14000
12000
10000
8000
6000
4000
2000
20000
15000
10000
5000
12000
10000
8000
6000
4000
2000
25000
20000
15000
10000
5000
25000
20000
15000
10000
5000
6553
6553
6553
6553
6553

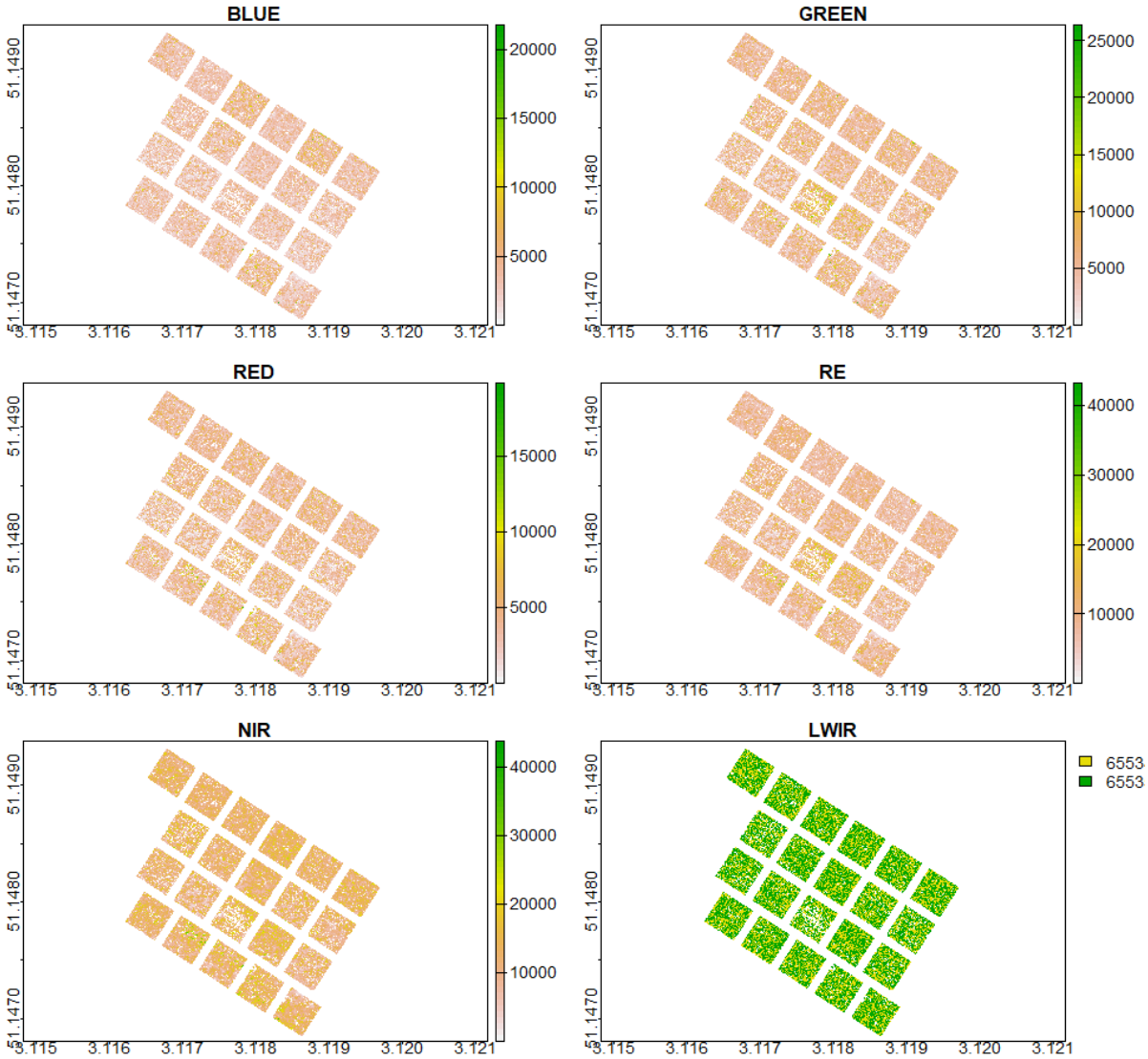
BLUE
GREEN
RED
RE
NIR
LWIR
51.1490
51.1480
51.1470
3.115
3.116
3.117
3.118
3.119
3.120
3.121
20000
15000
10000
5000
25000
40000
30000
6553
6553

Appendix XII DTM (left) and DSM (right) in meters derived from MAPEO-preprocessed drone data. The results of the five different flight missions over the FORBIO site in Gedine (three in Gribelle and two in Gouverneurs) are given (continued next page).

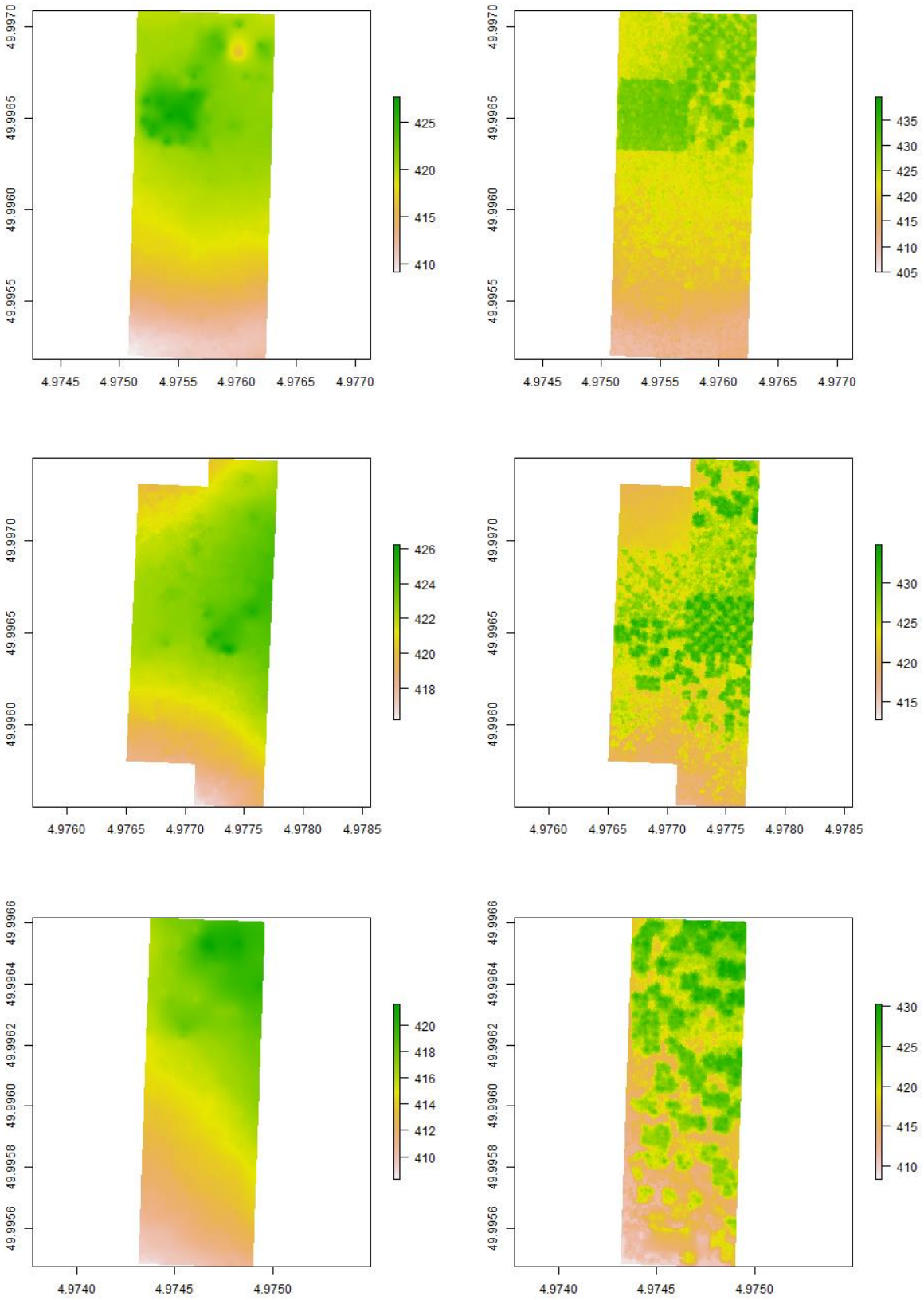

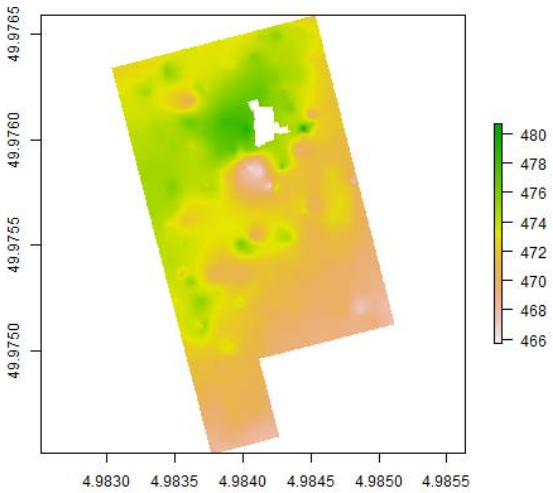
49.9765
49.9760
49.9755
49.9750
4.9830
4.9835
4.9840
4.9845
4.9850
4.9855
480
478
476
474
472
470
468
466

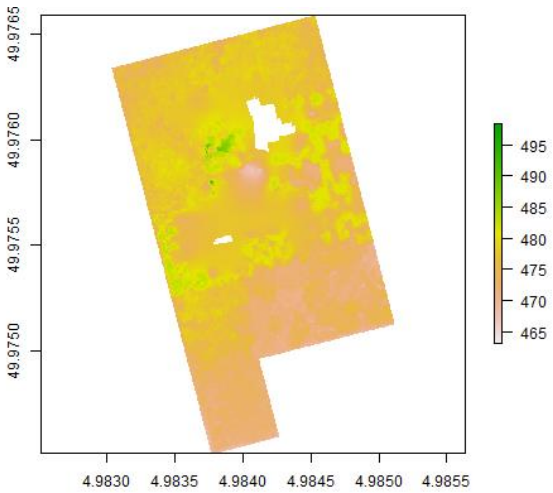
49.9765
49.9760
49.9755
49.9750
4.9830
4.9835
4.9840
4.9845
4.9850
4.9855
495
490
485
480
475
470
465

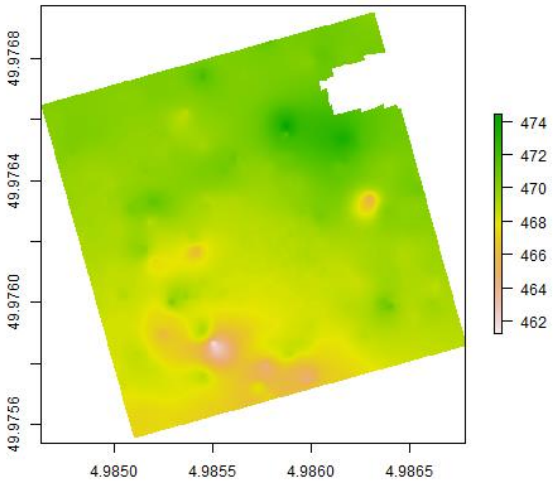
49.9768
49.9764
49.9760
49.9756
4.9850
4.9855
4.9860
4.9865
474
472
470
468
466
464
462

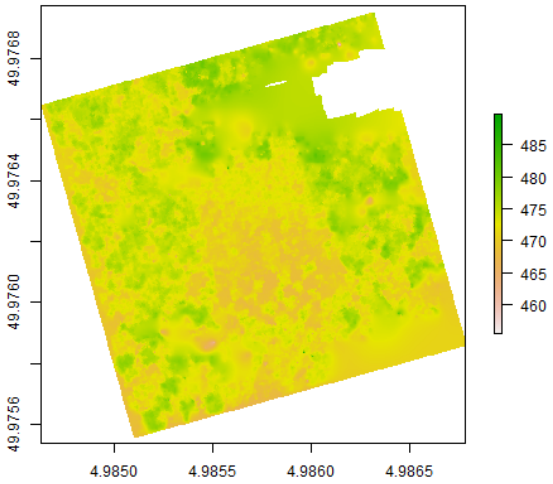
49.9768
49.9764
49.9760
49.9756
4.9850
4.9855
4.9860
4.9865
485
480
475
470
465
460

Appendix XIII Mask layer (right) derived from the NDVI layer (left) where values are lower than 0.3. The results of the five different flight missions over the FORBIO site in Gedine (three in Gribelle and two in Gouverneurs) are given (continued next page).

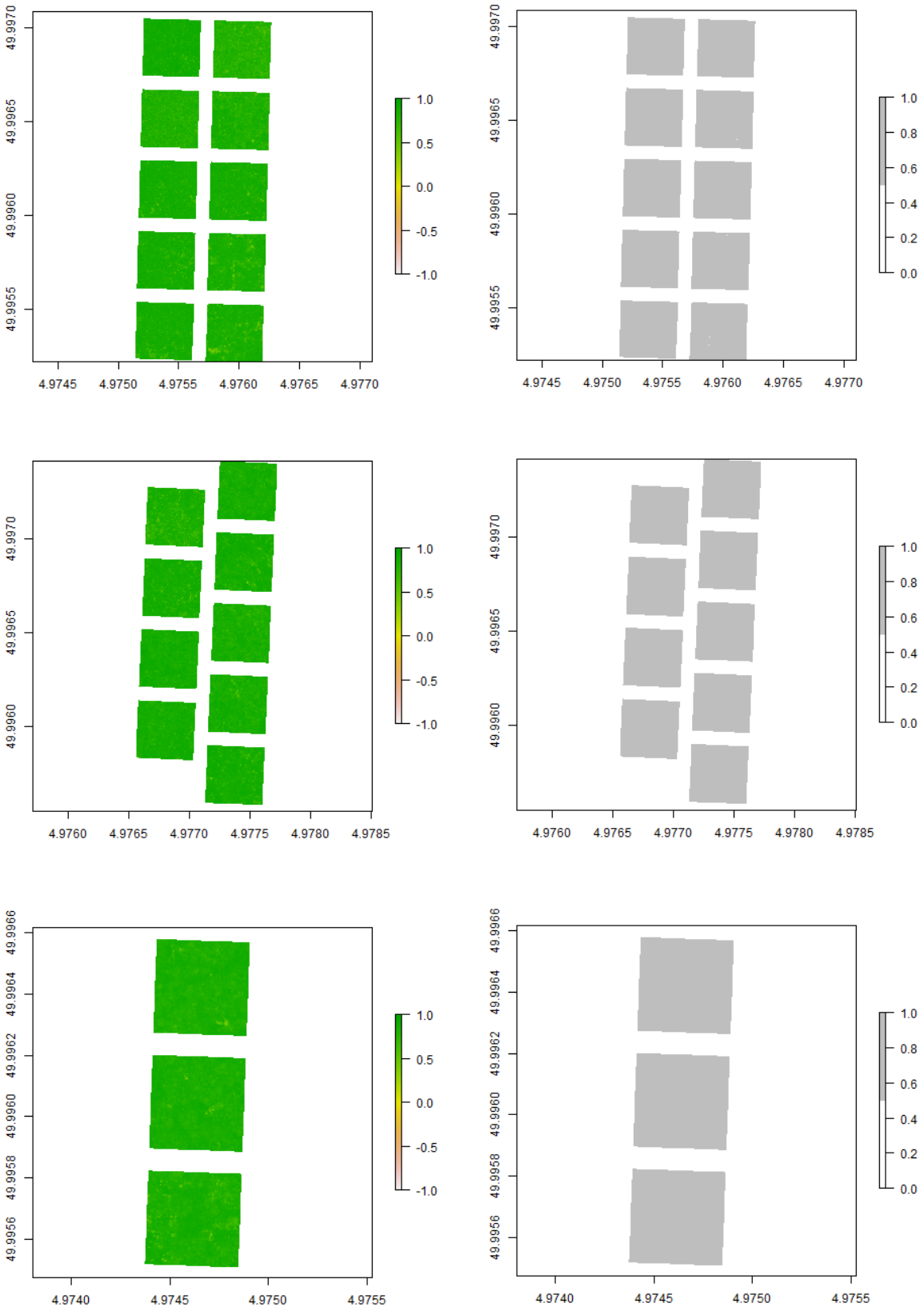

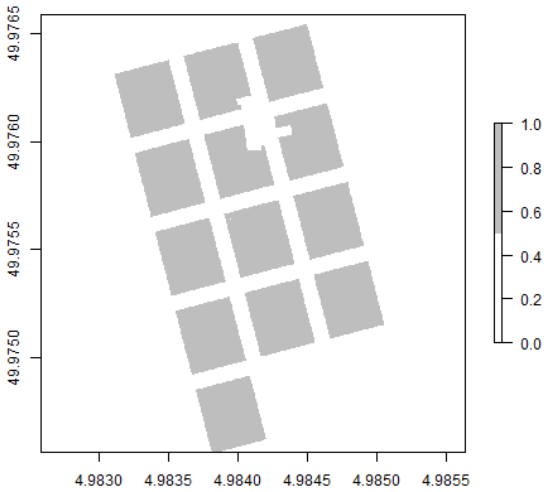
49.9765
49.9760
49.9755
49.9750
4.9830
4.9835
4.9840
4.9845
4.9850
4.9855
1.0
0.8
0.6
0.4
0.2
0.0

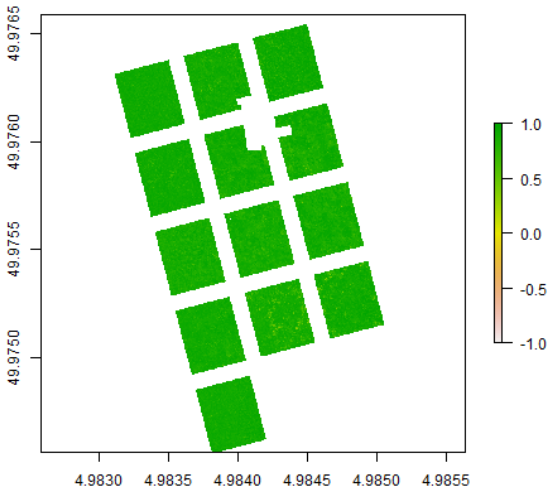
49.9765
49.9760
49.9755
49.9750
4.9830
4.9835
4.9840
4.9845
4.9850
4.9855
1.0
0.5
0.0
-0.5
-1.0

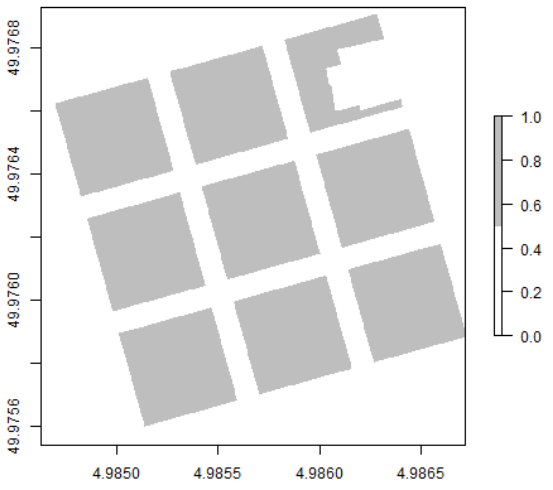
49.9768
49.9764
49.9760
49.9756
4.9850
4.9855
4.9860
4.9865
1.0
0.8
0.6
0.4
0.2
0.0

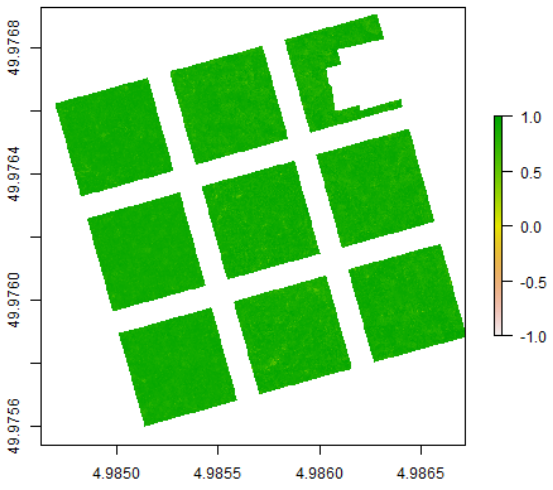
49.9768
49.9764
49.9760
49.9756
4.9850
4.9855
4.9860
4.9865
1.0
0.5
0.0
-0.5
-1.0

Appendix XIV Plant height in meters derived by subtracting the DTM of Flanders from the MAPEO-preprocessed DSM result. The results of the five different flight missions over the FORBIO site in Gedine (three in Gribelle and two in Gouverneurs) are given.

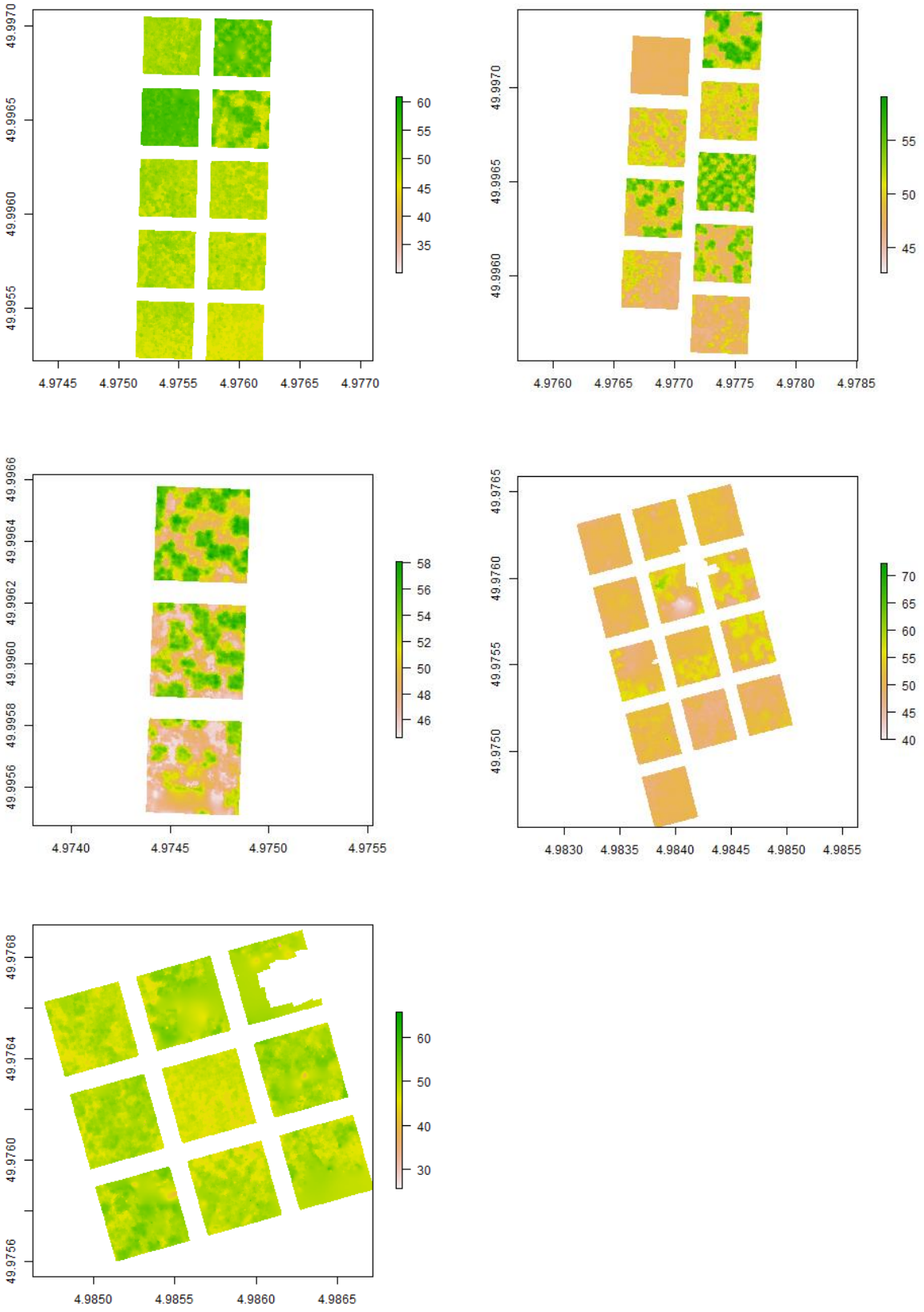

Appendix XV Reflectance drone data after clipping with size-reduced plots of the FORBIO site in Gedinne. Six different bands are presented from left to right: blue, green, red, red edge (RE), near-infrared (NIR), longwave infrared (LWIR). The results of the five different flight missions over the FORBIO site in Gedine (three in Gribelle and two in Gouverneurs) are given (continued next pages).

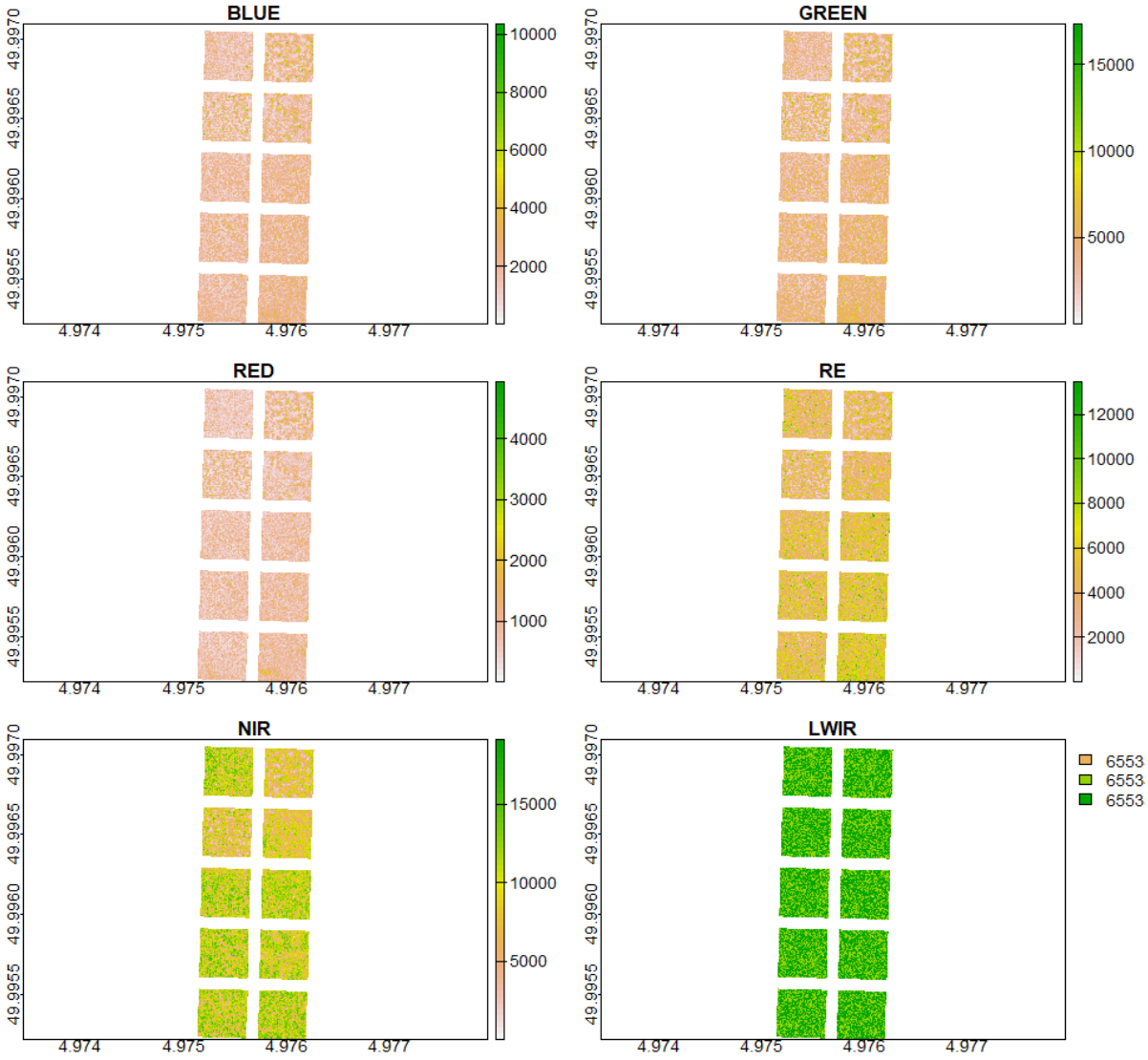

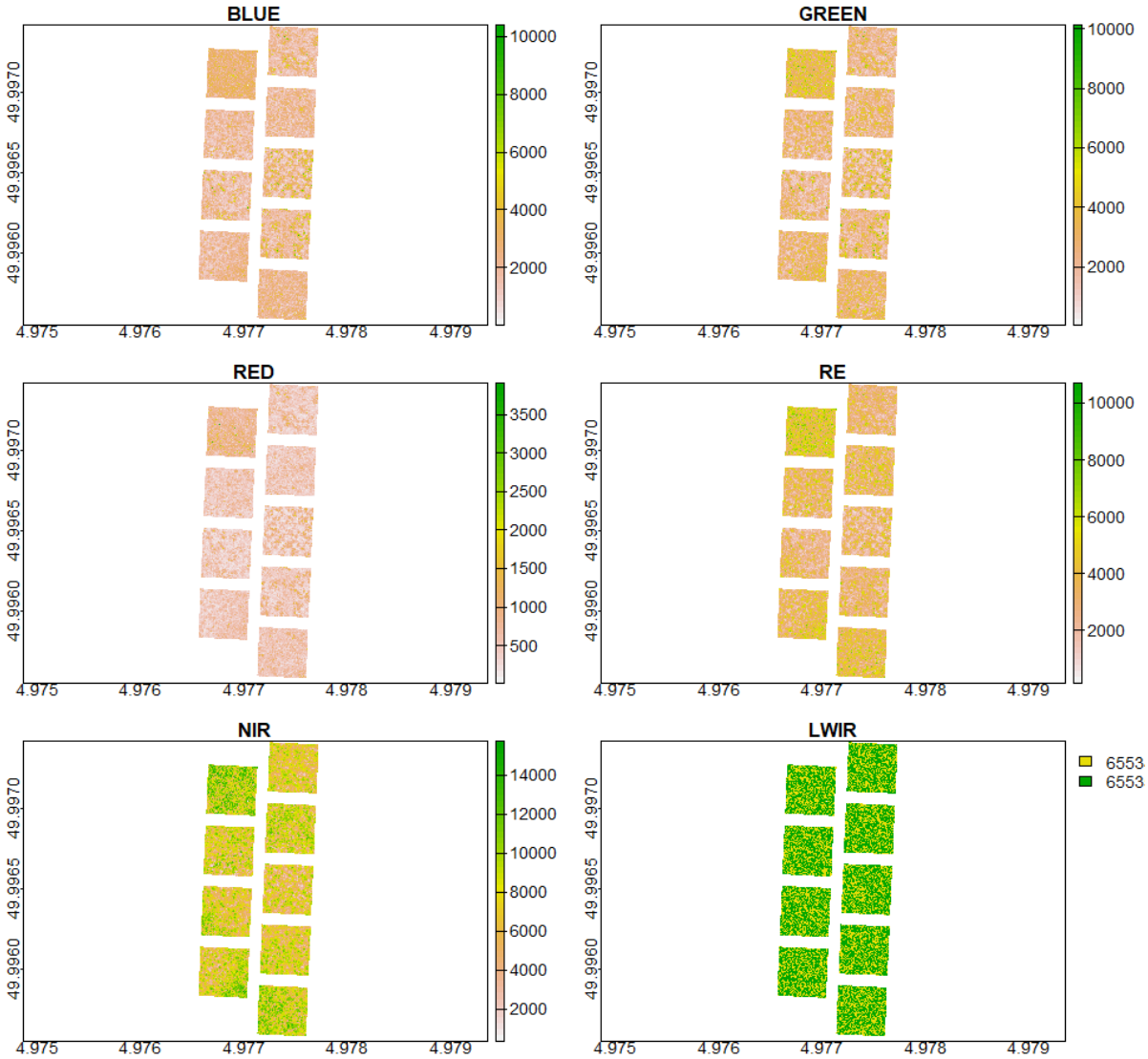
BLUE
GREEN
RED
RE
NIR
LWIR
49.9970
49.9965
49.9960
4.975
4.976
4.977
4.978
4.979
10000
8000
6000
4000
2000
3500
3000
2500
2000
1500
1000
500
14000
12000
10000
6553
6553

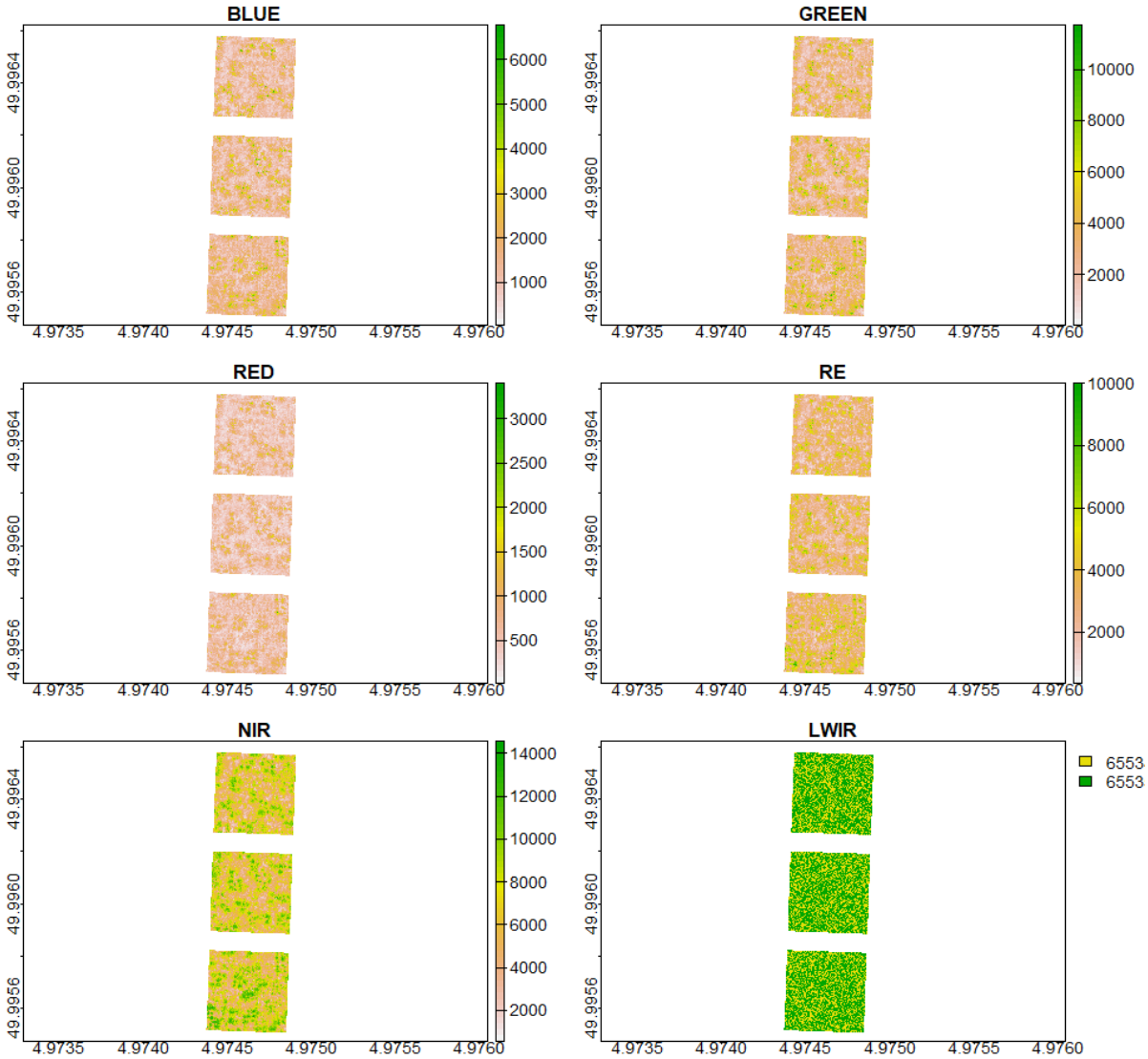
BLUE
GREEN
RED
RE
NIR
LWIR
49.9964
49.9960
49.9956
4.9735
4.9740
4.9745
4.9750
4.9755
4.9760
6000
5000
4000
3000
2000
1000
10000
8000
6000
4000
2000
3000
2500
2000
1500
1000
500
14000
12000
10000
8000
6000
4000
2000
6553
6553

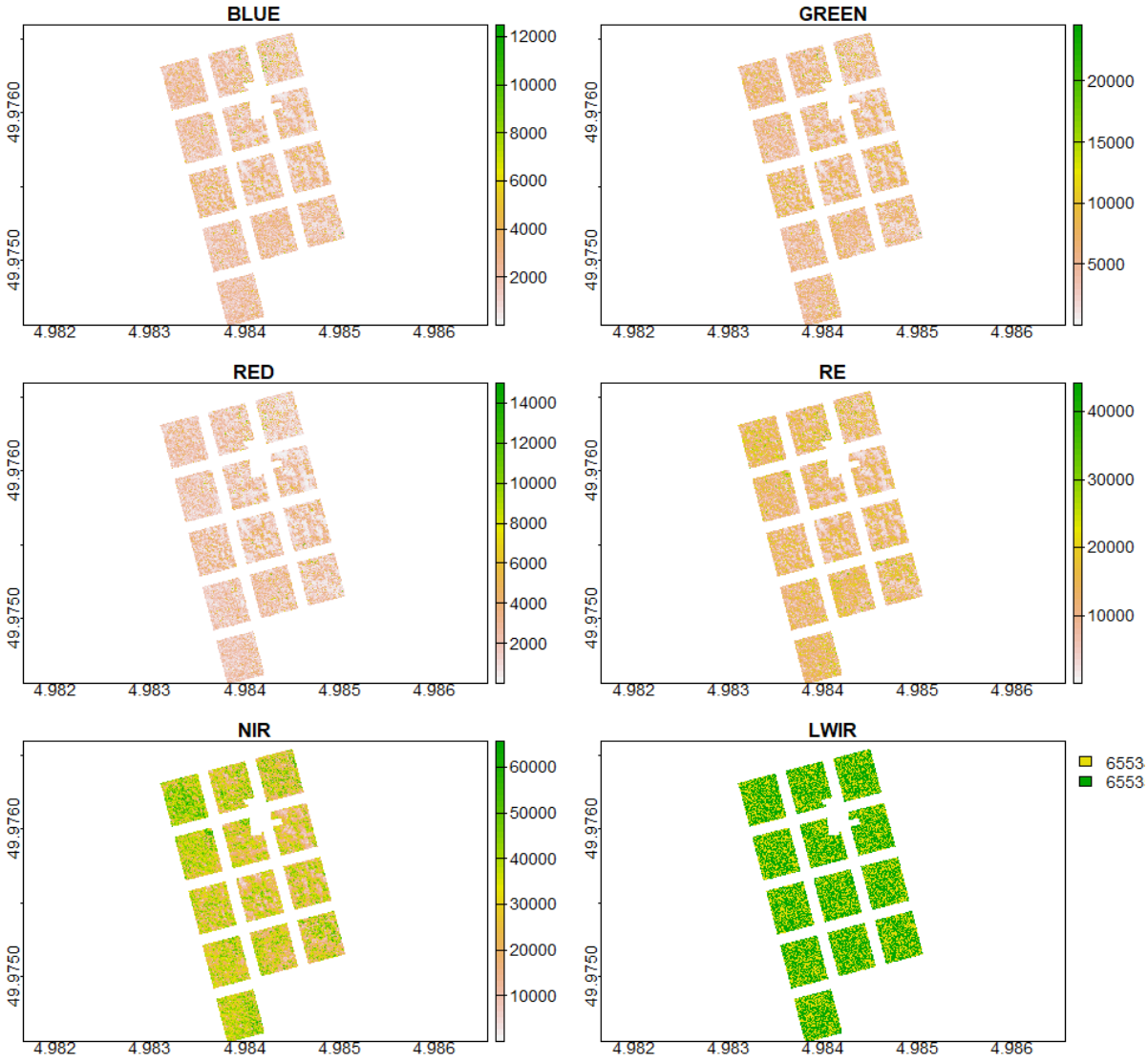
BLUE
12000
10000
8000
6000
4000
2000
GREEN
20000
15000
10000
5000
RED
14000
12000
10000
8000
6000
4000
2000
RE
40000
30000
20000
10000
NIR
60000
50000
40000
30000
20000
10000
LWIR
6553
6553
49.9760
49.9750
4.982
4.983
4.984
4.985
4.986

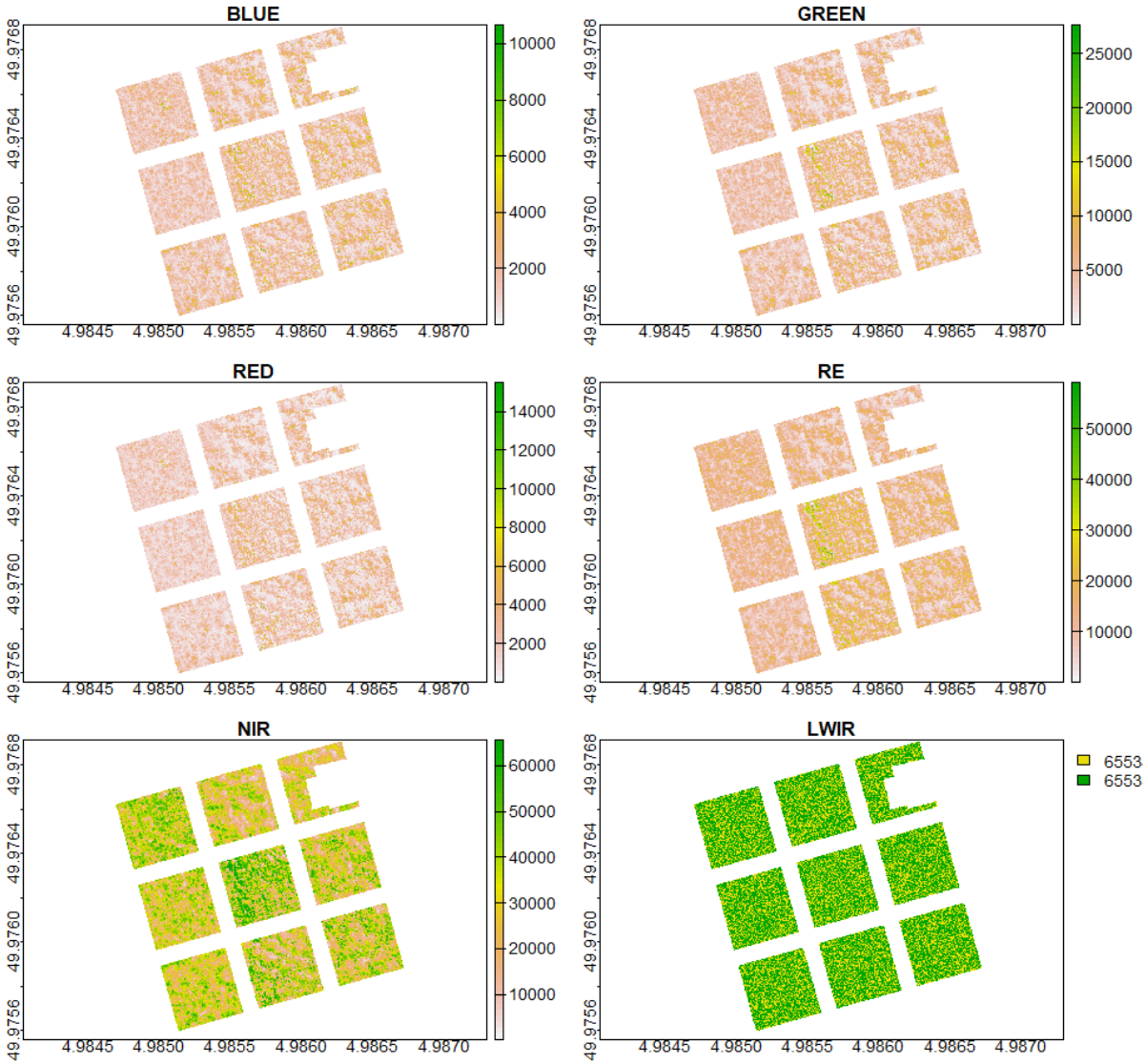
BLUE
GREEN
RED
RE
NIR
LWIR
49.9768
49.9764
49.9760
49.9756
4.9845
4.9850
4.9855
4.9860
4.9865
4.9870
10000
8000
6000
4000
2000
25000
20000
15000
10000
5000
14000
12000
10000
8000
6000
4000
2000
50000
40000
30000
20000
10000
60000
50000
40000
30000
20000
10000
6553
6553

Appendix XVI Absolute value of correlation between the different variables. The values higher than 0.7 are given in bold.

		Mean								sd								cv							
		Blue	Green	Red	NIR	RE	LWIR	NDVI	PH	Blue	Green	Red	NIR	RE	LWIR	NDVI	PH	Blue	Green	Red	NIR	RE	LWIR	NDVI	PH
Mean	Blue	**1.00**	**0.82**	**0.90**	0.40	0.48	0.51	0.48	0.10	**0.93**	**0.74**	**0.84**	0.29	0.41	0.42	0.43	0.21	0.11	0.11	0.18	0.23	0.10	0.42	0.44	0.00
	Green		**1.00**	**0.80**	0.64	**0.83**	**0.74**	0.24	0.04	**0.76**	**0.91**	**0.76**	0.55	**0.72**	0.61	0.19	0.16	0.11	0.11	0.14	0.18	0.09	0.61	0.25	0.10
	Red			**1.00**	0.48	0.59	0.46	0.58	0.23	**0.87**	**0.75**	**0.94**	0.33	0.51	0.36	0.55	0.17	0.05	0.02	0.05	0.23	0.01	0.36	0.57	0.30
	NIR				**1.00**	**0.83**	0.51	0.36	0.05	0.57	**0.78**	0.63	**0.90**	**0.85**	0.43	0.29	0.02	0.38	0.34	0.36	0.02	0.28	0.43	0.30	0.03
	RE					**1.00**	0.65	0.03	0.14	0.51	**0.85**	0.62	**0.78**	**0.93**	0.54	0.02	0.12	0.15	0.14	0.15	0.00	0.13	0.54	0.03	0.02
	LWIR						**1.00**	0.02	0.12	0.44	0.63	0.43	0.44	0.53	**0.85**	0.11	0.14	0.23	0.28	0.27	0.28	0.27	0.85	0.01	0.03
	NDVI							**1.00**	0.27	0.29	0.05	0.36	0.43	0.17	0.03	**0.87**	0.22	0.28	0.30	0.38	0.28	0.29	0.03	**0.94**	0.38
	PH								**1.00**	0.10	0.11	0.18	0.28	0.26	0.02	0.05	0.34	0.01	0.21	0.25	0.57	0.39	0.02	0.14	0.46
sd	Blue									**1.00**	**0.83**	**0.93**	0.49	0.55	0.35	0.35	0.13	0.24	0.22	0.15	0.04	0.19	0.35	0.31	0.16
	Green										**1.00**	**0.83**	**0.77**	**0.88**	0.52	0.14	0.09	0.27	0.29	0.25	0.11	0.28	0.52	0.13	0.05
	Red											**1.00**	0.52	0.63	0.33	0.44	0.11	0.29	0.27	0.21	0.08	0.22	0.33	0.41	0.20
	NIR												**1.00**	**0.91**	0.38	0.29	0.01	0.52	0.55	0.56	0.39	0.54	0.38	0.33	0.25
	RE													**1.00**	0.45	0.05	0.08	0.41	0.44	0.44	0.29	0.44	0.45	0.06	0.18
	LWIR														**1.00**	0.16	0.16	0.22	0.24	0.22	0.22	0.22	**1.00**	0.06	0.11
	NDVI															**1.00**	0.25	0.04	0.00	0.08	0.01	0.02	0.16	**0.96**	0.21
	PH																**1.00**	0.16	0.08	0.06	0.02	0.01	0.16	0.23	**0.73**
cv	Blue																	**1.00**	**0.94**	**0.94**	0.59	**0.85**	0.22	0.15	0.21
	Green																		**1.00**	**0.97**	**0.77**	**0.96**	0.24	0.14	0.32
	Red																			**1.00**	**0.75**	**0.95**	0.22	0.22	0.32
	NIR																				**1.00**	**0.88**	0.22	0.13	0.52
	RE																					**1.00**	0.22	0.12	0.38
	LWIR																						**1.00**	0.06	0.11
	NDVI																							**1.00**	0.28
	PH																								**1.00**

Appendix XVII For the plots at the FORBIO site in Hechtel-Eksel, represented by plot ID, the number of species and the number of trees per species are given.

Plot ID	No. species	No. Scots pine	No. sessile oak	No. silver birch	No. Douglas fir	No. Japanese larch	Total No. trees
1	1	0	0	576	0	0	576
2	3	192	0	192	192	0	576
3	2	288	0	0	288	0	576
4	2	0	288	288	0	0	576
6	4	144	144	144	0	144	576
7	2	288	288	0	0	0	576
8	4	144	0	144	144	144	576
10	4	0	144	144	144	144	576
11	1	0	0	0	576	0	576
12	1	0	576	0	0	0	576
13	3	0	192	0	192	192	576
14	3	192	192	0	0	192	576
15	4	144	144	0	144	144	576
16	1	0	0	0	0	576	576
17	3	0	192	192	192	0	576
18	1	576	0	0	0	0	576
19	3	192	0	192	0	192	576
20	4	144	144	144	144	0	576
21	4	144	144	144	0	144	576
22	1	0	0	576	0	0	576
23	2	288	0	0	288	0	576
25	3	192	0	192	0	192	576
26	1	576	0	0	0	0	576
27	4	0	144	144	144	144	576
29	1	0	0	0	576	0	576
30	1	0	576	0	0	0	576
31	1	0	0	0	0	576	576
33	3	0	192	0	192	192	576
34	3	0	192	192	192	0	576
35	3	192	192	0	0	192	576
37	4	144	144	0	144	144	576
38	2	0	288	288	0	0	576
40	3	192	0	192	192	0	576

Appendix XVIII For the plots at the FORBIO site in Hechtel-Eksel, represented by plot ID, the mean and standard deviation (sd) of different reflectance bands are given: blue, green, red, red edge (RE), near infrared (NIR) and longwave infrared (LWIR). These values are a result after clipping with the reduced plot sizes, correcting for the alpha band and applying the mask layer to eliminate dead or unhealthy vegetation pixels.

Plot ID	Blue	Green	Red	RE	NIR	LWIR	Blue sd	Green sd	Red sd	RE sd	NIR sd	LWIR sd
1	2092	4167	1717	10706	30120	65535	1305	2736	1286	6136	12528	0.49
2	2418	4138	1716	9259	24985	65535	1714	3033	1441	6464	14293	0.49
3	3036	4709	2080	8930	21526	65535	2026	3348	1610	5980	12627	0.49
4	2345	4626	2081	10985	27676	65535	1503	3247	1617	6999	14016	0.49
6	2335	4036	1646	8705	22886	65535	1724	3127	1436	6347	13652	0.49
7	2976	4632	1961	8979	23085	65535	2139	3466	1642	6123	12768	0.49
8	2322	4287	1669	9076	22537	65535	1708	3264	1440	6612	13999	0.49
10	1383	3062	1073	6653	18026	65535	921	2121	896	4140	8916	0.49
11	1511	3880	1030	8199	19386	65535	872	2393	701	4674	9293	0.49
12	1638	3891	1357	8051	19687	65535	974	2604	945	4880	10428	0.49
13	1641	3938	1243	7557	17341	65535	1043	2597	934	4593	9329	0.49
14	1135	1589	596	2791	6741	65535	841	1318	519	2296	5048	0.50
15	1389	2243	757	4199	10621	65535	1008	1703	632	2999	6467	0.50
16	1131	1890	624	3154	6939	65535	808	1448	515	2238	4564	0.50
17	894	1713	566	3762	9085	65535	651	1391	544	2943	6166	0.50
18	1869	2580	1035	4667	11660	65535	1270	1870	826	3141	6643	0.50
19	707	1051	374	2103	5907	65535	517	837	338	1613	3684	0.50
20	759	1136	423	2236	5781	65535	593	936	410	1802	3785	0.50
21	810	1288	460	2607	7000	65535	651	1103	460	2191	4763	0.50
22	778	1498	502	3663	11279	65535	584	1189	474	2630	5815	0.50
23	1501	1995	819	3690	9989	65535	1133	1632	757	2987	6944	0.50
25	2826	4754	2028	10127	23132	65535	1765	3169	1411	6334	12933	0.49
26	3441	5193	2415	9701	20359	65535	1967	3168	1594	5471	10881	0.49
27	2555	4878	1803	11143	28071	65535	1681	3471	1405	7180	14935	0.49
29	2261	5609	1393	12290	25960	65535	1371	3721	999	7624	14214	0.49
30	2916	5813	2150	11859	24530	65535	1696	4187	1609	8130	15582	0.49
31	3354	5879	2202	10353	22218	65535	2203	4206	1600	6844	13913	0.49
33	2583	5377	1683	10778	23574	65535	1733	3823	1275	7012	13404	0.49
34	2266	4500	1661	10444	24691	65535	1505	3243	1382	7013	13700	0.49
35	3048	4615	1991	8545	19287	65535	2128	3419	1603	6110	12907	0.49
37	2963	4871	1942	9358	21148	65535	2081	3529	1509	6332	13034	0.49
38	2318	4334	1788	10487	27032	65535	1497	3023	1410	6521	12530	0.49
40	2534	4027	1658	8540	21816	65535	1785	2855	1330	5594	12044	0.49

Appendix XIX For the plots at the FORBIO site in Hechtel-Eksel, represented by plot ID, the correlation of variance (cv) of different reflectance bands are given: blue, green, red, red edge (RE), near infrared (NIR) and longwave infrared (LWIR). The mean, standard deviation (sd) and cv of the NDVI and the corrected plant height (PH) are presented as well. These values are a result after clipping with the reduced plot sizes, correcting for the alpha band and applying the mask layer to eliminate dead or unhealthy vegetation pixels.

Plot ID	Blue cv	Green cv	Red cv	RE cv	NIR cv	LWIR cv	NDVI	NDVI sd	NDVI cv	PH	PH sd	PH cv
1	0.62	0.66	0.75	0.57	0.42	0.00	0.90	0.05	0.06	8.39	0.83	0.10
2	0.71	0.73	0.84	0.70	0.57	0.00	0.88	0.06	0.07	7.03	1.41	0.20
3	0.67	0.71	0.77	0.67	0.59	0.00	0.83	0.08	0.10	5.93	1.00	0.17
4	0.64	0.70	0.78	0.64	0.51	0.00	0.86	0.07	0.09	6.08	1.85	0.30
6	0.74	0.77	0.87	0.73	0.60	0.00	0.87	0.07	0.08	6.40	1.46	0.23
7	0.72	0.75	0.84	0.68	0.55	0.00	0.86	0.07	0.08	6.25	0.97	0.15
8	0.74	0.76	0.86	0.73	0.62	0.00	0.87	0.07	0.08	6.41	1.54	0.24
10	0.67	0.69	0.83	0.62	0.49	0.00	0.89	0.07	0.08	6.18	1.62	0.26
11	0.58	0.62	0.68	0.57	0.48	0.00	0.91	0.03	0.04	5.45	0.84	0.15
12	0.59	0.67	0.70	0.61	0.53	0.00	0.86	0.08	0.10	3.33	0.81	0.24
13	0.64	0.66	0.75	0.61	0.54	0.00	0.86	0.10	0.12	4.56	1.25	0.28
14	0.74	0.83	0.87	0.82	0.75	0.00	0.81	0.15	0.18	6.30	1.65	0.26
15	0.73	0.76	0.83	0.71	0.61	0.00	0.87	0.07	0.09	6.65	1.24	0.19
16	0.71	0.77	0.82	0.71	0.66	0.00	0.83	0.13	0.16	5.16	1.21	0.23
17	0.73	0.81	0.96	0.78	0.68	0.00	0.89	0.07	0.08	5.94	1.93	0.33
18	0.68	0.73	0.80	0.67	0.57	0.00	0.85	0.07	0.08	7.69	0.62	0.08
19	0.73	0.80	0.90	0.77	0.62	0.00	0.88	0.09	0.10	7.71	1.48	0.19
20	0.78	0.82	0.97	0.81	0.65	0.00	0.87	0.09	0.10	6.82	1.52	0.22
21	0.80	0.86	1.00	0.84	0.68	0.00	0.89	0.09	0.10	7.15	1.81	0.25
22	0.75	0.79	0.94	0.72	0.52	0.00	0.93	0.05	0.05	10.31	0.78	0.08
23	0.75	0.82	0.92	0.81	0.70	0.00	0.86	0.06	0.07	6.73	1.30	0.19
25	0.62	0.67	0.70	0.63	0.56	0.00	0.83	0.08	0.10	5.97	1.25	0.21
26	0.57	0.61	0.66	0.56	0.53	0.00	0.78	0.09	0.12	5.65	0.48	0.09
27	0.66	0.71	0.78	0.64	0.53	0.00	0.88	0.07	0.08	5.77	1.61	0.28
29	0.61	0.66	0.72	0.62	0.55	0.00	0.90	0.05	0.05	5.19	0.91	0.18
30	0.58	0.72	0.75	0.69	0.64	0.00	0.81	0.14	0.17	3.03	0.93	0.31
31	0.66	0.72	0.73	0.66	0.63	0.00	0.80	0.12	0.15	4.54	1.09	0.24
33	0.67	0.71	0.76	0.65	0.57	0.00	0.86	0.08	0.09	4.88	1.10	0.23
34	0.66	0.72	0.83	0.67	0.55	0.00	0.88	0.07	0.08	5.69	1.86	0.33
35	0.70	0.74	0.80	0.72	0.67	0.00	0.79	0.13	0.17	5.16	1.57	0.30
37	0.70	0.72	0.78	0.68	0.62	0.00	0.82	0.11	0.13	5.38	1.35	0.25
38	0.65	0.70	0.79	0.62	0.46	0.00	0.88	0.07	0.07	6.89	1.52	0.22
40	0.70	0.71	0.80	0.66	0.55	0.00	0.86	0.06	0.07	6.41	1.36	0.21

Appendix XX For the plots at the FORBIO site in Zedelgem, represented by plot ID, the number of species and the number of trees per species are given.

Plot ID	No. species	No. common beech	No. pedunculate oak	No. silver birch	No. small-leaved lime	No. Scots pine	Total No. trees
1	4	192	0	192	196	204	784
2	1	0	0	784	0	0	784
3	3	261	259	0	0	264	784
4	2	0	0	384	0	400	784
5	2	398	0	0	386	0	784
6	4	189	199	0	204	192	784
7	3	0	261	259	264	0	784
9	3	268	0	258	0	258	784
10	2	0	0	0	400	384	784
11	1	784	0	0	0	0	784
12	4	198	201	193	192	0	784
13	1	0	0	0	784	0	784
14	2	384	400	0	0	0	784
15	1	0	784	0	0	0	784
16	4	197	192	190	0	205	784
17	2	0	384	400	0	0	784
18	3	0	259	0	264	261	784
19	3	258	0	268	258	0	784
20	4	0	189	207	199	189	784
21	1	0	784	0	0	0	784
22	4	0	198	196	189	201	784
23	4	196	198	189	201	0	784
24	3	0	268	0	258	258	784
25	2	384	0	0	400	0	784
26	2	0	0	400	0	384	784
27	1	0	0	0	0	784	784
28	3	267	252	0	0	265	784
29	4	199	0	198	195	192	784
30	1	778	0	0	0	0	778
31	3	237	0	257	234	0	728
32	3	0	223	256	249	0	728
33	2	0	400	384	0	0	784
34	3	262	0	258	0	264	784
35	4	205	192	0	192	195	784
36	2	0	0	0	384	400	784
37	2	400	384	0	0	0	784
38	1	0	784	0	0	0	784
39	1	0	0	784	0	0	784
40	1	0	0	0	784	0	784
41	4	186	211	198	0	189	784
42	1	0	784	0	0	0	784

Appendix XXI For the plots at the FORBIO site in Zedelgem, represented by plot ID, the mean and standard deviation (sd) of different reflectance bands are given: blue, green, red, red edge (RE), near infrared (NIR) and longwave infrared (LWIR). These values are a result after clipping with the reduced plot sizes, correcting for the alpha band and applying the mask layer to eliminate dead or unhealthy vegetation pixels.

Plot ID	Blue	Green	Red	RE	NIR	LWIR	Blue sd	Green sd	Red sd	RE sd	NIR sd	LWIR sd
1	2979	3597	2875	5844	29283	65535	2466	3102	2683	4428	14776	0.49
2	3279	4068	3501	6814	29167	65535	2448	3087	2672	4241	14386	0.49
3	6192	7293	5910	10606	43236	65535	4740	5468	4863	7164	15210	0.49
4	6058	8265	7244	14632	48504	65535	4598	6518	5978	10312	15795	0.49
5	762	661	563	1440	3373	65535	496	440	406	781	1331	0.50
6	1205	877	784	1627	4190	65535	792	544	531	859	1558	0.50
7	766	612	583	1333	3420	65535	547	432	453	779	1440	0.50
9	3151	3936	3405	6589	30849	65535	2439	3096	2872	4356	14985	0.49
10	5198	5657	4381	7719	37446	65535	3704	3883	3337	4599	15224	0.49
11	4370	6335	4365	10724	50415	65535	2983	4257	3280	5948	14241	0.49
12	4804	6342	5019	10551	46381	65535	3628	4640	4064	6297	15573	0.49
13	806	706	651	1575	3268	65535	478	434	415	767	1227	0.50
14	1157	916	812	1812	4611	65535	820	609	603	1016	1760	0.50
15	985	782	699	1539	3617	65535	727	529	536	852	1418	0.50
16	844	655	619	1362	3396	65535	598	447	459	760	1388	0.50
17	927	774	762	1708	4129	65535	679	576	581	1044	2052	0.51
18	1069	771	689	1441	3522	65535	733	505	486	789	1368	0.50
19	2839	4377	3332	8025	11848	65535	1609	2605	1991	3926	4481	0.49
20	2793	4045	3060	7075	10183	65535	1859	2678	2089	4034	4333	0.49
21	2974	4568	3166	7390	10647	65535	1693	2651	1931	3710	4129	0.49
22	3368	4870	3677	7860	12646	65535	1780	2469	1848	3247	4180	0.49
23	4218	6151	4220	10231	17839	65535	2092	3140	2181	4093	5215	0.49
24	3996	5345	3928	8394	13032	65535	2377	3083	2370	4277	4788	0.49
25	2834	5094	3347	9667	12725	65535	1747	3211	2247	5089	4814	0.49
26	3165	4592	3619	7852	11121	65535	1635	2466	1846	3788	4739	0.49
27	4492	5264	4021	6973	11677	65535	2412	2745	2019	3117	4120	0.49
28	5373	7204	4641	10457	18195	65535	2966	3690	2480	4316	5372	0.49
29	3215	4598	3539	7932	11706	65535	1845	2673	2119	4245	4829	0.49
30	3315	6815	3989	11327	12535	65535	1768	3805	2334	5641	5084	0.49
31	2977	4589	3285	8157	11863	65535	1512	2431	1888	3748	4190	0.49
32	3135	4746	3542	8182	13129	65535	1483	2275	1791	3198	3960	0.49
33	3076	4751	3730	8677	12345	65535	1846	3061	2424	5025	5659	0.49
34	2759	3959	3029	6947	9668	65535	1834	2575	2060	4092	4581	0.49
35	3611	4910	3450	7579	11223	65535	2065	2663	1988	3574	3869	0.49
36	4197	5096	3819	7106	11747	65535	2207	2432	1860	2707	3587	0.49
37	2995	4744	3258	8187	12104	65535	1668	2665	1977	3904	4086	0.49
38	2823	4289	3047	7549	10986	65535	1842	2820	2181	4165	4292	0.49
39	3169	4946	3840	8732	11879	65535	1554	2574	1814	3911	4867	0.49
40	3062	5033	3659	9107	11874	65535	1236	2206	1510	3062	3013	0.49
41	3349	4609	3544	7389	11929	65535	1719	2195	1702	2967	3807	0.49
42	2986	4363	3188	7191	11744	65535	1787	2509	1983	3334	3955	0.50

Appendix XXII For the plots at the FORBIO site in Zedelgem, represented by plot ID, the correlation of variance (cv) of different reflectance bands are given: blue, green, red, red edge (RE), near infrared (NIR) and longwave infrared (LWIR). The mean, standard deviation (sd) and cv of the NDVI and the corrected plant height (PH) are presented as well. These values are a result after clipping with the reduced plot sizes, correcting for the alpha band and applying the mask layer to eliminate dead or unhealthy vegetation pixels.

Plot ID	Blue cv	Green cv	Red cv	RE cv	NIR cv	LWIR cv	NDVI	NDVI sd	NDVI cv	PH	PH sd	PH cv
1	0.83	0.86	0.93	0.76	0.50	0.00	0.85	0.09	0.10	12.60	1.48	0.12
2	0.75	0.76	0.76	0.62	0.49	0.00	0.80	0.09	0.11	13.68	2.52	0.18
3	0.77	0.75	0.82	0.68	0.35	0.00	0.79	0.13	0.16	10.80	0.82	0.08
4	0.76	0.79	0.83	0.70	0.33	0.00	0.77	0.14	0.19	13.36	1.90	0.14
5	0.65	0.66	0.72	0.54	0.39	0.00	0.74	0.12	0.16	9.42	1.06	0.11
6	0.66	0.62	0.68	0.53	0.37	0.00	0.71	0.12	0.17	10.20	0.87	0.08
7	0.71	0.71	0.78	0.58	0.42	0.00	0.74	0.12	0.16	12.33	2.15	0.17
9	0.77	0.79	0.84	0.66	0.49	0.00	0.82	0.09	0.11	13.20	1.91	0.14
10	0.71	0.69	0.76	0.60	0.41	0.00	0.82	0.09	0.11	10.93	0.68	0.06
11	0.68	0.67	0.75	0.55	0.28	0.00	0.86	0.08	0.09	8.89	0.89	0.10
12	0.76	0.73	0.81	0.60	0.34	0.00	0.83	0.10	0.12	11.61	1.61	0.14
13	0.59	0.62	0.64	0.49	0.38	0.00	0.69	0.12	0.18	9.15	0.88	0.10
14	0.71	0.66	0.74	0.56	0.38	0.00	0.73	0.13	0.18	9.46	1.43	0.15
15	0.74	0.68	0.77	0.55	0.39	0.00	0.71	0.14	0.19	9.80	1.45	0.15
16	0.71	0.68	0.74	0.56	0.41	0.00	0.72	0.13	0.17	12.77	1.50	0.12
17	0.73	0.74	0.76	0.61	0.50	0.00	0.72	0.13	0.19	12.67	0.94	0.07
18	0.69	0.66	0.71	0.55	0.39	0.00	0.70	0.12	0.17	11.21	0.81	0.07
19	0.57	0.60	0.60	0.49	0.38	0.00	0.56	0.17	0.30	11.97	1.60	0.13
20	0.67	0.66	0.68	0.57	0.43	0.00	0.55	0.17	0.31	11.90	1.30	0.11
21	0.57	0.58	0.61	0.50	0.39	0.00	0.53	0.19	0.36	10.15	1.00	0.10
22	0.53	0.51	0.50	0.41	0.33	0.00	0.55	0.13	0.23	12.16	1.35	0.11
23	0.50	0.51	0.52	0.40	0.29	0.00	0.63	0.11	0.18	11.44	1.96	0.17
24	0.59	0.58	0.60	0.51	0.37	0.00	0.54	0.17	0.32	11.72	0.87	0.07
25	0.62	0.63	0.67	0.53	0.38	0.00	0.60	0.16	0.27	9.14	0.92	0.10
26	0.52	0.54	0.51	0.48	0.43	0.00	0.49	0.14	0.29	13.42	1.01	0.08
27	0.54	0.52	0.50	0.45	0.35	0.00	0.49	0.12	0.24	12.13	0.65	0.05
28	0.55	0.51	0.53	0.41	0.30	0.00	0.60	0.13	0.21	9.43	0.69	0.07
29	0.57	0.58	0.60	0.54	0.41	0.00	0.54	0.16	0.29	12.55	2.09	0.17
30	0.53	0.56	0.59	0.50	0.41	0.00	0.43	0.24	0.57	6.40	1.24	0.19
31	0.51	0.53	0.57	0.46	0.35	0.00	0.58	0.14	0.24	11.52	2.17	0.19
32	0.47	0.48	0.51	0.39	0.30	0.00	0.58	0.13	0.22	12.80	1.71	0.13
33	0.60	0.64	0.65	0.58	0.46	0.00	0.54	0.17	0.31	13.48	1.38	0.10
34	0.66	0.65	0.68	0.59	0.47	0.00	0.53	0.17	0.31	11.92	1.96	0.16
35	0.57	0.54	0.58	0.47	0.34	0.00	0.53	0.16	0.30	10.37	1.26	0.03
36	0.53	0.48	0.49	0.38	0.31	0.00	0.51	0.12	0.24	11.05	0.96	0.02
37	0.56	0.56	0.61	0.48	0.34	0.00	0.58	0.16	0.28	10.65	0.95	0.02
38	0.65	0.66	0.72	0.55	0.39	0.00	0.57	0.21	0.36	9.60	0.97	0.02
39	0.49	0.52	0.47	0.45	0.41	0.00	0.47	0.16	0.33	13.76	0.84	0.02
40	0.40	0.44	0.41	0.34	0.25	0.00	0.52	0.13	0.26	8.43	0.63	0.01
41	0.51	0.48	0.48	0.40	0.32	0.00	0.54	0.13	0.24	11.36	1.54	0.03
42	0.60	0.58	0.62	0.46	0.34	0.00	0.58	0.16	0.28	12.75	0.81	0.02

Appendix XXIII For the plots at the FORBIO site in Gedinne, represented by plot ID, the number of species and the number of trees per species are given.

Plot ID	No. species	No. common beech	No. pedunculate oak	No. silver birch	No. small-leaved lime	No. Scots pine	Total No. trees
1	4	0	204	196	192	192	784
2	1	0	0	0	784	0	784
3	3	259	264	0	0	261	784
4	2	0	400	0	384	0	784
5	2	0	0	384	0	400	784
6	4	199	192	207	0	186	784
7	3	261	0	264	259	0	784
8	1	0	784	0	0	0	784
9	3	0	267	0	256	261	784
10	2	0	384	400	0	0	784
11	1	0	0	0	0	784	784
12	4	201	0	192	193	198	784
13	1	0	0	784	0	0	784
14	2	400	0	0	0	384	784
15	1	784	0	0	0	0	784
16	4	192	205	0	189	198	784
17	2	384	0	0	400	0	784
18	3	259	261	264	0	0	784
19	3	0	0	258	259	267	784
20	4	189	189	199	207	0	784
22	4	198	201	189	196	0	784
23	4	198	0	201	189	196	784
24	3	268	258	258	0	0	784
25	1	784	0	0	0	0	784
26	2	0	384	0	400	0	784
27	3	252	265	0	0	267	784
28	1	0	784	0	0	0	784
29	4	0	192	195	198	199	784
30	1	0	0	0	0	700	700
31	3	0	0	240	223	237	700
32	3	240	0	244	216	0	700
33	2	348	0	0	352	0	700
34	3	0	240	0	235	225	700
35	4	153	166	189	0	192	700
36	2	0	348	352	0	0	700
37	1	0	0	0	700	0	700
38	1	700	0	0	0	0	700
39	2	352	0	0	0	348	700
40	1	0	0	700	0	0	700
41	4	162	183	0	172	183	700
42	1	700	0	0	0	0	700
43	1	784	0	0	0	0	784
44	1	784	0	0	0	0	784

Appendix XXIV For the plots at the FORBIO site in Gedinne, represented by plot ID, the mean and standard deviation (sd) of different reflectance bands are given: blue, green, red, red edge (RE), near infrared (NIR) and longwave infrared (LWIR). These values are a result after clipping with the reduced plot sizes, correcting for the alpha band and applying the mask layer to eliminate dead or unhealthy vegetation pixels.

Plot ID	Blue	Green	Red	RE	NIR	LWIR	Blue sd	Green sd	Red sd	RE sd	NIR sd	LWIR sd
1	1927	2283	489	2868	6765	65535	996	1096	257	1061	2076	0.49
2	2644	3556	803	4586	9212	65535	764	1201	326	1386	2641	0.49
3	1844	2411	476	3347	7472	65535	773	1111	209	1330	2455	0.49
4	1744	2319	475	3190	7049	65535	755	1018	206	1204	2372	0.49
5	2142	2396	518	2632	6130	65535	1310	1427	325	1260	2328	0.49
6	1809	2185	441	2676	6957	65535	1010	1164	244	1110	2310	0.49
7	2131	2458	520	2935	6960	65535	1157	1286	275	1133	2190	0.49
8	1881	2641	490	3539	7648	65535	712	1072	199	1263	2454	0.49
9	2137	2727	541	3805	8478	65535	786	1060	219	1241	2385	0.49
10	1999	3787	820	3814	6840	65535	1286	2284	509	1864	2929	0.49
11	1486	3071	588	4199	9977	65535	788	1555	326	1911	3209	0.49
12	1868	3622	733	4126	7930	65535	1092	2031	408	1689	2647	0.49
13	1767	3603	754	3630	7200	65535	1215	2366	502	1964	3249	0.49
14	1874	3869	736	5077	10111	65535	803	1697	325	1910	2928	0.49
15	1611	3462	668	4478	9891	65535	732	1658	323	1847	3216	0.49
16	1930	4091	800	5270	9397	65535	783	1744	357	1933	3014	0.49
17	1687	3646	699	4754	10034	65535	808	1758	353	1975	3295	0.49
18	1337	2688	525	2830	6292	65535	746	1427	290	1163	2253	0.49
19	1430	2831	528	2896	6555	65535	796	1554	297	1212	2228	0.49
20	1526	3064	592	3281	6978	65535	737	1503	293	1285	2400	0.49
22	1653	4109	1821	10950	29910	65535	1205	2868	1383	6363	13031	0.49
23	1614	4080	1786	10823	30761	65535	1217	2901	1430	6510	13475	0.49
24	1469	3785	1643	9513	26472	65535	1094	2623	1252	5414	12086	0.49
25	1755	5064	2066	14649	37981	65535	1251	3601	1552	8835	15804	0.49
26	1529	4155	1871	12630	29810	65535	1102	2865	1520	7624	14645	0.49
27	1421	3933	1599	11242	35317	65535	791	2012	911	4991	12301	0.49
28	1245	3630	1449	10649	30300	65535	654	1771	801	4664	11614	0.49
29	1466	3745	1588	9334	31022	65535	978	2352	1035	4497	11362	0.49
30	1712	3774	1659	9790	29334	65535	1524	3047	1605	6511	12549	0.49
31	1612	3859	1703	8602	23330	65535	1296	3021	1504	5815	11638	0.49
32	1812	4398	1857	9742	26350	65535	1358	3226	1515	6061	11934	0.49
33	1692	4013	1844	10726	27761	65535	1325	3071	1632	6934	13213	0.49
34	1818	4328	1909	11606	29927	65535	1432	3067	1555	6816	12647	0.49
35	1729	4191	1849	9916	27600	65535	1297	2939	1455	5902	11274	0.49
36	1707	4096	1842	9056	24434	65535	1261	2859	1474	5412	11558	0.49
37	1926	4558	2189	12150	28309	65535	1182	2686	1579	6065	11693	0.49
38	1867	4742	1928	13070	38343	65535	1086	2806	1228	6318	11660	0.49
39	1744	4136	1737	11137	33570	65535	1209	2608	1288	5790	10886	0.49
40	2122	5210	2097	10506	28843	65535	1483	3424	1468	5619	11213	0.49
41	1706	4123	1736	10948	30298	65535	1137	2473	1214	5371	10314	0.49
42	1757	4519	1808	12081	35071	65535	983	2610	1104	5608	10233	0.49
43	2112	4494	863	5818	10516	65535	746	1628	363	1857	3161	0.49
44	1703	3719	690	4721	9916	65535	699	1694	327	1905	3295	0.49

Appendix XXV For the plots at the FORBIO site in Gedinne, represented by plot ID, the correlation of variance (cv) of different reflectance bands are given: blue, green, red, red edge (RE), near infrared (NIR) and longwave infrared (LWIR). The mean, standard deviation (sd) and cv of the NDVI and the corrected plant height (PH) are presented as well. These values are a result after clipping with the reduced plot sizes, correcting for the alpha band and applying the mask layer to eliminate dead or unhealthy vegetation pixels.

Plot ID	Blue cv	Green cv	Red cv	RE cv	NIR cv	LWIR cv	NDVI	NDVI sd	NDVI cv	PH	PH sd	PH cv
1	0.52	0.48	0.53	0.37	0.31	0.00	0.87	0.05	0.06	13.43	3.08	0.23
2	0.29	0.34	0.41	0.30	0.29	0.00	0.83	0.08	0.09	8.58	0.25	0.03
3	0.42	0.46	0.44	0.40	0.33	0.00	0.87	0.06	0.07	11.04	1.44	0.13
4	0.43	0.44	0.43	0.38	0.34	0.00	0.87	0.06	0.07	10.53	1.71	0.16
5	0.61	0.60	0.63	0.48	0.38	0.00	0.85	0.05	0.06	14.66	2.07	0.14
6	0.56	0.53	0.55	0.41	0.33	0.00	0.88	0.04	0.05	12.22	2.87	0.23
7	0.54	0.52	0.53	0.39	0.31	0.00	0.86	0.06	0.06	11.48	2.94	0.26
8	0.38	0.41	0.41	0.36	0.32	0.00	0.88	0.04	0.05	9.13	1.67	0.18
9	0.37	0.39	0.41	0.33	0.28	0.00	0.88	0.06	0.06	8.83	1.30	0.15
10	0.64	0.60	0.62	0.49	0.43	0.00	0.79	0.07	0.08	14.10	1.93	0.14
11	0.53	0.51	0.55	0.46	0.32	0.00	0.89	0.04	0.05	10.20	1.02	0.10
12	0.58	0.56	0.56	0.41	0.33	0.00	0.83	0.07	0.08	11.32	2.86	0.25
13	0.69	0.66	0.67	0.54	0.45	0.00	0.82	0.06	0.07	15.69	0.95	0.06
14	0.43	0.44	0.44	0.38	0.29	0.00	0.86	0.06	0.07	8.88	1.00	0.11
15	0.45	0.48	0.48	0.41	0.33	0.00	0.87	0.05	0.06	9.56	1.15	0.12
16	0.41	0.43	0.45	0.37	0.32	0.00	0.84	0.07	0.09	8.59	1.06	0.12
17	0.48	0.48	0.51	0.42	0.33	0.00	0.87	0.06	0.07	9.30	1.22	0.13
18	0.56	0.53	0.55	0.41	0.36	0.00	0.85	0.05	0.06	13.32	2.78	0.21
19	0.56	0.55	0.56	0.42	0.34	0.00	0.86	0.05	0.06	12.15	3.27	0.27
20	0.48	0.49	0.49	0.39	0.34	0.00	0.84	0.06	0.08	9.93	2.50	0.25
22	0.73	0.70	0.76	0.58	0.44	0.00	0.89	0.05	0.06	10.92	1.78	0.16
23	0.75	0.71	0.80	0.60	0.44	0.00	0.90	0.05	0.06	9.81	1.63	0.17
24	0.74	0.69	0.76	0.57	0.46	0.00	0.89	0.05	0.06	10.65	1.99	0.19
25	0.71	0.71	0.75	0.60	0.42	0.00	0.90	0.05	0.06	7.83	1.08	0.14
26	0.72	0.69	0.81	0.60	0.49	0.00	0.89	0.06	0.07	9.50	1.73	0.18
27	0.56	0.51	0.57	0.44	0.35	0.00	0.91	0.04	0.04	9.34	1.61	0.17
28	0.53	0.49	0.55	0.44	0.38	0.00	0.91	0.03	0.03	10.61	1.56	0.15
29	0.67	0.63	0.65	0.48	0.37	0.00	0.91	0.04	0.04	11.37	2.29	0.20
30	0.89	0.81	0.97	0.67	0.43	0.00	0.91	0.06	0.07	12.55	1.00	0.08
31	0.80	0.78	0.88	0.68	0.50	0.00	0.88	0.07	0.08	13.72	2.98	0.22
32	0.75	0.73	0.82	0.62	0.45	0.00	0.89	0.06	0.07	13.96	2.46	0.18
33	0.78	0.77	0.89	0.65	0.48	0.00	0.89	0.08	0.09	11.33	1.55	0.14
34	0.79	0.71	0.81	0.59	0.42	0.00	0.89	0.06	0.06	12.48	1.10	0.09
35	0.75	0.70	0.79	0.60	0.41	0.00	0.89	0.06	0.07	12.17	4.20	0.35
36	0.74	0.70	0.80	0.60	0.47	0.00	0.88	0.06	0.07	13.46	1.66	0.12
37	0.61	0.59	0.72	0.50	0.41	0.00	0.86	0.09	0.11	9.77	1.43	0.15
38	0.58	0.59	0.64	0.48	0.30	0.00	0.91	0.04	0.04	11.08	0.95	0.09
39	0.69	0.63	0.74	0.52	0.32	0.00	0.91	0.05	0.05	11.56	1.19	0.10
40	0.70	0.66	0.70	0.53	0.39	0.00	0.88	0.05	0.06	12.09	2.51	0.21
41	0.67	0.60	0.70	0.49	0.34	0.00	0.90	0.05	0.05	12.41	1.24	0.10
42	0.56	0.58	0.61	0.46	0.29	0.00	0.91	0.04	0.04	10.97	0.89	0.08
43	0.35	0.36	0.42	0.32	0.30	0.00	0.84	0.08	0.10	7.25	0.77	0.11
44	0.41	0.46	0.47	0.40	0.33	0.00	0.87	0.06	0.07	8.47	1.08	0.13

8 Popularised Summary

Today, biodiversity is declining faster than ever known in human history. This huge loss of species threatens all kind of benefits that nature provides us. Think off clean drinking water, carbon uptake, recreation… Without taking conservation actions, the rate of species extinction will accelerate even more, which is a direct threat to human existence. To be able to conserve species, one needs to have a clear picture of how many species live where and how well they are performing. However, doing this through traditional field surveys is very time-consuming and costly. A recently discovered solution for this is using drones. Drones can easily collect very detailed data and can even capture information that is not visible to the naked eye. Because this is a rather new field of research, much remains to be discovered.

In this research, we tried to predict species diversity and productivity at the FORBIO tree experiment sites in Belgium. At these sites, different tree species are planted in plots where some plots contain one species only (monocultures) and in other plots different species are mixed together. To collect data, drone flight missions were carried out over these sites. A multispectral sensor attached to the drone captured reflectance data in different parts of the electromagnetic spectrum e.g. visible part, infrared part… For all these bands, the mean, standard deviation and correlation of variance were calculated per plot and this information was used to build models to predict tree species richness on the one hand and tree productivity on the other hand. Different models were tested, but none were very good in predicting species richness. However, by adding information of the tree height the model accuracy increased significantly.

The models to predict tree productivity performed better. Generally, a higher productivity was found in mixed-species plots compared to monoculture plots. This confirms the theory that it is better to plant mixed forest. These research results indicate that data collected with drones can indeed be used in tree biodiversity and productivity studies in addition to traditional field surveys.